Subcellular localization and visualization of RecA and ImuA′ in mycobacteria.

Atondaho Angelah Ramudzuli, RMDATO001

Supervisor: Prof. Digby Warner

Co-supervisors: Dr Sophia Gessner

Prof. Valerie Mizrahi

This thesis is submitted to the Division of Medical Microbiology, Department of Pathology, Faculty of Health Sciences, University of Cape Town in fulfilment of the requirements for a Master of Science in Medical Microbiology.

March 2021.

Declaration

I declare that this thesis is my own unaided work. It is being submitted for the degree of Master of Science at the University of Cape Town. It has not been submitted for any degree or examination at any other university.

Signature Signed by candidate

Date ____March 2021____

Abstract

Antibiotic-resistant strains of *Mycobacterium tuberculosis* (*Mtb*) are threatening global efforts to eradicate tuberculosis (TB). One attractive approach for target-based drug design proposes to curb the evolution of *Mtb* during both immune and drug assault. The potential target: mycobacterial DNA metabolism. For this, an in-depth understanding of the mechanisms of DNA repair and mutagenesis in mycobacteria is required. RecA and ImuA′ are DNA damage-inducible proteins implicated in DNA damage repair and tolerance in *Mtb*. RecA is a key regulatory protein of the SOS response and ImuA′ is a component of the mycobacterial mutasome, effecting DNA damage tolerance and mutagenesis. In this study, a comprehensive panel of *M. smegmatis (Msm)* RecA and ImuA′ reporter strains was generated to explore the dynamics of their expression and subcellular localization within live *Msm* cells. To this end, fluorescently tagged versions of ImuA′ and RecA were constructed and shown to retain functional activity in UV-induced mutagenesis but not survival of mitomycin C (MMC) treatment. The discrepant complementation phenotypes observed in UV and MMC assays was unexpected and suggested disruption of a critical protein-protein interaction(s) owing to the presence of the fluorophore. Using fluorescence microscopy, RecA and ImuA′ expression were monitored in *Msm* exposed to different types of genotoxic stresses conditions. When mScarlet-ImuA′ was introduced into wild-type (WT) and Δ*imuA′* backgrounds, diffuse bright red fluorescence was observed in cells treated with MMC and UV; in contrast, no fluorescence expression was observed in untreated cells, confirming the DNA damage-dependent induction of *imuA′*. Following the introduction of RecA-msfGFP into WT and Δ*recA* backgrounds, discrete green, fluorescent foci were observed in treated and untreated cells in both backgrounds, consistent with the role of RecA in DNA replication in the absence of external DNA damage, and elevated expression under genotoxic conditions. Taken together, these observations support the utility of the fluorescently tagged translational fusions as bioreporters to elucidate the function and regulation of ImuA’ and RecA in mycobacteria.

Acknowledgement

Firstly, I would like to thank God and give him praise for all his blessings, grace, and strength he bestowed upon me throughout this journey.

To my amazing late mom, thank you for being my best friend and for everything you have done for me, especially for your support and inspiring me to pursue my goals and dreams. To my sister, thank you for unselfishly taking over the motherly role when mom passed and for being the best cheerer in both good and bad times. To my brothers, Khahuliswe and Cooler, my nephews, Kharendiwe and Sechaba and my brother in-law Michael, thank you for your unwavering support. I hope I make all of you proud.

To my co-supervisor Dr. Sophia Gessner, I am grateful for your support and patience. Thank you for holding my hand and sharing your knowledge about this field with me and for teaching me the tips and tricks of running the experiments in the lab. And most importantly, thank you for being the most wonderful supervisor.

To my supervisor, Prof Digby Warner, thank you for believing in me and for giving me a chance to explore and learn more about this challenging research field. I appreciate all your encouragement, support, and everything you have taught me. Thank you for giving me an opportunity to work with you and learn from you.

To the MMRU, I'm grateful for everything and happy to have met such a wonderful family and group of people. To Rendani Mbau, Ditshego Ralefeta, Ryan Dinkele, and Joseph Gitari, thank you for all your assistance in the lab.

Finally, I would like to thank the Molecular Microbiology Research Unit (MMRU), the National Research Fund (NRF), and the university of Cape Town (UCT) for funding and financial assistance.

Table of Contents

List of abbreviations and units.

2YT	Two yeast tryptone
AFU	Arbitrary fluorescence unit
Amk	Amikacin
ATP	Adenosine triphosphate
attB	Bacterial tRNAGly attachment site
bp	Base pair
BER	Base excision repair
CFU	Colony forming unit
Cm	Capreomycin
cm^2	Square centimeter
CTAB	Cetyltrimethylammonium bromide
dH_2O	Distilled water
DMSO	Dimethyl sulfoxide
DNA	Deoxyribosenucleic acid
dNTP	Deoxyribonucleotide triphosphate
DSBs	Double-stranded DNA breaks
DsDNA	Double-stranded DNA
EMB	Ethambutol
EtBr	Ethidium Bromide
g	Gram
Gen	Gentamycin
Gen^R	Gentamycin-resistance
GFP	Green fluorescent protein
HIV	Human immunodeficiency virus
hr	Hour(s)
HR	Homologous recombination
ImuA′	Inducible mutagenesis protein A-prime

ImuB	Inducible mutagenesis protein B, encoded by *imuB*
INH	Isoniazid
Kan	Kanamycin
Kan^R	Kanamycin-resistance
KO	Knockout
LA	Luria-Bertani agar
LAL	LexA binding loop
LB	Luria-Bertani
LTBI	Latent TB infection
M	Molar
MDR	Multi-drug resistant
mg	Milligram
MIC	Minimum inhibitory concentration
min	Minute(s)
ml	Millilitre
mM	Millimolar
mm	Millimetre
MMR	Mismatch repair
MMC	Mitomycin C
Mox	Moxifloxacin
MScarlet	mScarlet fluorescent protein
msfGFP	monomeric super folder green fluorescent protein
Msm	*Mycobacterium smegmatis*
Mtb	*Mycobacterium tuberculosis*
NER	Nucleotide excision repair
Nfz	Nitrofurazone
ng	Nanogram
NHEJ	Non-homologous end-joining
No.	Number

Nov	Novobiocin
OADC	Oleic acid-albumin-dextrose-catalase
OD_{600}	Optical density at 600 nm wavelength light
Ofx	Ofloxacin
P1	RecA promoter 1, RecAP1
P2	RecA promoter 2, RecAP2
PBS	Phosphate-buffered saline
PCR	Polymerase chain reaction
PHP	Polyhistidinol phosphatase
Pol	Polymerase
PZA	Pyrazinamide
RE	Restriction endonuclease
RecA	RecA protein, encoded by *recA*
RecA*	Activated nucleoprotein filament of RecA
RecA-ND	RecA-independent mechanism
RecA-NDp	RecA non-dependent promoter
Rif	Rifampicin
Rif^R	Rifampicin resistant
RNS	Reactive nitrogen species
ROS	Reactive oxygen species
rpm	Revolutions per minute
sec	Second(s)
SSBs	Single-stranded breaks
ssDNA	Single-stranded DNA
TE	Tris-EDTA
TAE	Tris base, acetic acid, and EDTA
TB	Tuberculosis
TFB1	Transformation buffer 1
TFB2	Transformation buffer 2

TLS	Translesion DNA Synthesis
UV	Ultraviolet
V	Volt
VFP	Venus fluorescent protein
v/v	volume-per-volume
WHO	World Health Organisation
WT	Wild-type
XDR	Extensively drug resistant
°C	Degree Celsius
Ω	Resistance
µg	microgram
µF	microfarad
µJ	microjoules
µl	microlitre

List of Figures

List of Tables

1. Literature review

1.1. Background and TB epidemiology

Mycobacterium tuberculosis (*Mtb*), the causative agent of tuberculosis (TB), is classified as a gram positive, facultative intracellular pathogen that colonizes its obligate human host. According to the most recent World Health Organization (WHO) report, *Mtb* ranks in the top 10 causes of death and, with the exception of SARS-CoV-2/COVID-19, is responsible for the significant number of deaths from an infectious agent, with millions of new infections each year. It was reported that, in 2019, an estimated 10 million people developed TB and 1.4 million people succumbed to the disease, with 465 000 people infected with drug-resistant forms (Organization, 2020). Of the infected individuals, 12% were children under the age of 15 years and 8.2% were people living with TB-HIV comorbidity (Organization, 2020). In 2018, eight countries from Africa (Nigeria (4%) and South Africa (3%)) and Asia (China (9%), India (27%), Indonesia (8%), Philippines (6%), Bangladesh (4%) and Pakistan (6%)) reported the about two-thirds of the global new TB infections and TB associated deaths annually (Organization, 2020). These are low-income, resource-limited countries experiencing various socio-economic challenges, including poverty, high HIV incidence, inconsistent TB drug rollout campaigns, over-crowding, and stigma towards TB.

The emergence of antibiotic resistant strains threatens global efforts to eradicate TB. As a result, there is increasing interest in the development of ancillary therapies aimed at curbing the capacity of *Mtb* for adaptive mutagenesis. Among many possible strategies, crippling molecular mechanisms involved in DNA replication and repair represents a compelling approach (Minias et al., 2019, Ojha and Patil, 2019). However, the pathways involved in the maintenance of genome integrity remain poorly understood. Here, we will explore the aspects that are understood and identify the gaps that require urgent investigation.

1.2. TB pathogenesis

Mtb generally infects the lungs of the host (pulmonary TB) but can spread to other parts of the body (extrapulmonary TB) (Chen et al., 2010). Infection is thought to begin when *Mtb*-

containing aerosol droplets are released via cough by an individual with active TB (Patterson and Wood, 2019, Turner et al., 2017, Warner and Mizrahi, 2006). Upon inhalation, the *Mtb* bacilli enter the lung alveoli where they are phagocytosed by resident alveolar macrophages initiating the host immune response (Dover and Coxon, 2011, Huang et al., 2019, Sia and Rengarajan, 2019, Upadhyay et al., 2018, Warner and Mizrahi, 2007). Following macrophage phagocytosis, *Mtb* evades macrophage defences by tolerating their acidic, nitro-oxidative environment within the cells (Ankley et al., 2020, Ehrt and Schnappinger, 2009). The ability of *Mtb* to arrest phagosome maturation allows the bacilli to survive within the macrophages and to replicate within the cells (Ankley et al., 2020, Cambier et al., 2014, Ehrt and Schnappinger, 2009, Queval et al., 2017). Replication within macrophages causes apoptosis which results in other cells of the immune system being recruited to surround the infected macrophages, forming granulomas (Russell, 2007, Zhai et al., 2019). Macrophages within the granulomas can be dormant, preventing antigen presentation to lymphocytes and suppressing the immune response resulting in latent infection (Bozzano et al., 2014).

A hallmark of *Mtb* is its capacity to remain in a state of latency for prolonged periods (Barry et al., 2009, Cambier et al., 2014). In turn, this results in spreading of the primary infection to most organs of the body (Stallings and Glickman, 2010). However, *Mtb* infection is usually asymptomatic in healthy, immunocompetent hosts and generally doesn't lead to active TB (Philips and Ernst, 2011). Based on immunological tests, up to one quarter of the world's population is believed to be infected with *Mtb*, and are mostly latent infections (Carvalho et al., 2011, Ravimohan et al., 2018). This distinctive ability of *Mtb* to cause latent TB infection (LTBI) creates a huge reservoir of potential cases of disease reactivation and successive transmission of the bacillus (Mayito et al., 2019, Chao and Rubin, 2010).

1.3. TB treatment

Drug-susceptible TB is treated with first-line TB drugs, isoniazid (INH), rifampicin (RIF), ethambutol (EMB), and pyrazinamide (PZA) for two months, followed by a four months continuation phase with INH and RIF (Shin and Kwon, 2015, Stagg et al., 2016, Organization, 2020). This regimen is highly effective at curing drug-susceptible TB (Reiche et al., 2017). However, abandoning this course of treatment is common among infected TB patients and often leads to the development of multi-drug resistance TB (MDR-TB) (Dheda et al., 2017,

Reiche et al., 2017). Drug-resistant TB is far more complicated and challenging to treat and is therefore associated with high mortality rate (Dheda et al., 2014, Manjelievskaia et al., 2016). MDR-TB requires second-line TB drugs which are more expensive, toxic, and less effective (Dheda et al., 2017, Manjelievskaia et al., 2016). Emergence of resistance to second-line drugs such as fluoroquinolones and at least one injectable agent, amikacin (Amk), capreomycin (Cm) and kanamycin (Kan), is referred to as extensively drug resistance TB (XDR-TB) which is even more challenging to treat (Dheda et al., 2014). Drug-resistant TB requires prolonged periods of treatment which often leads to poor treatment adherence (Prasad et al., 2017, Warner and Mizrahi, 2006). The emergence of drug-resistant TB and the increase in MDR-TB and XDR-TB cases worldwide highlight the need for the development of new chemotherapeutic agents (Hoagland et al., 2016). New antimicrobial therapeutics have been approved recently. These include bedaquiline which is recommended by WHO to treat MDR-TB and XDR-TB (Mahajan, 2013, Pontali et al., 2016). Most recently a new drug, pretomanid, was approved by the Food and Drug Administration (FDA) and is administered with bedaquiline and linezolid to treat highly resistant TB (McKenna and Furin, 2019). Unlike other forms of MDR-TB treatment that is administered for a longer period and is less effective, pretomanid-containing regimen are more effective and have a shorter duration (McKenna and Furin, 2019).

Despite the promise these new drugs hold, antimicrobial resistance remains an escalating global problem that continues to threaten efficacy of antibiotics (Wipperman et al., 2018) and imperils progress in containing the global TB epidemic (Gygli et al., 2017). As such, understanding the mechanisms contributing to the evolution of drug resistance is crucial in efforts to control this pathogen (Miggiano et al., 2020, Mittal et al., 2020). *Mtb* is capable of overcoming DNA damage agents such as those generated by the host immune response and exposure to antibiotic treatment (Ehrt and Schnappinger, 2009, Singh and Mizrahi, 2017) and its ability to replicate and survive depends on mechanisms maintaining genome integrity (Bussi and Gutierrez, 2019, Queval et al., 2017, Smollett et al., 2012). However, in addition to maintaining genome integrity upon DNA damage, the bacillus is equipped with DNA damage tolerance mechanisms which might promote mutagenesis, especially under stress (Boshoff et al., 2003). Studies on how this bacillus maintains its genome integrity and induce mutagenesis after DNA damage forms part of an important area of research (Kurthkoti and Varshney, 2012).

1.4. DNA replication fidelity

Faithful, error-free replication of genomic DNA is essential for the ability of any organism to survive (Baños-Mateos et al., 2017, Ditse et al., 2017). To ensure error-free replication of DNA, bacteria employ high-fidelity polymerases that are capable of replicating DNA with very low error-rates (Timinskas et al., 2014, Zhao et al., 2006). Bacterial replication machinery utilises 3′ to 5′ exonuclease proofreading activity that removes misincorporated nucleotides (Baños-Mateos et al., 2017, Fijalkowska et al., 2012, Gu et al., 2016), either via intrinsic exonucleases in the replicative polymerases or through a dedicated proofreading subunit (Timinskas et al., 2014). In mycobacteria, DNA polIIIα is the major replicative polymerase and consists of polIII holoenzyme, a clamp loader complex and a β_2 sliding clamp processivity factor (Boshoff et al., 2003, Ditse et al., 2017, Gu et al., 2016, Johnson and O'Donnell, 2005, Warner et al., 2014). *Mtb* replicative polymerase IIIα subunit DnaE1 utilises a polymerase and histidinol phosphatase (PHP) domain that acts as the intrinsic proofreading replicative exonuclease (Rock et al., 2015).

1.5. DNA repair

In addition to high fidelity genome replication, DNA repair is essential to maintaining genome integrity (Müller et al., 2018). As an intracellular organism, *Mtb* is continually exposed to DNA damaging assaults such as host defence effectors and antimicrobial treatments (Dos Vultos et al., 2009). During infection, the host produces different anti-*Mtb* antimicrobial compounds such as reactive oxygen (ROS) and nitrogen (RNS) species (Adams et al., 1997, Burney et al., 1999, Echeverria-Valencia et al., 2018, Kumar et al., 2011, Warner and Mizrahi, 2006). However, *Mtb* persists in host macrophages, antagonizing host defences by withstanding the hostile environment and repairing any incurred DNA damage for continued survival (Ehrt and Schnappinger, 2009, Manganelli et al., 2004). *Mtb* employs a suite of different DNA repair mechanisms in response to damage, each thought to specialize in a different type of lesion or damage (Namouchi et al., 2016, Singh, 2017). Under both normal and DNA damaging conditions, DNA repair mechanisms have been shown to be fundamental for maintaining genome integrity and viability (Lin et al., 2014). However, a complete understanding of how *Mtb* is capable of maintaining genome integrity is an area of great interest and active research (Dos Vultos et al., 2009, Gorna et al., 2010, Kurthkoti and Varshney, 2012, Singh, 2017, Warner, 2010).

In *E. coli*, the mismatch repair (MMR) system is one of the main DNA repair mechanisms contributing to fidelity. Initially, mycobacteria were considered to lack MMR which recognizes and deletes mismatched bases erroneously incorporated during replication and missed during proofreading (Baños-Mateos et al., 2017, Friedberg et al., 2005, Mizrahi and Andersen, 1998). However, recent work has revealed that mycobacteria encode a putative non-canonical MMR system mediated by the NucS mismatch-specific endonuclease (Castaneda-Garcia et al., 2017, Castañeda-García et al., 2020). Mycobacterial NucS shares no structural homology with the canonical *E. coli* MMR system but it prevents acquisition of spontaneous DNA mutations in mycobacteria (Castaneda-Garcia et al., 2017, Castañeda-García et al., 2020).

Bacterial cells are capable of eliminating some damage to DNA by direct reversal repair (Yi and He, 2013). However, not all types of DNA lesions can be repaired by this mechanism (Friedberg, 1995). Single-strand DNA (ssDNA) damage involves excision repair pathways in which damaged DNA is removed and replaced using complementary strand as the template (Watson et al., 2008). Base excision repair (BER) recognises DNA bases with damage caused by chemical modifications. Excision is initiated when DNA glycosylases remove damaged DNA bases by cleaving the sugar-phosphate backbone, leaving an apurinic or apyrimidinic site. DNA PolI then removes damaged bases using the 5′ to 3′ exonuclease activity and fills in the missing bases using the complementary strand as a template before a DNA ligase seals the gap by forming a phosphodiester bond (Dos Vultos et al., 2009). Nucleotide excision repair (NER) is different to BER in which bulky damage such as pyrimidine dimerization caused by UV light is recognized. Instead of single bases, 12-24 nucleotide long strands of damaged DNA are clipped by an endonuclease on either side of the damaged lesion (Darwin and Nathan, 2005). Again, DNA PolI fills in the missing nucleotides and DNA ligase seals the gap.

DNA damage can also cause breaks in either one or both DNA strands, namely single-stranded breaks (SSBs), or double-stranded breaks (DSBs), respectively. Recombination repair involves strand exchange between two DNA molecules followed by joining of the DNA ends (Muttucumaru and Parish, 2004). Mechanisms which repair DSBs in mycobacteria include homologous recombination (HR) and non-homologous end-joining (NHEJ) (Gupta et al., 2011). HR requires an identical copy of a broken chromosome segment to use as a template

(Jasin and Rothstein, 2013, Smith, 2004). RecA plays a key role in the recombination processes (Clark and Margulies, 1965, Del Val et al., 2019, Huang et al., 2020, Singh et al., 2016). In HR, DSBs are repaired by RecBCD, a 3-subunit enzyme complex which binds the blunt end of DSB. The helicase subunits, RecB and RecD, unzip the DNA helix and RecB nuclease cuts the 3′ ssDNA from the unzipping process. The RecBCD unzips until it recognizes the Chi site close to the damaged region and degrades the 5′ end, leaving the 3′ end tail (Wigley, 2013). RecA is then recruited to the 3′ end of the generated ssDNA forming a nucleoprotein filament which allows strand evasion and exchange (Dillingham and Kowalczykowski, 2008, Taylor and Smith, 2003, Wigley, 2013). An alternative to RecBCD-mediated HR is RecFOR-mediated recombination. In this pathway, RecQ helicase unwinds the DNA and RecJ nuclease cut the 5′ end strand leaving the 3′ end strand. The RecA nucleoprotein filament then exchanges places with the identical strand in homologous DNA (Morimatsu and Kowalczykowski, 2003). Although the RecFOR pathway is sometimes used for DSB repair it is routinely used to repair SSB (Pagès, 2016). The second mechanism for DSB repair is NHEJ, in which a homologous template strand is not necessary and instead requires broken strand ends to be brought into contact (Dos Vultos et al., 2009). This process requires the presence of DNA-end-binding protein Ku which stimulates sealing of DSBs by specialised DNA ligase LigD (Dos Vultos et al., 2009, Weller et al., 2002).

1.6. Mycobacterial DNA damage response

Chromosomal mutations drive microevolution of *Mtb*, including the acquisition resistance to antimicrobial drugs (Warner, 2010, Warner et al., 2013). For the bacterium to survive and persist within hostile, potentially genotoxic environments, DNA repair mechanisms must be continually active within the course of prolonged infection (Warner et al., 2013). *Mtb* can respond to DNA damage by repair (mostly high fidelity) or tolerance (often error-prone) mechanisms but the DNA damage response in *Mtb* is not fully understood (**Fig. 1.1**) (Wang et al., 2011). As noted above, mechanisms of high-fidelity DNA damage repair employed by mycobacteria include base excision repair (BER), nucleotide excision repair (NER), and homologous recombination (HR) repair (Gupta et al., 2011, Kurthkoti and Varshney, 2012, Singh, 2017, Stephanou et al., 2007). DNA damage tolerance mechanisms include the process of error-prone translesion synthesis (TLS) which inserts bases to bypass lesions, preventing the replication fork from collapsing but with the consequence in some cases of introducing mutations into the strand. Another error-prone mechanism is non-homologous end-joining

(NHEJ) (**Fig. 1.1**) (Fuchs and Fujii, 2013). Most bacteria regulate these pathways and respond to DNA damage by triggering the classical LexA/RecA-dependent response mechanism (Little and Mount, 1982). However, *Mtb* is unusual in that it possesses both LexA/RecA-dependent and RecA-independent (RecA-ND) DNA damage response mechanisms (Davis et al., 2002, Gamulin et al., 2004, Müller et al., 2018, Rand et al., 2003).

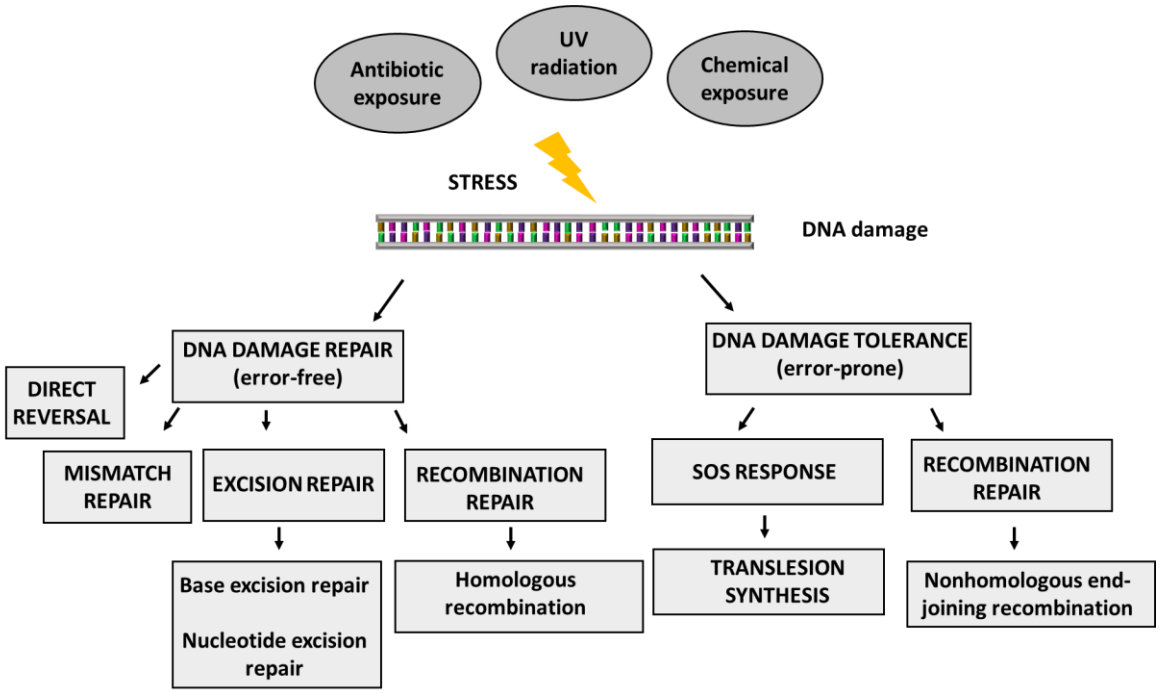

Figure 1.1: Mechanisms of DNA damage repair and tolerance in mycobacteria. Bacteria are constantly exposed to endogenous and environmental stresses. To maintain its genome integrity, bacteria either repair or tolerate the inflicted damage. DNA repair pathways are considered error-free, whereas damage tolerance pathways involve error-prone synthesis.

1.6.1. RecA/LexA-independent DNA damage response

Unlike many other bacterial species, in mycobacteria, the majority of DNA damage response genes, including DNA repair genes and *recA* itself (Davis et al., 2002), are regulated independently of RecA and LexA (Gamulin et al., 2004, Rand et al., 2003). A motif in the promoter regions of RecA/LexA-independent genes was identified that resembles a sigma70 recognition element; subsequently, the consensus sequence tTGTC(G/A)gtg-8nt-TAnnnT was renamed the RecA non-dependent promoter (RecA-NDp) (Gamulin et al., 2004). DNA repair genes regulated by the RecA-NDp promoter include genes for BER (*alkA*, *lhr*), recombination repair (*recA*, *ruvC*, *radA*), NER (*uvrA*, *uvrB*, *xthA*), and other genes encoding proteins involved

in DNA damage repair including single-stranded DNA-binding protein (*ssb*), ribonucleoside-diphosphate reductase (*nrdF2*) and DNA helicase (*dnaB*) (Gamulin et al., 2004). Recent studies have shown that PafBC (proteasome accessory factor B and C) is the global transcriptional regulator that regulates 150 DNA repair genes by recognizing a sequence similar to the RecA-NDp motif and is responsible for most genes regulated following Mitomycin C (MMC) stress (Müller et al., 2018, Müller et al., 2019, Olivencia et al., 2017).

1.6.2. The RecA/LexA-dependent mycobacterial SOS response

In most bacteria, a global regulatory network termed the SOS response controls the synthesis of factors that repair the genome (Ghodke et al., 2019). The SOS response was discovered and characterized in *E. coli* (Radman, 1975). Under conditions that damage DNA or inhibit its replication, induction of the SOS regulon is triggered and is associated with enhanced DNA repair and DNA damage tolerance (Little and Mount, 1982). This process is regulated primarily by RecA and LexA (Little and Mount, 1982, Maslowska et al., 2019). In this pathway, proteins that promote the integrity of DNA are induced which are associated with enhanced DNA repair, improved survival, and continuous replication of DNA, albeit at the cost sometimes of increased mutations (Little and Mount, 1982, Maslowska et al., 2019). In the classic system, LexA acts as a transcriptional repressor of SOS-regulated genes by binding to a specific operator sequence termed SOS box, preventing transcription of SOS regulon genes during non-DNA damaging conditions (**Fig. 1.2A**) (Gamulin et al., 2004, Little et al., 1981, Shinagawa, 1996, Walker, 1996). LexA is composed of a C-terminal catalytic domain responsible for homodimerization and N-terminal DNA binding domain which is crucial for SOS-box recognition (Maslowska et al., 2019). When bacteria encounter genotoxic conditions, ssDNA accumulates in the cell (owing to stalled replication forks, for example) initiating the SOS response (Sassanfar and Roberts, 1990). RecA is recruited to the ssDNA to form an activated nucleoprotein filament (RecA*) facilitating proteolytic autocleavage of the LexA dimer (Goodman et al., 2016, Jaszczur et al., 2016, Little, 1982). RecA thus acts as co-protease which mediates LexA cleavage, disabling binding to the SOS box and allowing the induction of the SOS regulon and expression of SOS response genes (**Fig. 1.2B**) (Gamulin et al., 2004, Little, 1991, Papavinasasundaram et al., 2001, Sutton et al., 2000). Once the cell recovers from the DNA damage, the numbers of ssDNA and RecA nucleofilaments are reduced, resulting in the accumulation of intact LexA dimers and binding to the SOS box repressing the SOS regulon and shutting down the SOS response (Friedberg, 1995, Sutton et al., 2000).

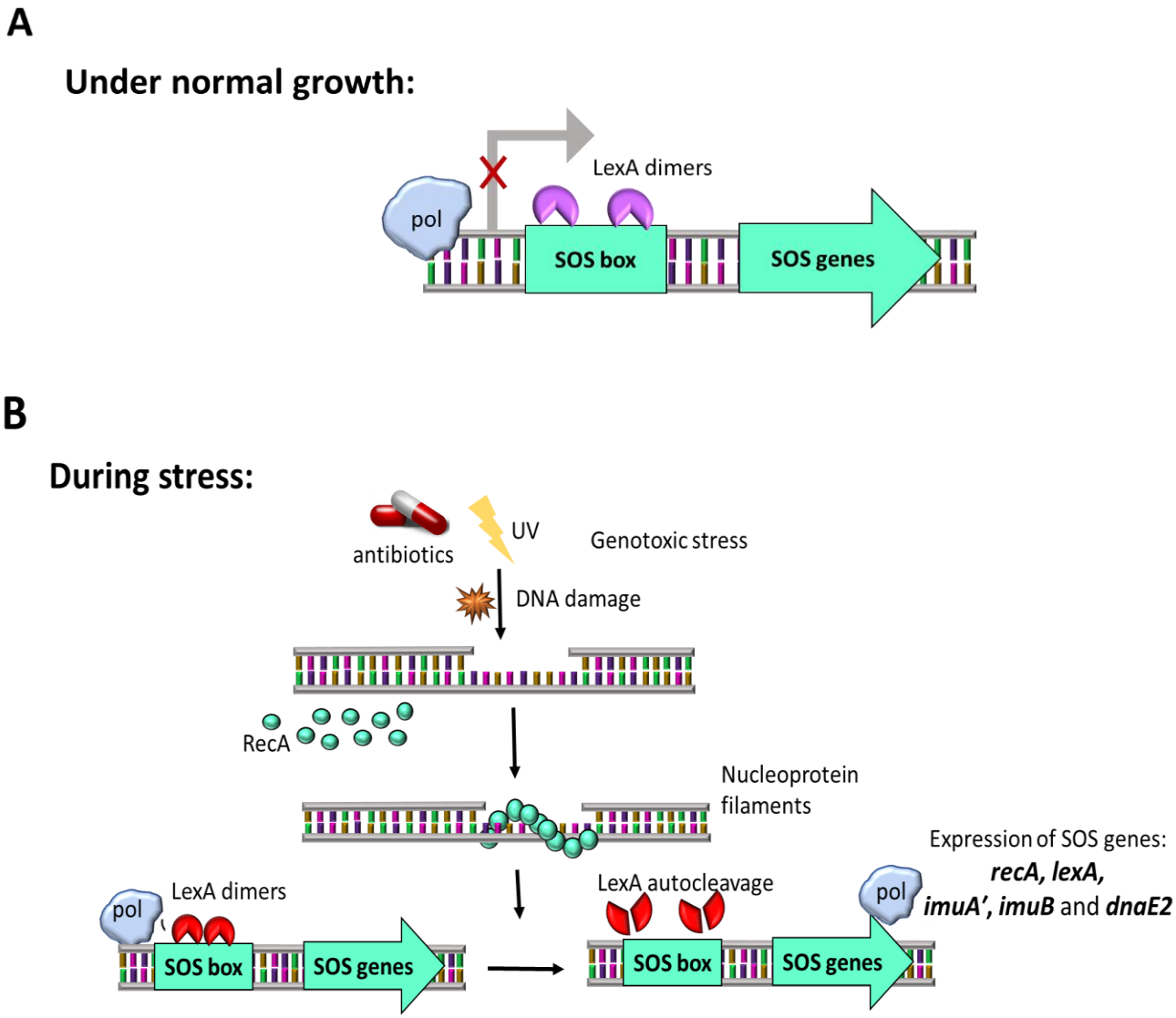

Figure 1.2: Bacterial SOS response system. A. Under normal conditions, the LexA dimer act as a transcriptional repressor which binds to the SOS box and blocks the activity of the polymerase, inhibiting the transcription of more than 50 SOS regulated genes including lexA and recA. **B.** When Mycobacteria encounters genotoxic stress conditions that compromise its genome integrity. RecA is recruited to the ssDNA to form activated nucleoprotein filaments (RecA*) facilitating proteolytic autocleavage of LexA. Once cleaved, LexA is unable to bind the SOS box allowing expression of SOS response genes including recA, lexA and components of the mutasome.

1.6.2.1. Translesion synthesis (TLS).

High-fidelity polymerases are unable to replicate past DNA damage and, when they encounter a lesion on a DNA template, replication is stalled and further DNA synthesis prevented (Lindahl, 1996, Liu et al., 2016). To bypass these lesions, bacterial cells are equipped with

specialized TLS DNA polymerases which are capable of replicating past lesion sites, allowing replication synthesis to continue (**Fig. 1.3**) (Bridges, 2005a, Bridges, 2005b, Yang and Woodgate, 2007). These specialized polymerases typically belong to the Y-family of DNA polymerases which play a significant role in DNA damage tolerance than in DNA replication (Nohmi, 2006, Ohmori et al., 2001, Yang and Gao, 2018). Typically, Y family DNA polymerases possess active sites that can accommodate large substrates and are able to replicate past damage to avoid the deleterious outcomes (Goodman and Woodgate, 2013). While these polymerases can exhibit the specialized function to replicate past lesions, their function across undamaged DNA templates is minimized (Bridges, 2005a, Bridges, 2005b, Yang and Woodgate, 2007) and may cause mutations (Andersson et al., 2010). Owing to this mutagenic function, TLS polymerases can be error-prone, and so have been associated with high increased mutagenesis and the acquisition of drug resistance (Fuchs and Fujii, 2013, Lange et al., 2011).

In *E. coli*, DNA PolII, a B family DNA polymerase, and PolIV and PolV (DinB and UmuD'$_2$C, respectively) – both Y family members, form part of the SOS response (Agashe, 2017, Goodman and Woodgate, 2013, Napolitano et al., 2000, Radman, 1975, Tippin et al., 2004). Y-family polymerases share common structural features with replicative polymerases such as the palm, finger, and thumb domains (Friedberg et al., 2001, Walsh et al., 2011, Yang and Woodgate, 2007). However, the sizes of replicative polymerase thumb and finger domains are smaller than those of other Y-family polymerases, which allow bulky lesions to enter the active site (Chandani et al., 2010, Ohmori et al., 2001). TLS polymerases lack the intrinsic 3′ to 5′ exonuclease proofreading, and the characteristic α-helix (O-helix) necessary for the high-fidelity function in replicative polymerases, but these deficiencies give them the ability to accommodate damage DNA templates and low fidelity function on undamaged DNA (Beard and Wilson, 2003, Ling et al., 2001).

In many bacteria, induced mutagenesis is mainly mediated by TLS **(Fig. 1.3)**. In *E. coli*, there are three different TLS DNA polymerases; PolII, PolIIV, and PolV which form part of the SOS response (Agashe, 2017, Goodman and Woodgate, 2013, Napolitano et al., 2000). All three TLS polymerases are required to bypass lesions in DNA (Goodman and Woodgate, 2013, Napolitano et al., 2000). PolV is the main polymerase that synthesizes DNA with decreased fidelity (Goodman and Woodgate, 2013, Jaszczur et al., 2016), and is associated with an increase in damage-induced mutagenesis (Patel et al., 2010, Tang et al., 2000). In *E. coli*, PolV

comprises the UmuD′$_2$C complex (Goodman et al., 2016, Ippoliti et al., 2012, Jaszczur et al., 2016). UmuD′$_2$C complex formation requires the interaction of UmuC as well as UmuD that is synthesised as a homodimer and undergoes autocatalytic cleavage facilitated by RecA to generate UmuD′$_2$ dimer (Bruck et al., 1996, Nohmi et al., 1988, Reuven et al., 1999, Schlacher et al., 2006, Tang et al., 1999, Timinskas and Venclovas, 2019). The ability to perform TLS depends on the formation of the UmuD′$_2$C complex, presence of β-clamp subunits, SSB as well as RecA nucleoprotein filament (Ippoliti et al., 2012, Tang et al., 2000). In TLS, PolV and RecA form a complex that activates PolV in the presence of ATP (Schlacher et al., 2005, Timinskas and Venclovas, 2019). A RecA nucleoprotein filament is required to activate PolV-catalysed TLS by transferring a RecA subunit and ATP from the nucleoprotein 3′-proximal end to PolV to form an activated PolV mutasome (Patel et al., 2010, Tang et al., 1999, Timinskas and Venclovas, 2019). PolV activity is greatly dependent on RecA and strongly enhanced when RecA is present, suggesting that RecA is essential to stimulate PolV activity in TLS (Pham et al., 2001, Schlacher et al., 2005, Timinskas and Venclovas, 2019).

The *Mtb* genome encodes two Y-family DNA PolIV homologs: DinB1, encoded by Rv3056, and DinB2 encoded by Rv1537. Unlike in *E. coli*, their expression does not depend on RecA and is not induced upon DNA (Boshoff et al., 2003, Boshoff et al., 2004, Brooks et al., 2001, Kana et al., 2010, Rand et al., 2003). In contrast to *E. coli*, *Mtb* utilises a C-family DNA polymerase, DnaE2, for TLS (**Fig. 1.3**) (Boshoff et al., 2003, McHenry, 2011a). Evidence from other models (Indiani et al., 2005, Indiani et al., 2009) suggests that the replicative polymerase (DnaE1) competes with TLS polymerase for access to the β -clamp, a homodimeric "doughnut"-shaped ring which encircles the DNA template strand and provides processivity to the replicative DNA polymerase (Johnson and O'Donnell, 2005, Zhao et al., 2017).

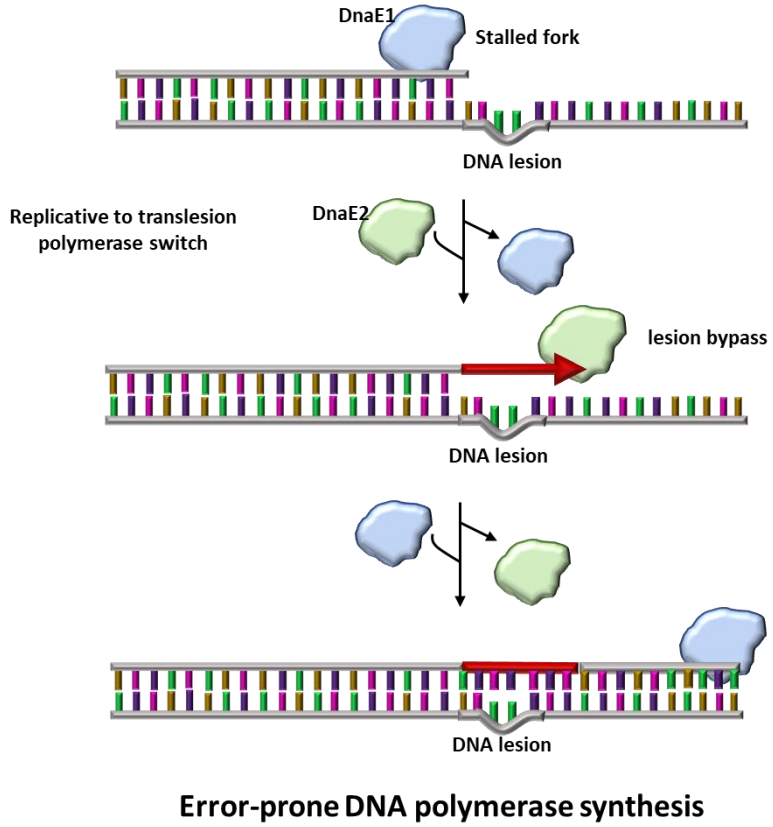

Figure 1.3: Bacterial Translesion Synthesis Model. When the replicative polymerase, DnaE1, encounters a bulky DNA lesion, replication is stalled. Current models hold that DnaE1 is replaced by the translesion polymerase, DnaE2, which is capable of replicating across the site of DNA damage. TLS DNA polymerases such as DnaE2 can be highly error prone.

1.6.2.2. The *imuA-imuB-dnaE2* cassette

Many bacteria, including mycobacteria, lack PolV and instead encode an SOS-regulated *imuA-imuB-dnaE2* gene cassette (Jatsenko et al., 2017, Timinskas and Venclovas, 2019). The cassette is composed of ImuA, a protein of unknown function which shares some homology to RecA; ImuB, a catalytically inactive Y-family polymerase homolog; and DnaE2 (also referred to as ImuC), an error-prone TLS polymerase (Abella et al., 2004, Erill et al., 2006, Galhardo et al., 2005, Warner et al., 2010). In these bacteria, the different components of the cassette were first discovered as *sulA*, *dinP* and *dnaE*, and were later renamed as *imuA*, *imuB* and *imuC*, respectively (Abella et al., 2004, Abella et al., 2007, Koorits et al., 2007). The designations, ImuA and ImuB, derive from *inducible mutagenesis* and, owing to their inter-related function, it has been proposed that DnaE2 should be renamed as ImuC (McHenry, 2011a, McHenry, 2011b). The function of ImuA is unknown; so, too, ImuB which, although it shares homology with Y-family polymerases, lacks active site residues (Warner et al., 2010). ImuB contains

structural features common to members of the Y-family DNA polymerases including a β-clamp binding motif to interact with the β-processivity clamp as well as an unstructured C-terminal domain (Koorits et al., 2007, Ippoliti et al., 2012, Warner et al., 2010). Both ImuA' and DnaE2 lack the consensus β-clamp binding motif which suggests that they depend on ImuB for access to the replication fork during TLS (**Fig. 1.4**) (Warner et al., 2010). *Mtb* ImuB was inferred from yeast two-hybrid assays to interact with the replicative subunit, DnaE1, as well as ImuA', DnaE2 and itself (Warner et al., 2010). The conserved nature of the β-binding motif in ImuB homologs suggests that it may facilitate replicative polymerase to TLS polymerase switching during DNA damage (Fuchs and Fujii, 2013, Goodman and Woodgate, 2013, Ippoliti et al., 2012).

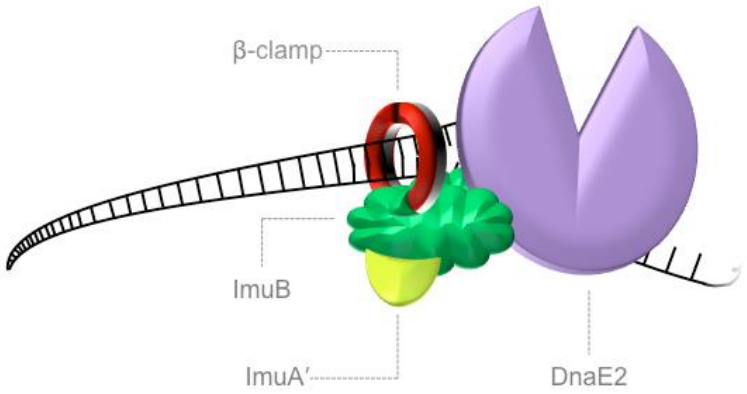

Figure 1.4: Proposed model for the mycobacterial mutasome. The β-clamp (red) binds to the accessory protein ImuB (green) which allows for the recruitment to the replication fork of other accessory protein, ImuA' (yellow) and the error-prone TLS polymerase DnaE2 (purple). (Adapted from Warner et al., 2010).

The precise arrangement of the *imuA-imuB-imuC* cassette is diverse and variable across bacterial species; in some, it is found organised in a single operon whereas in others the genes are split across different loci or with some genes missing (Erill et al., 2006, Ippoliti et al., 2012). *Caulobacter crescentus* contains the full *imuA*, *imuB* and *dnaE2* mutagenic cassette that is responsible for MMC and UV induced mutagenesis (**Fig. 1.5**) (Galhardo et al., 2005, Jatsenko et al., 2017). In contrast, *Streptomyces coelicolor* carries only *imuB* and *imuC* (**Fig. 1.5**) (Jatsenko et al., 2017, Tsai et al., 2012). In *Pseudomonas putida*, the *imuA-imuB-imuC* genes are regulated by a second copy of *lexA*, *lexA2* in a form of a single transcriptional unit (**Fig. 1.5**) (Abella et al., 2004, Jatsenko et al., 2017). Like *P. putida*, the *imuA*, *imuB* and *imuC* cassette of *P. aeruginosa* is regulated by a second LexA as a single operon (Abella et al., 2004, Jatsenko et al., 2017). In contrast, *Myxococcus xanthus imuA* and *imuB* are found in a single operon while DnaE2 is located 6.57kb downstream (**Fig. 1.5**) (Sheng et al., 2020).

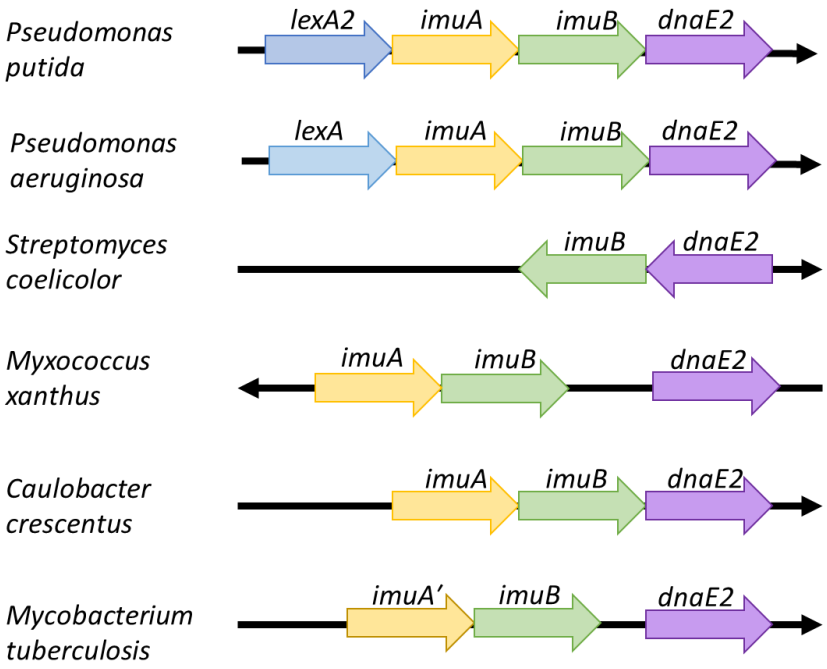

Figure 1.5: Bacterial mutagenesis cassette. Components of the mutagenic cassette in different bacteria. In *P. putida*, lexA2, imuA, imuB and dnaE2 are found together as one operon. In *P. aeruginosa*, lexA instead of lexA2, imuA, imuB and dnaE2 are found together in one operon. *S. coelicolor* is composed of only imuB and dnaE2. *M. xanthus* is consisted of imuA and imuB in one operon and dnaE2 is located 6.57kb downstream. *C. crescentus* have imuA, ImuB and dnaE2 as one operon. *Mtb* imuA' (Rv3395c) and imuB (Rv3394c) are found in one operon and dnaE2 (Rv3370c) is located ~24.7kb upstream.

In mycobacteria, induced mutagenesis is facilitated by ImuA′, ImuB and DnaE2, collectively referred to as the mycobacterial "mutasome" (**Fig. 1.4, 1.5**) (Warner et al., 2010). ImuA' and ImuB are accessory proteins, both of which play essential roles in DnaE2-mediated DNA damage induced mutagenesis and damage tolerance (Warner et al., 2010). Both *imuA'* and *imuB* are found in a two-gene operon which is located upstream of *dnaE2*, forming a split mutagenic *imuA'-imuB/dnaE2* cassette (**Fig. 1.5**). All three genes are regulated by LexA and are induced as part of the SOS response (Boshoff et al., 2003, Davis et al., 2002, Müller et al., 2018, Rand et al., 2003, Warner et al., 2010). Deleting any one of the three components disrupts function of the whole cassette, suggesting that all three components are part of the same pathway (Warner et al., 2010). This is similar but not identical to what was observed in *M. xanthus*, in which deletion of either *imuB* or *dnaE2*, but not deletion of *imuA*, resulted in reduced mutation frequency following exposure to UV-irradiation (Sheng et al., 2020). Deleting any of the genes in the *C. crescentus* cassette results in a mild increase in sensitivity to UV while double deletion

of both *imuB* and *dnaE2* doesn't affect the sensitivity further, suggesting that these proteins function in a single pathway (Da Rocha et al., 2008, Galhardo et al., 2005). In mycobacteria, DnaE2 polymerase was shown to be the error-prone TLS polymerase and responsible for DNA-damage induced mutagenesis (Boshoff et al., 2003, Warner et al., 2010). This is in contrast to *S. coelicolor* where DnaE2 was shown not to be required for UV mutagenesis (Jatsenko et al., 2017, Tsai et al., 2012) and *P. putida* where DnaE2 acted as an anti-mutator when exposed to UV (Galhardo et al., 2005, Jatsenko et al., 2017, Koorits et al., 2007, Sanders et al., 2006). It seems, therefore, that the cassette components, while conserved across many different species, have evolved functions specific to each species.

1.6.2.3. ImuA and Mycobacterial ImuA'

In general, bacterial ImuA proteins shows some degree of homology to *lexA*, *recA* and *sulA* (Erill et al., 2006, Galhardo et al., 2005, Ippoliti et al., 2012). In contrast, mycobacterial ImuA′, encoded by Rv3395c and MSMEG_1620 in *Mtb* and *Msm* respectively, shares very limited homology with the *imuA* found in *C. crescentus*, and was therefore denoted as *imuA′* (Galhardo et al., 2005, Ippoliti et al., 2012). Like ImuA, the precise function of the mycobacterial ImuA′ is still unknown. Recent work suggests that in *M. xanthus*, ImuA may play dual roles in DnaE2 mediated TLS, interacting with ImuB to facilitate DnaE2 assembly and inhibiting RecA nucleoprotein filament extension by interacting with RecA, thereby preventing homologous recombination (Sheng et al., 2020). Mycobacterial ImuA′ is distantly related to RecA, although it lacks a RecA equivalent C-terminus region responsible for binding ssDNA, conserved ATPase core domain and the ability to self-associate (Timinskas and Venclovas, 2019, Warner et al., 2010). Furthermore, in contrast to RecA, the DNA binding loops of ImuA' differ: L1 is almost absent and L2 is shorter. Instead, ImuA' consists of an N-terminal domain with putative DNA-binding capacity, as well as an interaction site with ImuB. Despite these differences, ImuA′ may play an analogous role to RecA, activating the TLS polymerase, DnaE2, as RecA does for PolV in *E. coli* (Timinskas and Venclovas, 2019). On the other hand, since ImuA′ was not seen to directly interact with DnaE2 (Warner et al., 2010), its role in DnaE2-catalysed TLS may not resemble that of RecA in PolV system (Sheng et al., 2020). Additionally, this suggests that ImuA may have evolved from RecA, losing sites required for homologous recombination and not those needed in TLS (Timinskas and Venclovas, 2019). Here, it is notable that, in bacteria that don't encode ImuA and only encode ImuB and DnaE2, ImuA function may be

substituted by RecA (Timinskas and Venclovas, 2019). Understanding the function and activity of ImuA′ is crucial in exploring the mutasome as a potential drug target for novel "anti-evolution" drugs which might eliminating the capacity of the bacillus to evade genotoxic stress through mutation (Gessner, 2017, Reiche et al., 2017).

1.6.2.4. RecA

RecA plays multiple critical roles in DNA metabolism. In *E. coli*, RecA is responsible for homologous recombination, DNA repair and induction of the DNA damage inducible SOS response (Del Val et al., 2019, Lusetti and Cox, 2002, McGrew and Knight, 2003, Walker, 1996). It is essential for error-free DNA strand exchange repair by mediating recombinational DNA repair at sites of single-stranded gaps, double-strand breaks, and failed replisomes (Lusetti and Cox, 2002, Patel et al., 2010). In addition, it mediates induction of the SOS response by facilitating autocatalytic cleavage of LexA (Goodman et al., 2016, Jaszczur et al., 2016). In mycobacteria, *recA* is expressed from two different DNA damage-inducible promoters, RecAP1, which is RecA/LexA independent (Davis et al., 2002, Manina et al., 2019) and RecAP2, which is recognised and repressed by LexA (**Fig. 1.6**). Initially, RecAP1 was thought to be regulated by ClpR which recognizes the promoter region and whose deletion impairs the induction levels of repair genes including *recA* (Gopaul et al., 2003, Manina et al., 2019, Wang et al., 2011). However, more recent work suggests that RecAP1 is regulated by proteosome accessory factors B and C (PafBC) as part of the RecA-NDp regulon (Müller et al., 2018).

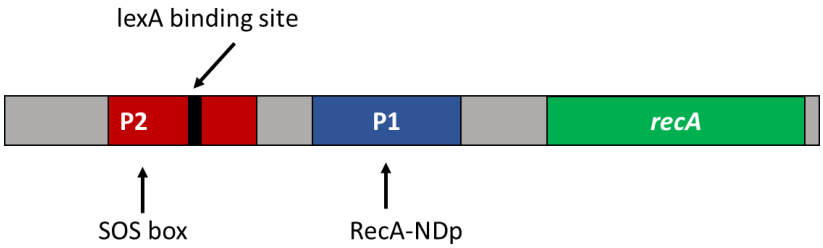

Figure 1.6: Mycobacterial *recA* promoters. The mycobacterial recA gene is unusual in that it is expressed from two promoters which are DNA damage inducible but by different mechanisms. The promoter proximal to the recA coding sequence was termed P1, while the other was termed P2. P1, is DNA damage inducible independently of LexA and RecA, whereas P2 is regulated by LexA.

In *E. coli*, in addition to regulating the SOS response, RecA facilitates autocatalytic cleavage of UmuD in generating PolV, and it binds PolV to activate TLS and SOS mutagenesis (Goodman, 2002, Jaszczur et al., 2019, Patel et al., 2010, Rangarajan et al., 2002). For RecA to function in all these processes, it must assemble on a ssDNA to form an active nucleoprotein filament (Story et al., 1992, Alekseev et al., 2020). The active nucleoprotein filament is a helical complex of RecA monomers wrapped around ssDNA (Bianco and Kowalczykowski, 2005). Similar to *E. coli*, mycobacterial RecA is a monomer with three domains; N-terminal domain, C-terminal domain, and M domain **(Fig. 1.7)** (Chandran et al., 2018, Datta et al., 2000, Datta et al., 2003b, Prabu et al., 2008). The C-terminal domain plays an important role in binding ssDNA during repair, recombination, and genome maintenance **(Fig. 1.7)** (Cox, 2007, Datta et al., 2003b, Prabu et al., 2008). The N-terminal domain is the smallest domain and is composed of an α helix and coil contributing to RecA self-association and filamentation **(Fig. 1.7)** (Cox, 2007, Prabu et al., 2008, Story et al., 1992). Lastly, the M domain consists of DNA binding loops 1 (L1) and 2 (L2), as well as nucleotide binding P-loop with the nucleotide triphosphate hydrolase fold and LexA binding loop (LAL) **(Fig. 1.7)** (Datta et al., 2003a, Prabu et al., 2008). *Mtb* RecA is composed of a single open reading frame interrupted by protein intein coding sequence that is excised by an unusual protein-splicing reaction (Davis et al., 1992). In contrast, *Msm* RecA is continuous and not interrupted by protein introns or intein (Davis et al., 1994, Frischkorn et al., 1998).

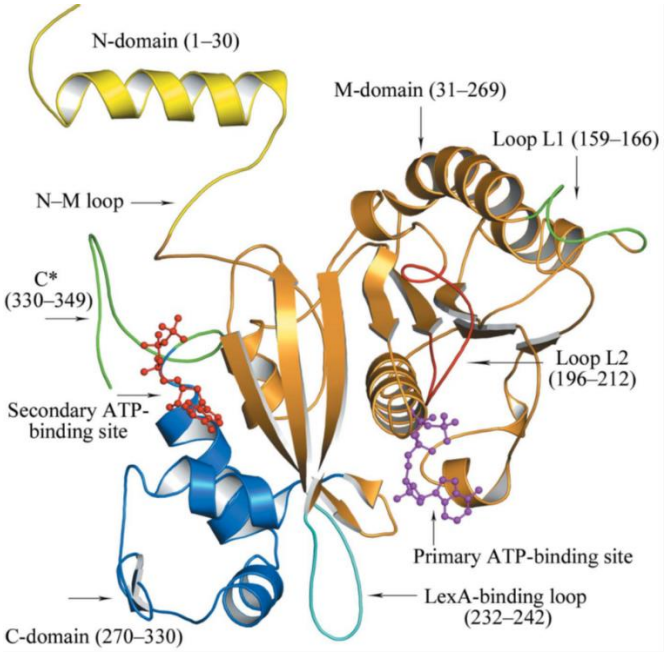

Figure 1.7: *Msm* RecA structure. Mycobacterial RecA is composed of N-terminal domain (yellow), M domain (orange), and C-terminal domain (blue). It is also consisted of DNA

binding loops, L1 (green) and L2 (red) as well nucleotide binding P-loop with the nucleotide triphosphate hydrolase fold (purple and red) and LexA-binding loop (blue). (Adapted from Prabu et al., 2008).

Studies in other organisms have used fluorescently labelled RecA to elucidate its function. For example, fluorescently tagged RecA has been used to monitor RecA location within cells and to investigate localization of recombinational processes in live *E. coli* (Renzette et al., 2005). It has also been used to investigate the roles of RecA bundles in facilitating DSB repair (Lesterlin et al., 2014). Additionally, repair of replication-dependent DSBs in *E. coli* involves localisation of RecA foci in the central region where DNA replication occurs (Amarh et al., 2018). Previously it has been shown that visualizing RecA-GFP in *E. coli* indicates the formation of foci following DNA damage by genotoxic agents (Lesterlin et al., 2014, Renzette et al., 2005, Simmons et al., 2007). Under normal conditions, RecA is concealed in storage structures and, following exposure of *E. coli* to UV, the storage structures dissolve and cytosolic RecA nucleates on DNA to form early SOS signalling complexes that later form RecA bundles. Upon completion of repair, RecA storage structures form again (Ghodke et al., 2019). However, very little is known about the localization of RecA protein in mycobacteria. A previous study showed that, following DNA damage, RecA associates with the membrane and cardiolipin can impair the LexA co-protease function of RecA without impairing its ATPase or strand-exchange activities. However, this was not visible using fluorescently labelled RecA (Wipperman et al., 2018). A more recent study of RecA localization in mycobacteria has shown that the protein is distributed unevenly throughout the cell but becomes more uniform following exposure to DNA-damaging agents (Manina et al., 2019).

1.6.2.5. Targeting the SOS response regulon as drug target

RecA plays a central role in DNA repair, the SOS response, antibiotic-induced mutagenesis, and drug resistance acquisition, suggesting that inhibiting its activity is crucial for managing the evolution of drug resistance (Pavlopoulou, 2018). Therefore, understanding the functions of RecA in response to DNA damage is important, especially given its potential as new TB drug target (Manina et al., 2019, Nautiyal et al., 2014, Prasad et al., 2019, Wipperman et al., 2018). Since RecA function is activated upon binding to ssDNA to form an activated RecA nucleoprotein filament (Goodman et al., 2016, Jaszczur et al., 2016, Little et al., 1981), inhibiting this ability could interfere with DNA repair, blocking the activation of SOS response and reducing acquisition of antibiotic resistance (Alam et al., 2016, Ojha and Patil, 2019).

Studies in *E. coli* have shown that inactivating the SOS regulon by either engineering an uncleavable LexA or deleting *recA* inhibit SOS response initiation, rendering cells hypersensitive to drug treatment and resulting in decreased mutation rates (Cirz et al., 2005, Culyba et al., 2015). In addition to directly reducing the expression of the mutagenic SOS response, inhibiting the DNA repair functions of RecA can be crucial during antibiotic exposure and enhance the activity of bactericidal antibiotics (Alam et al., 2016). Therefore, RecA inhibitors can be used as adjuvants to existing therapeutic agents, potentially enhancing their activity (Ojha and Patil, 2019). In *Mtb*, the RecA inhibitor Sumarin has been shown to inhibit recombinational and co-protease activity of RecA and to suppress antibiotic-induced RecA expression (Nautiyal et al., 2014). By analogy, deleting the TLS polymerase, DnaE2, results in decreased *Mtb* virulence in mouse infection and reduced acquisition of rifampicin resistance (Boshoff et al., 2003). The findings in these studies suggest a potential antimicrobial therapeutic benefit in targeting the regulators and effectors of the SOS response (Culyba et al., 2015).

1.7. Rationale for this work

The emergence of antibiotic resistant strains threatens global efforts to eradicate TB. As a result, there is increasing interest in the development of ancillary therapies aimed at curbing the capacity of *Mtb* for adaptive mutagenesis. Among many possible strategies, crippling molecular mechanisms involved in DNA replication and repair represents a compelling approach (Minias et al., 2019, Ojha and Patil, 2019). However, the pathways involved in the maintenance of genome integrity remain poorly understood. *Mtb* can respond to DNA damage by repairing its DNA while inducing mutations that enable it to survive. SOS response activation results in the emergence of mutations and acquisition of drug resistance (Galhardo et al., 2009, Ojha and Patil, 2019). Understanding the regulation of these factors and elucidating the molecular interactions which determine whether DNA repair is error-free or error-prone is central to the development of antimicrobial therapeutic intervention which might eliminate the capacity of the bacillus to evade lethal stress by acquiring mutations. RecA and ImuA′ are DNA damage-inducible proteins that have been shown to be involved damage tolerance and mutagenesis. RecA plays a central role in regulating the SOS response (Maslowska et al., 2019) and ImuA′ forms part of the mycobacterial mutasome which has been shown to upregulate mutation rates in stressed cells (Warner et al., 2010). ImuA’ has also been shown to partially resemble the structure of RecA (Warner et al., 2010). It is interesting, therefore, that ImuA′

shows weak homology to RecA which, together with PolV, forms the mutasome in *E. coli*. However, *E. coli* lacks ImuA and since mycobacteria encode both ImuA′ and RecA proteins, the question of how these two proteins function together in the same cell becomes salient.

Fluorescence microscopy has been utilized to visualize protein localization in both prokaryote and eukaryote cells (Spring and Davidson). In this approach, proteins of interest are fused with fluorescent tags which allow for expression and enable visualization of target proteins in cells (Lodish, 1995). Fluorescent proteins allow for movements and interactions of proteins to be monitored through imaging in real-time (Shashkova and Leake). Live fluorescence microscopy to study the expression and localization patterns of ImuA′ and RecA can be valuable in adding important molecular insights into the functions of proteins whose precise mechanistic roles remain unknown, largely because previous studies have tended to utilize genetic approaches without applying imaging tools to elucidate recruitment and localization in real-time. By understanding the endogenous roles of these proteins, how they relate and are similar, we could potentially increase putative drug targets as well as block the evolution and acquisition of adaptive mutations.

.

2. Aims and Objectives.

The weak homology of mycobacterial ImuA′ to RecA, combined with genetic evidence implicating ImuA’ in the DnaE2-dependent mycobacterial mutasome, suggests that the competitive or co-ordinated interaction of ImuA’ and RecA might be critical to the regulation and function of DNA damage repair.

2.1. Aim.

The aim of this study was to visualize the expression and subcellular localizations of fluorescently labelled RecA and ImuA’ proteins in *M. smegmatis (Msm)* towards understanding how these proteins behave in the same cell.

2.2. Objectives.

- Design and construct recombinant reporter alleles, *mScarlet-imuA′* and *recA-msfGFP*.
- Generate *Msm* reporter strains in which the reporter alleles are expressed in Δ*imuA′* and Δ*recA* backgrounds.
- Evaluate the functionality of the fluorescently-tagged fusion proteins using DNA damage sensitivity and UV mutagenesis assays.
- Visualize the expression and localization patterns of fluorescent proteins in live bacterial cells using fluorescence microscopy.

3. Methods and materials

All DNA manipulations and culturing were carried out using standard protocols (Parish and Stoker, 1998, Sambrook et al., 1989, Sambrook and Russell, 2001). Enzymes and chemicals were supplied by Thermo Fischer Scientific, New England Bio-Labs, Sigma-Aldrich, Qiagen, Bio-Rad, Fermentas, and Roche. Details of growth media and general solutions used in this study are provided in **Appendix I**.

3.1. Bacterial strains and culture conditions.

E. coli strains were grown in Luria-Bertani (LB) liquid or on solid media (LA) supplemented with the appropriate selection antibiotic and incubated at 37ºC. Bacterial strains generated and/or used in this study are listed in **Table 1**. *Msm* mc^2155 and all its derivative mutants were grown in Middlebrook 7H9 liquid medium (Difco) supplemented with 0.2% glycerol, 0.05% Tween-80 and 10% Oleic Acid Dextrose Catalase (OADC) enrichment (Difco) or on solid 7H10 medium (Difco) supplemented with 0.5% glycerol and 10% OADC. Media were supplemented with the appropriate antibiotics when required.

Table 1: Strains used in this study.

Strain name	**description**	**source**
***Escherichia coli* DH5α**	*supE44 ΔlacU169 (F80 lacZΔM15) hsdR17 recA1 endA1 gyrA96 thi-1 relA1*	Promega
***M. smegmatis* mc^2155 (WT)**	high frequency transformation mutant of *Msm* ATCC 706	Snapper et al., 1990
Δ*imuA′*	*imuA′* (MSMEG_1620) knockout of mc^2155	Warner et al., 2010
Δ*recA*	*recA* (MSMEG_2723) knockout of mc^2155	Machowski et al., 2007
Δ*imuA′*::T*mScarlet-imuA′*	Δ*imuA′* carrying pTT1B::*mScarlet-imuA′* at the *attB* integration site; Gen^R	This study
Δ*imuA′*::P*mScarlet-imuA′*	Δ*imuA′* carrying pMCpAINT::*mScarlet-imuA′* at the *attB* integration site; Kan^R	This study

WT::T*mScarlet-imuA′*	*Msm* mc^{2}155 carrying pTT1B::*mScarlet-imuA′* at the *attB* integration site; Gen^R	This study
WT::P*mScarlet-imuA′*	*Msm* mc^{2}155 carrying pMCpAINT::*mScarlet-imuA′* at the *attB* integration site; Kan^R	This study
Δ*recA*::T*recA-msfGFP*	Δ*recA* carrying pTT1B::*recA-msfGFP* at the *attB* integration site; Gen^R	This study
Δ*recA*::P*recA-msfGFP*	Δ*recA* carrying pMCpAINT::*recA-msfGFP* at the *attB* integration site; Kan^R	This study
WT::T*recA-msfGFP*	*Msm* mc^{2}155 carrying pTT1B::*recA-msfGFP* at the *attB* integration site; Gen^R	This study
WT::P*recA-msfGFP*	*Msm* mc^{2}155 carrying pMCpAINT::*recA-msfGFP* at the *attB* integration site; Kan^R	This study
Δ*imuA′*-T*mScarlet-imuA′* ::P*recA-msfGFP*	Δ*imuA′* carrying pTT1B::*mScarlet-imuA′* and pMCpAINT::*recA-msfGFP* at *attB* integration sites; Gen^R Kan^R	This study
Δ*recA*::P*recA-msfGFP* ::T*mScarlet-imuA′*	Δ*recA* carrying pMCpAINT::*recA-msfGFP* and pTT1B::*mScarlet-imuA′* at *attB* integration sites; Kan^R Gen^R	This study

Table 2: Plasmids used in this study.

Plasmid name	**description**	**source**
pUC57::*mScarlet-imuA'*	Cloning vector pUC57 containing 5′- region of designed mScarlet-FLAG tag-ImuA ′ -3 ′ construct; Kan^R	Genewiz. USA
pUC57::*recA-msfGFP*	Cloning vector pUC57 containing 5 ′ region of designed RecA-FLAG tag-msfGFP-3 ′ construct; Kan^R	Genewiz. USA
pMCpAINT	Integrating vector; Kan^R	Warner et al., 2010
pMCpAINT::*mScarlet-imuA'*	Resulting *Eco*RI ligation product of	This study

	pMCpAINT and pUC57::mScarlet-ImuA ′; Kan^R	
pMCpAINT::*recA-msfGFP*	Resulting *Eco*RI ligation product of pMCpAINT and pUC57::RecA-msfGFP; Kan^R	This study
pTT1B (pTT1B)	Integrating vector; Gen^R	Pham et al., 2007
pTT1B::*mScarlet-imuA'*	Resulting *Eco*RI ligation product of pTT1B and pUC57::mScarlet-ImuA ′; Gen^R	This study
pTT1B::*recA-msfGFP*	Resulting *Eco*RI ligation product of pTT1B and pUC57::RecA-msfGFP; Gen^R	This study

3.2. Bacterial selection

E. coli and *Msm* strains were grown on media supplemented with antibiotics at the following concentrations.

Table 3. Antibiotic working concentrations.

Antibiotic	*E. coli*	*M. smegmatis*
1. Kanamycin	50 µg/ml	25 µg/ml
2. Gentamycin	20 µg/ml	5 µg/ml
3. Mitomycin C	N/A	0.2 µg/ml

Primers that flank the beginning and end of mScarlet-ImuA′ and RecA-msfGFP constructs were designed for PCR screening and DNA sequencing.

Table 4. Primers used in this study.

Primer name	Direction	Sequence 5' → 3'	Description
PAINTSCREEN F2	Forward	CCACCTCTGACTTGAGCGT	pMCpAINT plasmid screen
PAINTSCREEN R2	Reverse	GACTCTTCTGACCTGGGCA	pMCpAINT plasmid screen
ImuA R2	Reverse	GTGAGGACACCCAGACCAT	mScarlet-ImuA' construct screen

mScarlet F1	Forward	GCGAGGCAGTGATCAAGGA	mScarlet-ImuA' construct screen
mScarlet R1	Reverse	GGCGCAGGGCCATCTTAAT	mScarlet-ImuA' construct screen
ImuA' F1	Forward	CGCAAGATGGCCTCGGTAT	mScarlet-ImuA' construct screen
ImuA R1	Reverse	CCAGCAGGGTGCAACCTTT	mScarlet-ImuA' construct screen
ImuA F2	Forward	CCCGGTATTTCGGATCCGA	mScarlet-ImuA' construct screen
PTT1BCREEN F1	Forward	CTGGCAAGTGTAGCGGTCA	pTT1B plasmid screen
PTT1BSCREEN R2	Reverse	GCGGGTGTGGATGAGCAAA	pTT1B plasmid screen
RECA R2	Reverse	GCTTCGACCTGATCACCGA	RecA-msfGFP construct screen
RECA F1	Forward	GCTCCATCTCGCTGGATGT	RecA-msfGFP construct screen
RECA R1	Reverse	GAGCCGAACATCACACCGA	RecA-msfGFP construct screen
MSFGFP F1	Forward	GCGACGTAAACGGCCACAA	RecA-msfGFP construct screen
MSFGFP R1	Reverse	CGACGTTGTGGCGGATCTT	RecA-msfGFP construct screen
RECA F2	Forward	CTCAACGCCGGAAAAGGCA	RecA-msfGFP construct screen
P2NILSCREEN F5	Forward	CACTCGTGCACCCAACTGA	RecA-KO construct screen

3.3. DNA extractions and purification

3.3.1. Small scale *E. coli* DNA extractions

Small-scale DNA extractions in *E. coli* were performed using the Zyppy™ plasmid miniprep kit (Zymo Research) as per manufacturer's instructions. Briefly, 600 µl of bacterial culture was added to a 1.5 ml microcentrifuge tube. 100 µl of 7X Lysis Buffer (Blue) was added to the culture and mixed by inverting the tubes 6 times and incubated at room temperature for 2 min. 350 µl of cold Neutralization Buffer (Yellow) was added and mixed thoroughly by inverting the samples an additional 2-3 times to ensure complete neutralization. The tubes were centrifuged at 11,000 × *g* for 4 minutes. The supernatant was transferred into the provided Zymo-Spin™ IIN column placed on a collection tube and centrifuged for 15 seconds, while avoiding disturbing the cell debris pellet. 200 µl of Endo-Wash Buffer was added to the column and centrifuged for 30 seconds. 400 µl of Zyppy™ Wash Buffer was added to the column and centrifuged for 1 minute. The column was transferred into a clean 1.5 ml microcentrifuge tube and 20 µl of Zyppy™ Elution Buffer was added directly to the column matrix and let to stand for one minute at room temperature. The tubes were centrifuge for 30 seconds to elute the plasmid DNA. The DNA was quantified using NanoDrop ND-1000 Spectrophotometer (Thermo Scientific).

3.3.2. Large scale *E. coli* plasmid DNA extraction and purification

E. coli cultures were grown at 37^0C overnight. 100ml cultures were pelleted by centrifugation (4500 × *g*, 20ºC, 10 min). Following centrifugation, the supernatant was discarded, and the pellet was resuspended in 1 ml resuspension buffer (solution I) after which 2 ml lysis buffer (solution II) was added and inverted to mix. 1.5 ml of neutralizing buffer (Solution III) was immediately added. The suspension was aliquoted in 1.5 mL Eppendorf tubes and centrifuged (13 000 rpm, 10 min) at room temperature, followed by treatment with 10 µl RNaseA (10 µg/ml) for 30 min at 42ºC. 700 µl isopropanol was added to precipitate the plasmid DNA and incubated at room temperature for 10 min followed by centrifugation (13 000 rpm, 10 min). The pellet was resuspended in 100 µl dH_2O and 700 µl of phenol: chloroform and 50 µl 3M sodium acetate was added, vortexed until cloudy white followed by centrifugation (13 000 rpm, 10 min). The top layer supernatant was transferred to a new Eppendorf tube and 350 µl of 1:24 chloroform: isoamyl alcohol and centrifuged at 13 000 rpm, for 10 min. The top layer supernatant was transferred to new Eppendorf tube and 1 ml ice-cold 100% ethanol was added and allow to precipitate the plasmid DNA for an hour following by centrifugation at 13 000 rpm, for 10 min. The pelleted DNA was washed with 70% ice-cold ethanol by centrifugation (13 000 rpm, 10 min), dried in a speedvac and resuspended in 100 µl nuclease-free water. The

plasmid was run on 1% agarose gel and the concentration was also determined using the Nanodrop.

3.3.3. Small-scale chromosomal DNA extraction from Msm

Small-scale chromosomal DNA extraction was performed using quick DNA bacterial/fungal miniprep kit (Zymo Research) as per manufacturer's instructions. Briefly, 20 ml of bacterial cell cultures was centrifuged (4000 × *g*, 10 min) and resuspended in 500 µl of water and added into a ZR BashingBead™ Lysis Tube (0.1 mm & 0.5 mm). 750 µl of Bead Bashing buffer was also added to the tube. The tube was secured in a bead beater fitted with a 2 ml tube holder assembly and processed at maximum speed for 40 sec. The tubes were then centrifuged at (8 000 rpm, 30 sec). 400 µl of supernatant was transferred to a Zymo-Spin™ IV Spin Filter (Orange Top) in a collection tube and centrifuged (7,000 rpm,1 min). 1,200 µl of Genomic Lysis Buffer was added to the filtrate in the collection tube from the previous step. 800 µl of the mixture from previous step was transferred to a Zymo-Spin™ IIC Column in a collection tube and centrifuged at (10,000 rpm,1 min). 200 µl DNA Pre-Wash Buffer was added to the Zymo-Spin™ IIC Column in a new collection tube and centrifuge at (10,000 rpm, 1 min). 500 µl gDNA Wash Buffer was added to the Zymo-Spin™ IIC Column and centrifuge at (10,000 rpm, 1 min). The Zymo-Spin™ IIC Column was transferred to a clean 1.5 ml microcentrifuge tube and 50 µl DNA Elution Buffer was added directly to the column matrix and centrifuged at (10,000 rpm, 30 sec) to elute the DNA. The DNA was quantified using the NanoDrop ND-1000 Spectrophotometer (Thermo Scientific).

3.3.4. CTAB bulk DNA extraction and purification from Msm

For *Msm*, 20 ml cells were grown to log phase (OD_{600} ~ 0.6-0.8) and harvested by centrifugation (4500 × *g*, 4 ºC, 10 min). The pellet was resuspended in 1 ml ddH_2O and heat killed at 65 ^{0}C for 20 min. The cells were pelleted by centrifuged (13 000 rpm, 10 min*)* and resuspended in 500 µl fresh TE buffer (pH. 8.0). 50 µl lysozyme (10 mg/ml) and 10 µl RNase (10mg/ml) were added and the mixture was incubated overnight at 37^{0}C. The next day, 70 µl of 10% SDS and 10 µl proteinase K (10mg/ml) was added and incubated in the Thermomixer Compact (Eppendorf) at 65 ^{0}C for 1 hr with shaking at 400 rpm. 100 µl 10% cetyltrimethylammonium bromide (CTAB) and 100 µl 5M NaCl were added and incubated at 65 ^{0}C for 15 min with shaking at 400 rpm. 700 µl chloroform:isoamyl alcohol (24:1) was added, gently mixed and centrifuged (3 000 rpm, 10 min) to separate the cell debris from the aqueous

solution. The aqueous phase was recovered, and an equal volume of ice-cold isopropanol was added and incubated at -20^{0}C for 30 min. The DNA was recovered by centrifugation (13 000 rpm, 20 min). The pelleted DNA was washed with ice-cold 70% ethanol, dried in a vacuum centrifuge, and resuspended in 50 µl nuclease free water. The extracted DNA was run on a 1% gel to check for quality and quantified using the NanoDrop ND-1000 Spectrophotometer (Thermo Scientific).

3.3.5. Ethanol precipitation and purification of DNA

Before electroporation of plasmid DNA into Msm strains, the plasmids are purified. 20 µl of DNA was measured and added to a new Eppendorf tube. 20 µl of 3M sodium acetate was added to the DNA sample and mixed well. 40 µl of ice cold 100% ethanol was also added to the tube and mixed to combine. The mixture was placed on ice for 20 minutes to incubate. The DNA was harvested by centrifugation (14 000 rpm, 10 min). The pellet was washed with 70% ethanol and dried in speedvvac and resuspended in 20 µl.

3.4. DNA manipulations

3.4.1. Polymerase Chain Reaction (PCR)

PCR amplification of DNA fragments for cloning purposes were amplified using Q5 high fidelity polymerase (New England Bio-labs) and Phusion High-Fidelity polymerase (New England Bio-labs) due to their high-fidelity action. For PCR screening, FastStart Taq polymerase (Roche) was used. 25 µl PCR reactions were prepared according to the manufacturer's instructions and annealing temperatures were set according to the melting temperature of the primers. All PCR reactions were performed in the MyCycler™ thermal cycler (Bio-Rad). The PCR cycling conditions for each polymerase used are tabulated below.

Table 5: Thermocycling conditions for Phusion PCR

Step	Temperature (ºC)	Time	Cycles
Initial denaturation	98 ºC	10 sec	1
Denaturation Annealing Elongation	98 ºC 55 ºC 55 ºC - 70 ºC	10 sec 10 sec 30 sec – 2 min	35
Final elongation	72 ºC	5 min	1

Hold	4ºC	∞	hold

Table 6: Thermocycling conditions for Q5 high fidelity PCR

Step	Temperature	Time	Cycles
Initial denaturation	98ºC	10 sec	1
Denaturation Annealing Elongation	98 ºC 55 ºC 55 ºC - 65 ºC	10 sec 30 sec 1 min – 2.30 min	35
Final elongation	72ºC	5 min	1
Hold	4ºC	∞	hold

Table 7: Thermocycling conditions for Fast-start PCR

Step	Temperature	Time	Cycles
Initial denaturation	95ºC	3 min	1
Denaturation Annealing Elongation	98ºC 55ºC 55ºC - 65ºC	30 sec 30 sec 30 sec - 2 min	35
Final extension	72ºC	5 min	1
Hold	4ºC	∞	hold

3.4.2. Agarose gel electrophoresis

DNA molecular weight fragments were separated on 1% agarose gel dissolved in 1xTAE buffer. DNA samples were loaded with loading dye. Fragment sizes were assessed using DNA molecular weight markers (IV and VI; Roche Applied Science, Germany). Gels were electrophoresed in a Mini-Sub Cell GT mini gel horizontal submarine unit (Bio-Rad) at 100 volts and visualized under UV-light using the Gel Doc (WealTech Keta Imaging System).

3.4.3. Gel and PCR purification

After gel electrophoresis, DNA fragments of the expected size were cut from the agarose gel using a sterile scalpel blade. The bands were gel-extracted using the Nucleospin Extract II Kit (Macherey-Nagel) according to the manufacturer's instructions. For PCR reactions, the

amplicons were also cleaned using the Nucleospin Extract II Kit (Macherey-Nagel) according to the manufacturer's instructions. The DNA was quantified using NanoDrop ND-1000 Spectrophotometer (Thermo Scientific).

DNA fragment was excised from the agarose gel slice. The DNA fragment was then weighed and transferred to a clean Eppendorf tube. 2x the volume NTI buffer was added to the size of the agarose gel (for each 100 mg agarose gel, add 200 µl NTI buffer). For PCR, 2 volumes of NTI buffer were added to 1 volume of PCR sample (200 µl of NTI buffer in 100 µl of PCR sample). The sample was incubated for 5-10 min or until it dissolves at 50 °C, while vortexing every 3 min. A NucleoSpin® Gel and PCR clean-up column was placed into a collection tube and 700 µl of the sample was loaded followed by centrifugation for 30s at 11 000 *x* g. The flow-through was discarded and the process was repeated with the remaining sample. 700 µl NT3 buffer was added to the NucleoSpin® Gel and PCR clean-up column and centrifuged for 30s at 11 000 × g and the flow-through was discarded. This step was repeated twice. To completely remove the NT3 buffer, the column was centrifuge for 1 min at 11 000 *x* g and the flow-through was discarded. To elute DNA, the column was moved to a new Eppendorf tube and 30 µl of NE buffer was added and left to incubate at room temperature for 1 min. The tube was then centrifuged for 1 min at 11 000 × g and the NucleoSpin® Gel and PCR clean-up column was discarded.

3.4.4. Restriction digestion

Restriction digests were performed at the manufacturer recommended temperature for each respective enzyme (New England Biolabs). Plasmid DNA was digested from 1 hr to overnight in an appropriate buffer (New England Biolabs). Digested fragments were run on a gel and visualized using the gel doc as previously described. Digested plasmid DNA was run on the gel and purified using the Nucleospin Extract II Kit as previously described.

3.4.5. Plasmid DNA dephosphorylation

Digested linearized plasmid vectors for cloning were treated with Antarctic Alkaline Phosphatase (New England Biolabs Inc) for 1 hr at 37ºC followed by heat inactivation for 20 min at 65ºC to remove the 5′ phosphate group and minimize vector re-ligation. Dephosphorylated plasmid DNA was purified using the Nucleospin Extract II Kit according to the manufacturer's instructions.

3.4.6. Ligation reactions

The Quick ligase (New England Biolabs Inc) was used for ligation reactions. Briefly, 50 ng dephosphorylated plasmid DNA and insert were added together in different plasmid:insert ratios (1;1, 1:3 and 1:5). 1 µl buffer, 1 µl quick ligase and water was added to each ligation reaction. Ligations were performed at 25°C for 15 min in the MyCycler thermal cycler (Bio-Rad).

3.5. Transformation reactions

3.5.1. *E. coli* DH5α competent cells preparation and transformation

E. coli DH5α overnight cultures were resuspended in fresh 100ml LB and grown to OD_{600} 0.6-0.8 at 37 ºC. The cultures were transferred to 50 ml falcon tubes and incubated on ice for 15 min followed by centrifugation (4500 × *g*, 4 ºC, 5 min). Following centrifugation, the supernatant was discarded, and the pellet was resuspended in 20 ml transformation buffer I (TFBI) and incubated on ice for 15 min. The pellet was collected by centrifugation at 3000 × *g* for 5 min and resuspended in 2 ml transformation buffer II (TFBII). The cells were kept on ice for 15 min for immediate use or 0.5 ml aliquots was added to 1.5 ml Eppendorf tubes and stored at 70 ºC for future use.

Stored chemical competent cells were thawed on ice and 100 µl of cells were added to the ligation reactions as previously described and incubated on ice for 20 min. The cells were heat-shocked at 42 °C for 90 sec, and immediately placed on ice for 2 min. 400 µl of 2 Tryptone Yeast (TY) broth media was added to rescue the cells. The cells were then incubated for 1 hr at 37 °C in a shaking incubator. Cells were harvested by centrifugation (11 000 rpm, 1 min) and pellet resuspended in fresh 1 ml 2TY media. The entire 100 ul was plated on LA plates supplemented with the appropriate antibiotic. The plates were incubated overnight at 37 °C and single colonies were picked and cultured in 2 ml LB for plasmid DNA extraction and screening by enzyme restriction. The transformants were also screened by PCR and the putative positive clones were further confirmed by sequencing.

3.5.2. Electroporation of *Msm*

100 ml wild-type *Msm* cells were cultured in 7H9/OADC media to log phase (OD600 of ~0.6 - 0.8) at 37 °C with shaking. Cells were harvested by centrifugation (4000 × *g*, 10 min, 4^0C)

and washed three times with 10 ml ice-cold 10% glycerol. The cells were harvested by centrifugation between each washing step. After washing, the cell pellet was resuspended in 2 ml ice-cold 10% glycerol. A minimum of 1 µg to 4 µg plasmid DNA was added to a pre-chilled 2 mm electroporation cuvette (0.2 cm electrode gap, Bio-Rad). 400 µl of electrocompetent *Msm* cells were added to the electroporation cuvettes containing the plasmid DNA and pulsed once in a GenePulser™ (Bio-Rad). The pulsing conditions were as follows; 2 500 V, 1000 Ω, and 25 µF. Cells were rescued immediately with 800 µl LB and then transferred to a fresh Eppendorf tube. The tubes were incubated at 37 °C for 4 hrs and the cells were plated on 7H10/OADC supplemented with the appropriate antibiotic. The plates were then incubated at 37 °C for 3-5 days.

3.6. DNA sequencing

All Sanger sequencing of constructs, plasmids or PCR products were performed by the Central Analytical Sequencing Facility (CAF) at the University of Stellenbosch using Sanger sequencing. Sequencing reads were visualized using Benchling software (https://benchling.com) and CLC DNA Workbench 7.5 software (http://www.clcbio.com/blog/clc genomics-workbench-7-5/).

3.7. Cloning of reporter constructs.

3.7.1. Cloning of *mScarlet-imuA'* and *recA-msfGFP* constructs.

Nucleotide sequences of the *Msm* mc^{2}155 *imuA'* (MSMEG_1620) and *recA* (MSMEG_2723) genes and promoter elements regions were obtained from the Mycobrowser database (https://mycobrowser.efpl.ch). For each construct, extra base pairs were added for upstream and downstream promoter elements of the gene. All constructs were synthesized commercially by Genewiz (Sigma, USA) in the pUC57 (Kan^R) background.

Cloning of the reporter constructs was done using added flacking *Eco*RI into two different integrating vectors, pMCpAINT and pTT1B, that integrates at different *attB* sites in the mycobacterial genome to allow introduction of both fusion proteins in the same background.

The pMCpAINT and pTT1B vectors were digested with *Eco*RI as detailed in **section 3.4.4**. pUC57::mScarlet-ImuA' and pUC57::RecA-msfGFP were also digested with *Eco*RI. The digested products were run on 1% agarose gel and the expected fragments were excised and

purified using the Gel purification kit as per user manual. The mScarlet-ImuA' and RecA-msfGFP fragments were each ligated to pMCpAINT and pTT1B vectors using the ligation procedure detailed in **section 3.4.6**. The ligation reactions were used to transform chemically competent *E. coli* DH5α as detailed in **section 3.5.1**. The transformants were plated on LA plates with appropriate antibiotic. Single colonies were randomly picked, cultured and plasmid DNA extracted as detailed in **section 3.3.2**. Putative positive clones were identified following PCR and restriction digest confirmation. Following this, putative positive constructs were sequenced as described in **section 3.7.1.** Positive mScarlet-ImuA′ and RecA-msfGFP clones were introduced into wild-type *Msm*, Δ*imuA′* and Δ*recA Msm* strains respectively by electroporation as detailed in **section 3.5.2** to allow integration at the *attB* site.

3.8. Microscopy.

Msm strains were grown to an OD_{600} ~ 0.4 in 7H9/OADC media at 37ºC with shaking. 5ml of the cells were treated with 1x MIC of MMC at 37ºC for 4-6 hrs. The cells were then harvested by centrifugation (4500 × *g*, 10 min) and washed 3× with PBS. After the last wash, the cells were resuspended in 100 µl of PBS. The filtered cells were spread on the microscope coverslip and allowed to air dry. The coverslips were then mounted on a microscope slide and cells imaged using a Zeiss Axio Observer fluorescent microscope Agarose pads were also prepared for microscopy imaging. Briefly, 0.15 g of agarose low melting powder (Sigma) was resuspended in 10 ml dH_2O and heated to melt. 100 µl of the gel was placed on microscope slides and allowed to dry. 2 µl of culture was added on each gel pad and allowed to air dry, before placing the coverslips. The cells were then imaged with Zeiss Axio Observer fluorescent microscope. The images were analysed using microbeJ plugin of ImageJ-Fiji (https://imagej.net/) (Ducret et al., 2016).

3.9. Statistical analysis.

Data were exported from microbeJ and analyses were performed using prism 7.04 (GraphPad software). Unpaired nonparametric T-test with Mann-Whitney test was used to compare multiple groups. A p value <0.05 was considered statistically significant.

3.10. DNA damage and UV mutagenesis assays

Different DNA damaging agents and treatments were used to test the functionality of the different reporter strains following introduction into *Msm*.

3.10.1. UV mutagenesis assays

50 ml cultures were grown to an OD_{600} of 0.6-0.8. 2 ml of each culture was used for UV-pre-exposure CFU/ml counts which were obtained by plating 100 µl of 10-fold dilutions for each strain (10^{-5}, 10^{-6}, 10^{-7}) onto 7H10/OADC and incubating the plates at 37°C for 4 days. The remaining cells in the 48 ml culture were harvested by centrifugation (3000 × *g*, 10 min). The pelleted cells were resuspended in 4 ml fresh 7H9/OADC liquid media and irradiated with 250×100µJ (UV Stratalinker 1800, Stratagene) in open petri dishes. The cells were rescued in a total volume of 48 ml 7H9/OADC for 3 h at 37°C after which 1 ml of each strain was plated on 7H10/OADC containing 200 µg/ml Rifampicin (Rif) to calculate Rifampicin resistant (Rif^R) frequencies. Plates were incubated at 37°C for 5-6 days (**Fig. 2.1**). As for before UV exposure, 10-fold dilutions were plated for CFU determination to study UV treatment survival, with plates incubated for 7 days at 37°C.

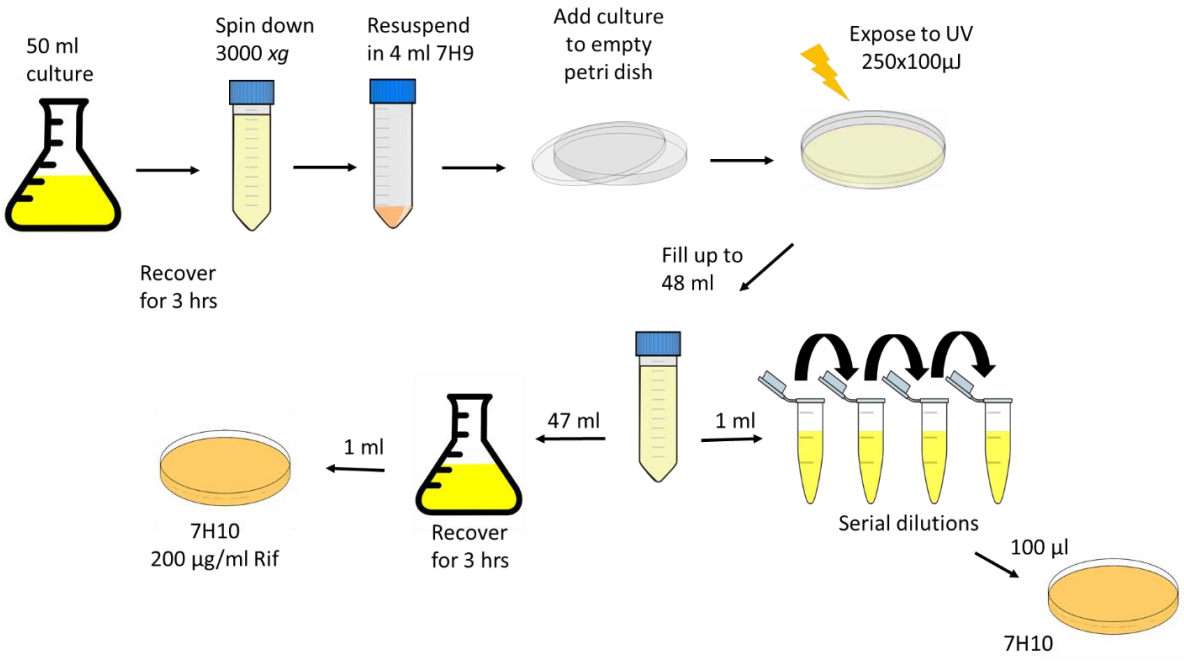

Figure 2.1: UV mutagenesis assay. Msm cultures were grown to an OD600~0.6-0.8, centrifuged and resuspended in fresh media. The cells were exposed to UV and allowed to recover before plating on Rifampicin-containing plates for enumeration of Rifampicin-resistant CFUs.

3.10.2. DNA damage assays

Cultures were grown to an OD_{600}~0.6-0.8 after which 5µl of 10-fold dilutions (10^{-1} to 10^{-7}) were spotted onto plain 7H10/OADC and 7H10/OADC supplemented with MMC at 0.02 µg/ml (0.1x MIC) and 0.04 µg/ml (0.2x MIC). Plates were incubated for 5-7 days at 37°C (**Fig. 2.2**).

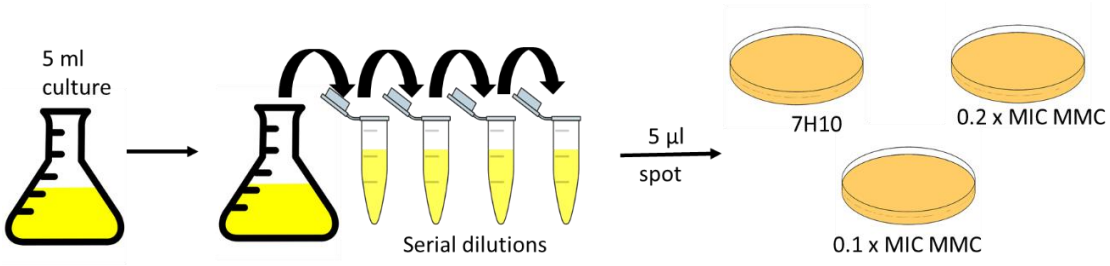

Figure 2.2: MMC sensitivity assay. Cultures were grown to an OD_{600}~0.6-0.8. Serial dilutions were performed and spotted on 7H10 only and MMC-supplemented solid 7H10 plates.

Cultures were spotted onto 7H10/OADC and 7H10/OADC supplemented with different types of DNA-damaging agents: namely, Moxifloxacin (Mox), Nitrofurazone (Nfz), Novobiocin (Nov), or Ofloxacin (Ofx). For UV irradiation, cultures were plated on 7H10 solid media only and exposed to UV. The plates were allowed to dry and incubate for 3-5 days at 37 °C.

Table 8: Antimicrobial agents' minimum inhibitory concentrations (MIC) in *Msm*.

Agent	MIC	Tested concentrations
1. Mitomycin C	0.2 µg/ml	0.02 µg/ml, 0.04 µg/ml
2. Moxifloxacin	0.125 µg/ml	0.0125 µg/ml, 0.025 µg/ml
3. Nitrofurazone	160 µg/ml	64 µg/ml, 80 µg/ml
4. Novobiocin	8 µg/ml	16 µg/ml, 32 µg/ml
5. Ofloxacin	0.67 µg/ml	0.201 µg/ml, 0.268 /ml

4. Results.

4.1. Design of constructs

4.1.1. Design and construction of fluorescent reporter alleles: *mScarlet-imuA′* and *recA-msfGFP*.

The *mScarlet-imuA′* and *recA-msfGFP* constructs were designed with the aim to generate fluorescence reporter proteins to investigate DNA damage-induced expression in live *Msm* cells. mScarlet was fused to the N-terminus of *imuA'* by cloning *imuA′* downstream of mScarlet and a flag tag was included between the fluorophore and the *imuA′* ORF for possible pull-downs of protein in the future **(Fig. 3.1)**. *Msm recA* was cloned upstream of msfGFP and the flag tag to generate a C-terminal fusion (Renzette et al., 2005) **(Fig. 3.3)**. For both constructs, 500 bp upstream and downstream sequence was utilized to ensure the native promoter elements including the SOS box as well as the transcription terminator elements were retained. *Eco*RI sites were introduced on either side of the flanking sequences to facilitate cloning into the integrating vectors, pMCpAINT and pTT1B **(Fig. 3.2, 3.4)**. When both pUC57::*mScarlet-imuA′* and pUC57::*recA-msfGFP* were digested with *Eco*RI, the plasmids resulted in fragment sizes that were too close to each other to separate visually. Therefore, *Dra*I, which cut the pUC57 backbone into two smaller bands (1367 bp and 1193 bp) was used in addition to *Eco*RI. Thus, to generate *mScarlet-imuA′* and *recA-msfGFP* constructs, pUC57::*mScarlet-imuA′* and pUC57::*recA-msfGFP* were digested with *Eco*RI and *Dra*I to yield inserts of 2434 bp and 2794 bp, respectively. At the same time, integrating vectors pMCpAINT and pTT1B were also digested with *Eco*RI to yield 3995 bp and 7983 bp backbones, respectively. After digestion, the plasmids were separated by agarose gel electrophoresis, and the fragments of interest excised from the gels. Vector fragments were dephosphorylated to prevent re-ligation. The insert fragments (mScarlet-ImuA′ and RecA-msfGFP) were then ligated into both pMCpAINT and pTT1B. The ligation products were transformed into *E. coli* DH5α competent cells and grown on LB agar with appropriate antibiotics (kanamycin and gentamycin for the pMCpAINT and pTT1B backbones, respectively) at 37°C overnight. No growth was observed on the vector-only control whereas colonies were observed on various ratios of insert:vector ligation plates indicating successful ligation. Random colonies were picked and resuspended in LB broth with the appropriate antibiotic, propagated overnight for plasmid extracted. Plasmid screening was done using restriction mapping as well as PCR. Both cloned products were confirmed with

multiple restriction enzymes. pMCpAINT::*mScarlet-imuA′* plasmids were confirmed with *Eco*RI, *Not*I, *Pvu*I, *Pvu*II and *Xho*I **(Fig. 3.5);** and pTT1B::*mScarlet-imuA'* plasmids were confirmed with *Bsa*AI, *Bst*BI, *Pvu*I, *Pvu*II and *Pst*I **(Fig. 3.6)**. Similarly, pMCpAINT::*recA-msfGFP* plasmids were confirmed with *Bam*HI, *Pvu*I, *Pvu*II, *Sma*I and, *Xho*I **(Fig. 3.7)** while pTT1B::*recA-msfGFP* plasmids were confirmed with *Bam*HI, *Bsa*AI, *Bst*BI, *Dra*I, *Pvu*I, *Pvu*II and *Stu*I **(Fig. 3.8)**. The plasmids that screened positive were further confirmed by DNA sequencing. Sequence-confirmed constructs were electroporated into different *Msm* background strains: PMCpAINT::*recA-msfGFP* and pTTB1::*recA-msfGFP* were electroporated in to Δ*recA* deletion strain, and pMCpAINT::*mScarlet-imuA′* and pTTB1::*mScarlet-imuA′* were electroporated in Δ*imuA′* deletion strain to evaluate the ability of the reporter proteins to complement the functions of the deleted genes. Both constructs were also electroporated into the WT parental strain as controls.

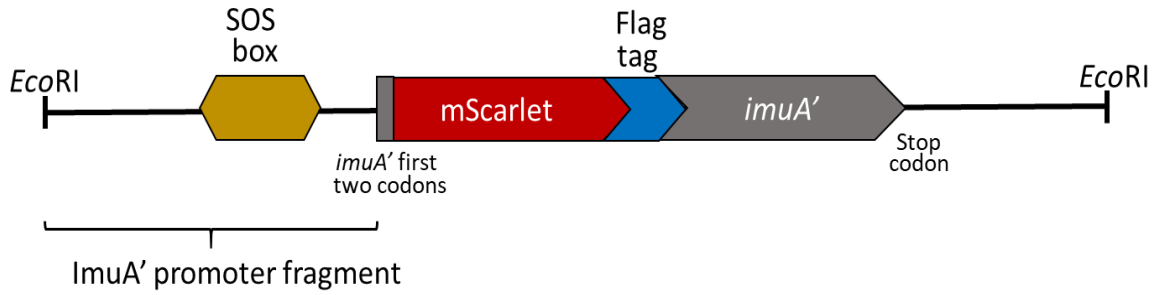

Figure 3.1. Schematic design of *mScarlet-imuA'*. The reporter construct consists of the imuA′ promoter which contains an SOS box. This is followed by the first two codons of imuA′, and mScarlet fluorophore with a flag tag in between the gene and the fluorophore. The EcoRI restriction sites were added on either side of the 500 bp upstream and downstream flanking regions to allow ligation into integrating vectors.

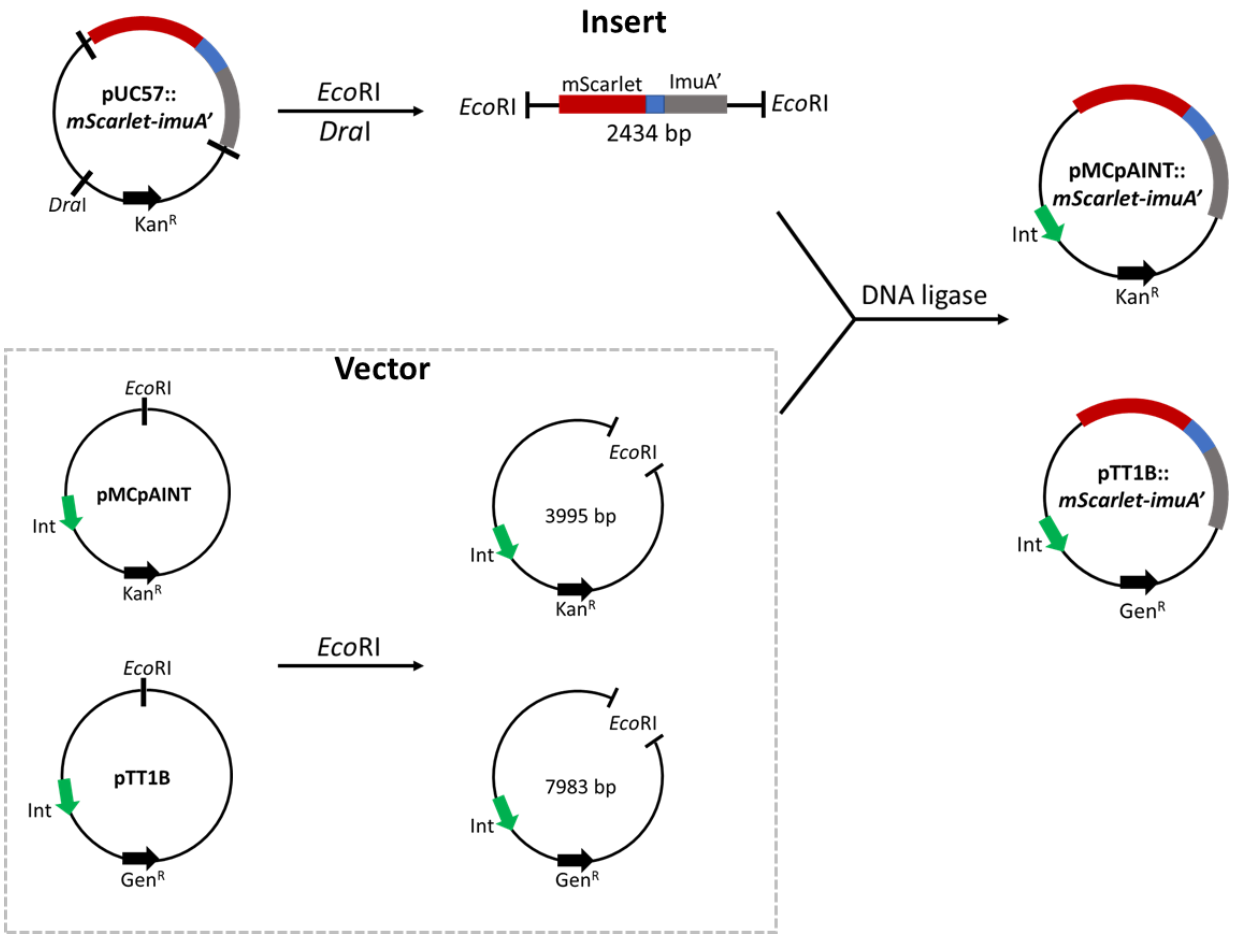

Figure 3.2. Cloning strategy for pMCpAINT::*mScarlet-imuA'* and pTT1B::*mScarlet-imuA'*. The schematic diagram represents steps followed to construct pMCpAINT::mScarlet-imuA′ and pTT1B::mScarlet-imuA′ reporters.

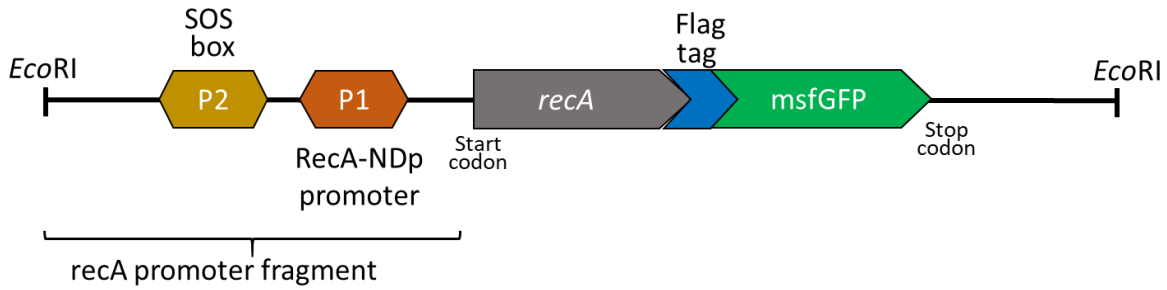

Figure 3.3: Schematic design of *recA-msfGFP*. The reporter construct consists of the recA promoters (RecA independent (P1) and RecA dependent SOS box (P2)), a flag tag in between the gene and the fluorophore, msfGFP, downstream of the recA gene. The EcoRI restriction enzymes were also added on either side of the 500 bp upstream and downstream flanking regions to allow ligation into integrative vectors.

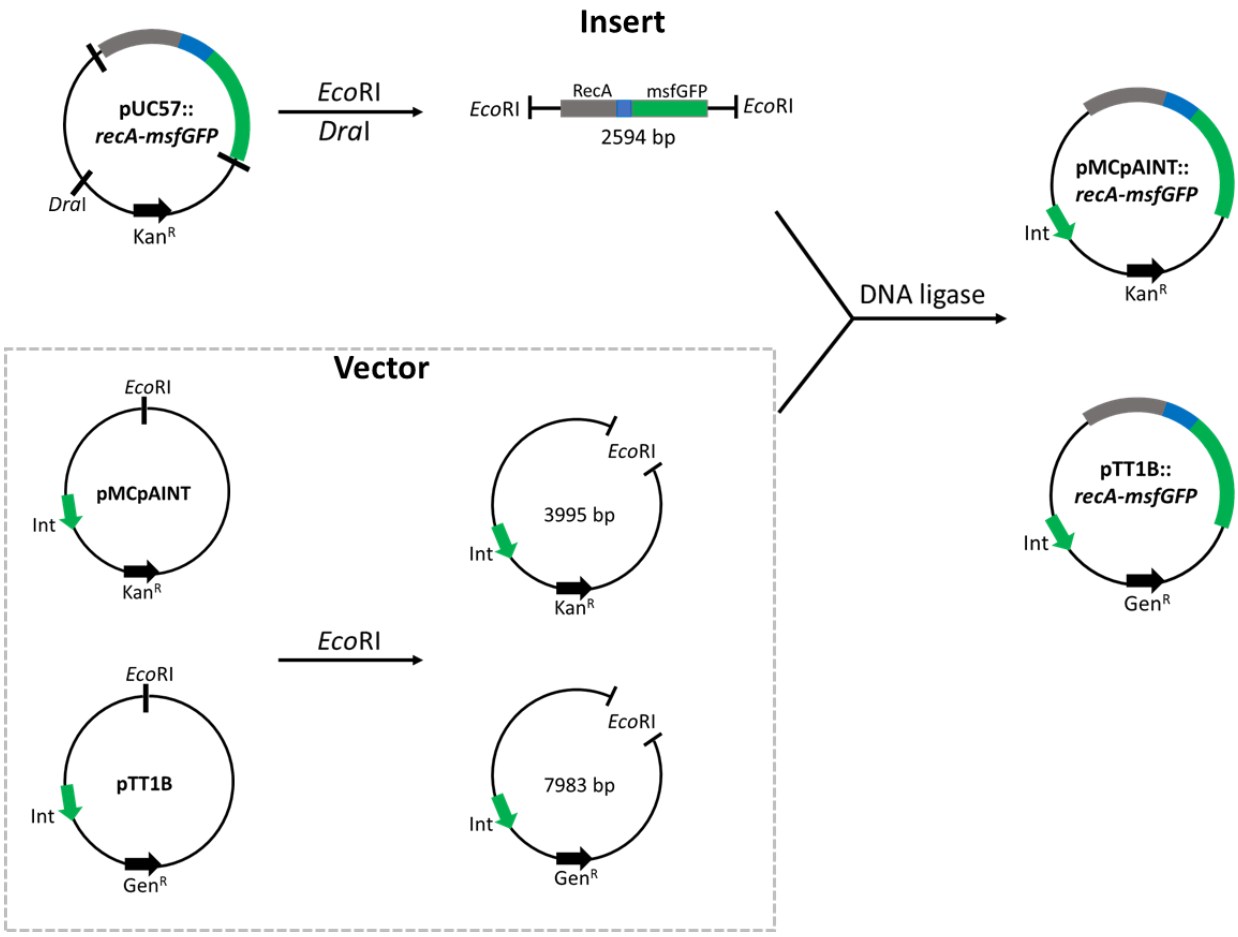

Figure 3.4: Cloning approach of pMCpAINT::*recA-msfGFP* and pTT1B::*recA-msfGFP*. The schematic diagram that represents steps which were taken to clone and generate pMCpAINT::recA-msfGFP and pTT1B::recA-msfGFP construct.

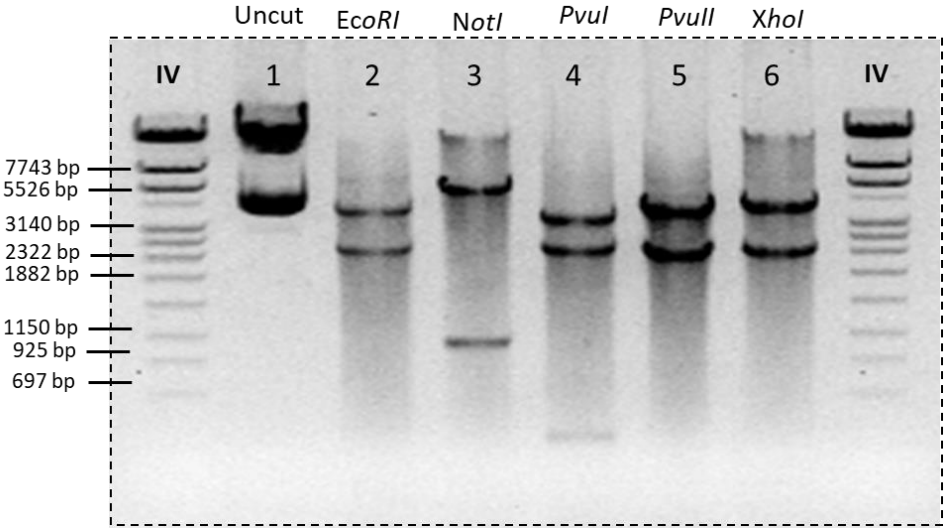

Figure 3.5: Restriction screening of putative clones of pMCpAINT::*mScarlet-imuA'*. Restriction digest mapping screen of pMCpAINT::mScarlet-imuA′ transformants. Multiple REs were used to screen the clones. EcoRI (3995 bp, 2440 bp), NotI (5355 bp, 1074 bp), PvuI

(3546 bp, 2434 bp, 488 bp), PvuII (4059 bp, 2370 bp) and XhoI (4066 bp, 2363 bp). The uncut control was also added. The molecular weight marker IV (Roche, USA) fragments of selected sizes are clearly indicated. Expected fragment sizes are indicated in brackets.

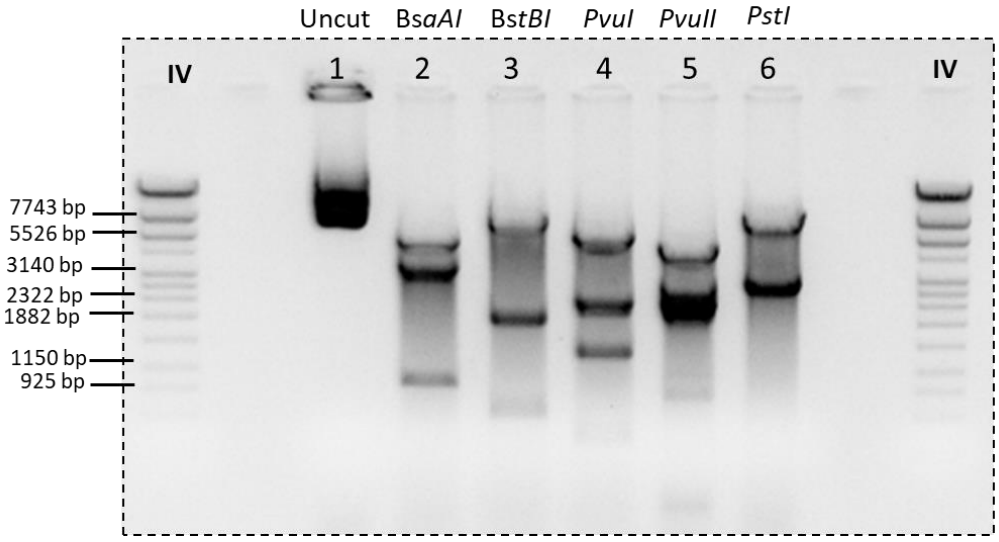

Figure 3.6: Restriction screening of putative clones of pTT1B::*mScarlet-imuA′*. Restriction digest mapping screen of pTT1B::mScarlet-imuA′ transformants. Multiple Res were used to screen the clones. BsaAI (5497 bp, 3939 bp, 940 bp), BstBI (7841 bp, 1967 bp, 609 bp), PvuI (6177 bp, 2345 bp, 1386 bp), PvuII (5126 bp, 2836 bp, 2452 bp) and PstI (7308 bp, 3198 bp). The uncut control was also added. The molecular weight marker IV (Roche, USA) fragments of selected sizes are clearly indicated. Expected fragment sizes are indicated in brackets.

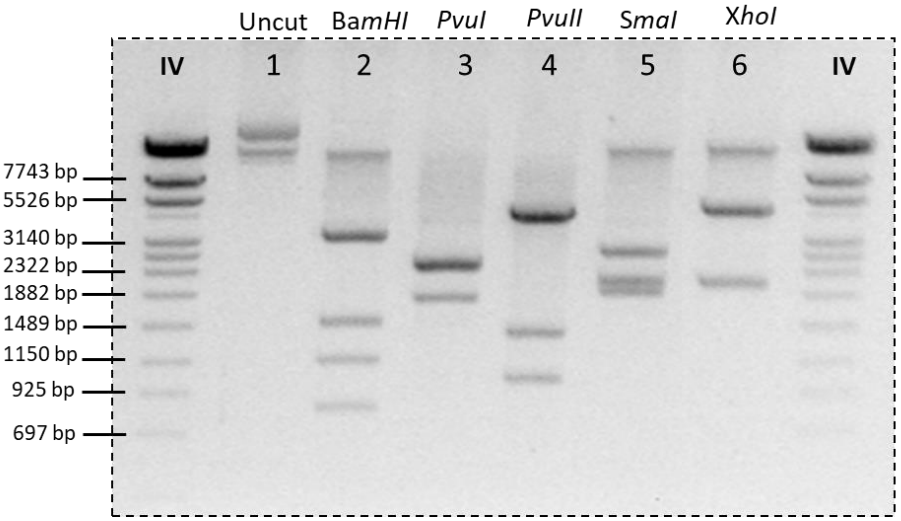

Figure 3.7: Restriction screening of putative clones of pMCpAINT::*recA-msfGFP*. Restriction digest mapping screen of pMCpAINT::recA-msfGFP transformants. Multiple REs were used to screen the clones. BamHI (3284 bp, 1519 bp, 1156 bp, 821 bp), PvuI (2435 bp, 2375bp, 1808 bp), PvuII (4366 bp, 1408 bp, 1035 bp), SmaI (2750 bp, 2098 bp, 1941 bp), and XhoI (4676 bp, 2113 bp). The uncut control was also added. The molecular weight marker IV (Roche, USA) fragments of selected sizes are clearly indicated. Expected fragment sizes are indicated in brackets.

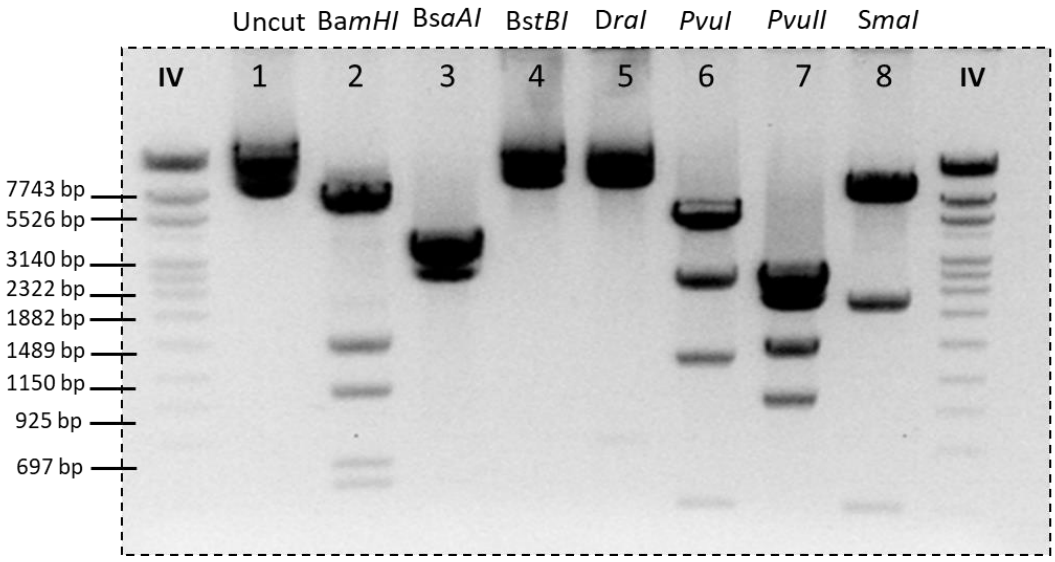

Figure 3.8: Restriction screening of putative clones of pTT1B::*recA-msfGFP*. Restriction digest mapping screen of pTT1B::recA-msfGFP transformants. Multiple REs were used to screen the clones. BamHI (7154 bp, 1519 bp, 1035 bp, 581 bp, 488 bp), BsaAI (3988 bp, 3939 bp, 2850 bp), BstBI (10168 bp, 609 bp), DraI (10066 bp, 692 bp), PvuI (6177 bp, 2651 bp, 1386 bp, 409 bp), PvuII (5436 bp, 2836 bp, 1490 bp, 1015 bp) and SmaI (8264bp, 2098 bp). The uncut control was also added. The molecular weight marker IV (Roche, USA) fragments of selected sizes are clearly indicated. Expected fragment sizes are indicated in brackets.

4.2. Evaluating the functionalities of the fluorescently tagged ImuA' and RecA proteins.

The use of fluorescently tagged reporter strains to deduce protein expression and localization may be cofounded where the fluorescent tag interferes with the function of the tagged protein. Therefore, to find out whether mScarlet- and msfGFP-tagged proteins retained their normal functions in knockout backgrounds, separate DNA damage tolerance and UV induced mutagenesis assay were performed.

UV-induced mutagenesis was used to evaluate the mutation frequency in *Msm* and was performed as previously described (Boshoff et al., 2003, Warner et al., 2010). Here, the frequency of emergence of rifampicin resistant (Rif^R) mutants is measured using the number of Rif^R colonies that grow after exposure to UV treatment. The assay was conducted using Δ*imuA'*::*mScarlet-imuA',* WT::*mScarlet-imuA',* Δ*recA*::*recA-msfGFP* and WT::*recA-msfGFP* strains with both the pMCpAINT and pTT1B vectors and with Δ*imuA',* Δ*recA* and WT parental strains as controls. Mid-log cultures were exposed to UV irradiation and plated on solid 7H10

plates containing 200 μg/ml Rif. Consistent with previous observations, no colonies were observed for Δ*imuA'* or Δ*recA* strains following UV exposure, confirming that deletion of either gene abolishes induced mutagenesis (Boshoff et al., 2003, Warner et al., 2010). When *mScarlet-imuA′* was introduced into Δ*imuA′*, the mutation frequency was restored to WT levels; this was an important result since it indicated functional complementation of the *imuA′* deletion. Similarly, the presence of *mScarlet-imuA′* did not significantly alter the mutation frequency in the WT background (which retains a functional *imuA′* at the native chromosomal locus) **(Fig. 3.9A)**. Similar results were observed when *recA-msfGFP* was introduced into WT and Δ*recA* strains **(Fig. 3.9B)**. As before, the Δ*recA*::*recA-msfGFP* strain showed a mutation frequency similar to that of WT, suggesting that the fluorescent tag did not impact RecA function in the induced mutagenesis assay.

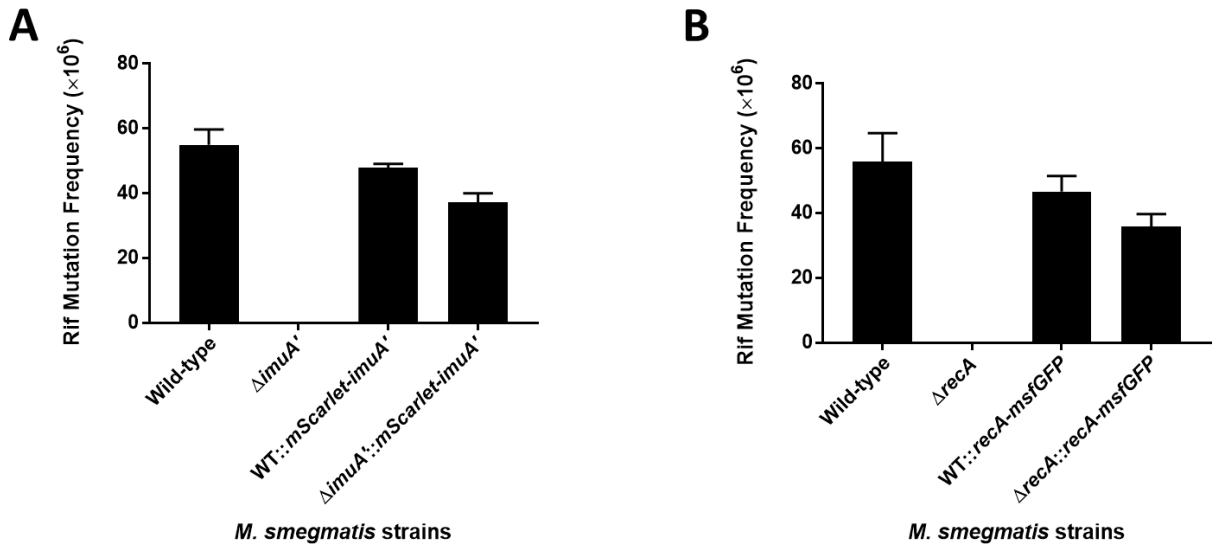

Figure 3.9: UV-induced mutation frequency to rifampicin resistance (Rif^R). Mutation frequency for **A.** mScarlet-ImuA′ and **B.** RecA-msfGFP reporter strains. Cells were grown to mid-log phase and exposed to UV radiation at 250×100 μJ before being allowed to recover in fresh medium for 3 hr. After exposure, an aliquot of cells was plated on 7H10 only plates and, the rest of the cells were allowed to recover for 3 hr. After recovery, cells were plated on solid medium supplemented with 200 μg/ml Rif and the frequency of Rif^R mutants determined as a function of total viable cells. The experiments were conducted as three independent biological replicates; error bars indicate standard deviations.

The functionalities of the fusion proteins were also evaluated in DNA damage tolerance assays. Here, a dilution series of the *Msm* strains was spotted on solid plates containing a suite of different DNA damaging agents to determine tolerance of induced DNA damage. To conduct the assay, cultures were grown to an OD_{600} of 0.6 – 0.8 and 10-fold serial dilutions spotted on solid plates containing 7H10 medium only or 7H10 supplemented with (i) 0.1 × MIC or 0.2 ×

MIC MMC; (ii) 0.1 × MIC or 0.2 × MIC Mox; (iii) 0.3 × MIC or 0.4 × MIC Ofx; (iv) 0.4 × MIC or 0.5 × MIC Nfz; and (v) 2 × MIC and 4 × MIC Nov. The plates were incubated for 3-5 days at 37 °C.

The first DNA damaging agent tested was MMC owing to its use in our lab previously (Warner et al, 2010). When spotted on plates supplemented with MMC, Δ*imuA′* and Δ*imuA′*::*mScarlet-imuA′* mutants appeared hypersensitive, exhibiting 1 log-fold greater sensitivity to 0.02 µg/ml MMC than WT. At the higher concentration of 0.04 µg/ml MMC, Δ*imuA′* and Δ*imuA′*::*mScarlet-imuA′* mutants were again hypersusceptible to DNA damage, exhibiting ~2 log-fold greater sensitivity than WT. The observation that the complemented Δ*imuA′* strain phenocopied the Δ*imuA′* mutant was surprising and suggested that the mScarlet-ImuA′ fluorescent protein was not able to functionally complement loss of wild-type ImuA'. Moreover, when *mScarlet-imuA′* was electroporated into the WT parental strain, the resulting WT::*mScarlet-imuA′* mutant (which is effectively heterologous for ImuA', expressing both wild-type and fluorescently tagged proteins) showed greater susceptibility to MMC than the other three strains: a 3 log growth inhibition was observed at the lower MMC concentration of 0.02 µg/ml and this increased to 4 log inhibition at 0.04 µg/ml MMC. This result was unexpected since the strain expresses both mScarlet tagged ImuA′ as well as the native ImuA′ and was predicted to show comparable sensitivity to WT. Instead, this observation suggested that the *mScarlet-imuA′* allele might have a dominant negative effect on WT **(Fig. 3.10)**.

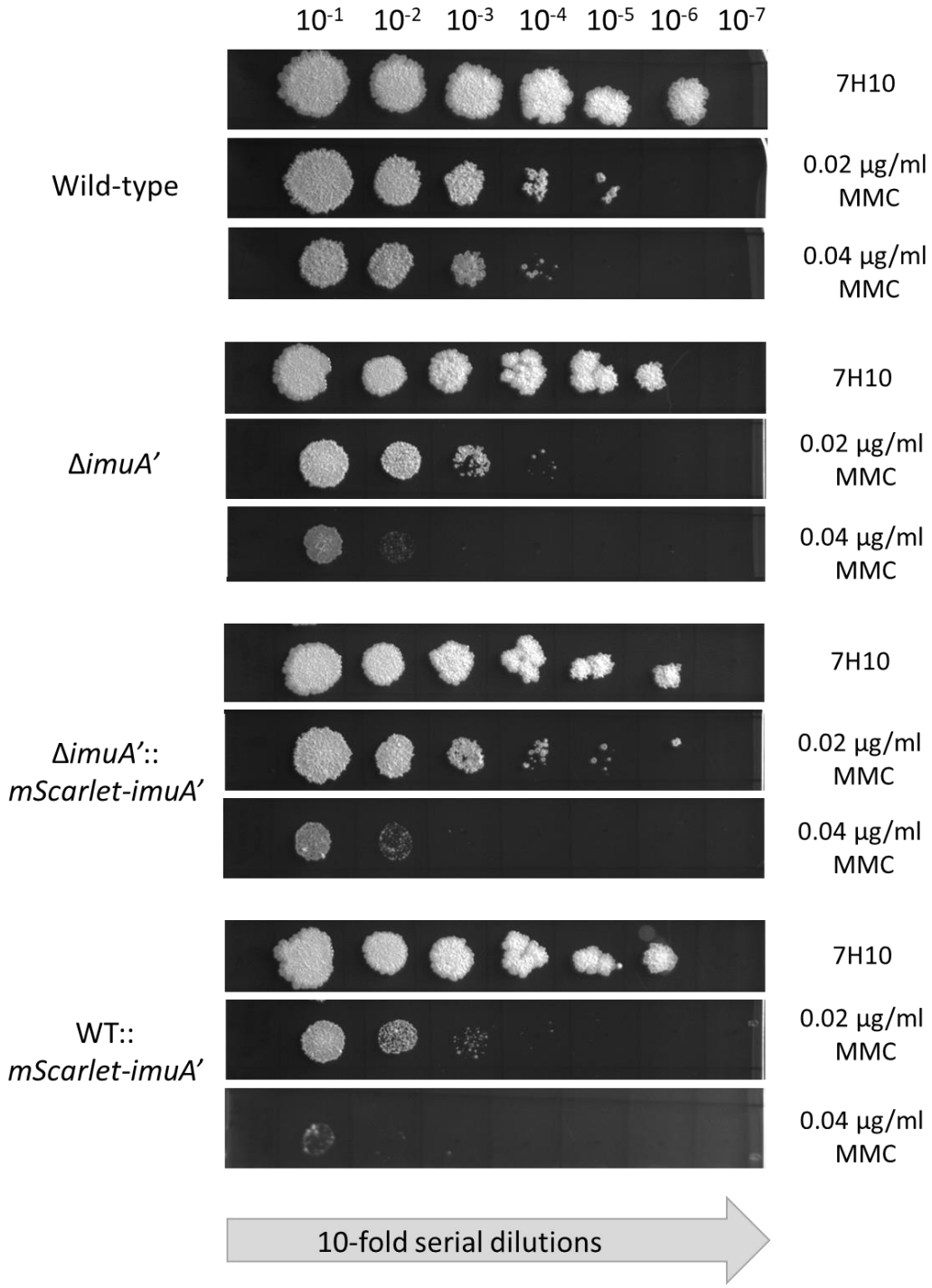

Figure 3.10: mScarlet-ImuA' DNA damage tolerence assay. DNA damage tolerance of WT, ΔimuA′, WT::mScarlet-imuA′ and ΔimuA′::mScarlet-imuA′ strains was assessed following exposure to MMC. Cells were grown to mid-log phase and ten-fold serial dilutions were spotted on solid 7H10 medium and 7H10 supplemented with 0.02 and 0.04 µg/ml MMC, respectively. The experiments were conducted as three independent biological replicates.

In equivalent MMC tolerance assays, Δ*recA* and Δ*recA*::*recA-msfGFP* were hypersensitive exhibiting 1-2 log greater sensitivity than WT when exposed to 0.02 μg/ml and 0.04 μg/ml MMC, respectively. This hypersensitivity was also observed in the merodiploid WT::*recA-msfGFP* mutant. While the ability of the *recA*-msfGFP to complement recA deletion was questionable, visual inspection of the plates suggested a larger spot size for the Δ*recA*::*recA-msfGFP* mutant at the higher MMC concentration, perhaps indicating slightly reduced sensitivity to MMC compared to either Δ*recA* or WT:: *recA-msfGFP* strains. In summary, therefore, it seemed prudent to conclude that, similar to mScarlet-ImuA′, RecA-msfGFP fluorescent protein failed to complement *recA* knockout and exhibited a dominant negative effect when introduced into WT **(Fig. 3.11)**.

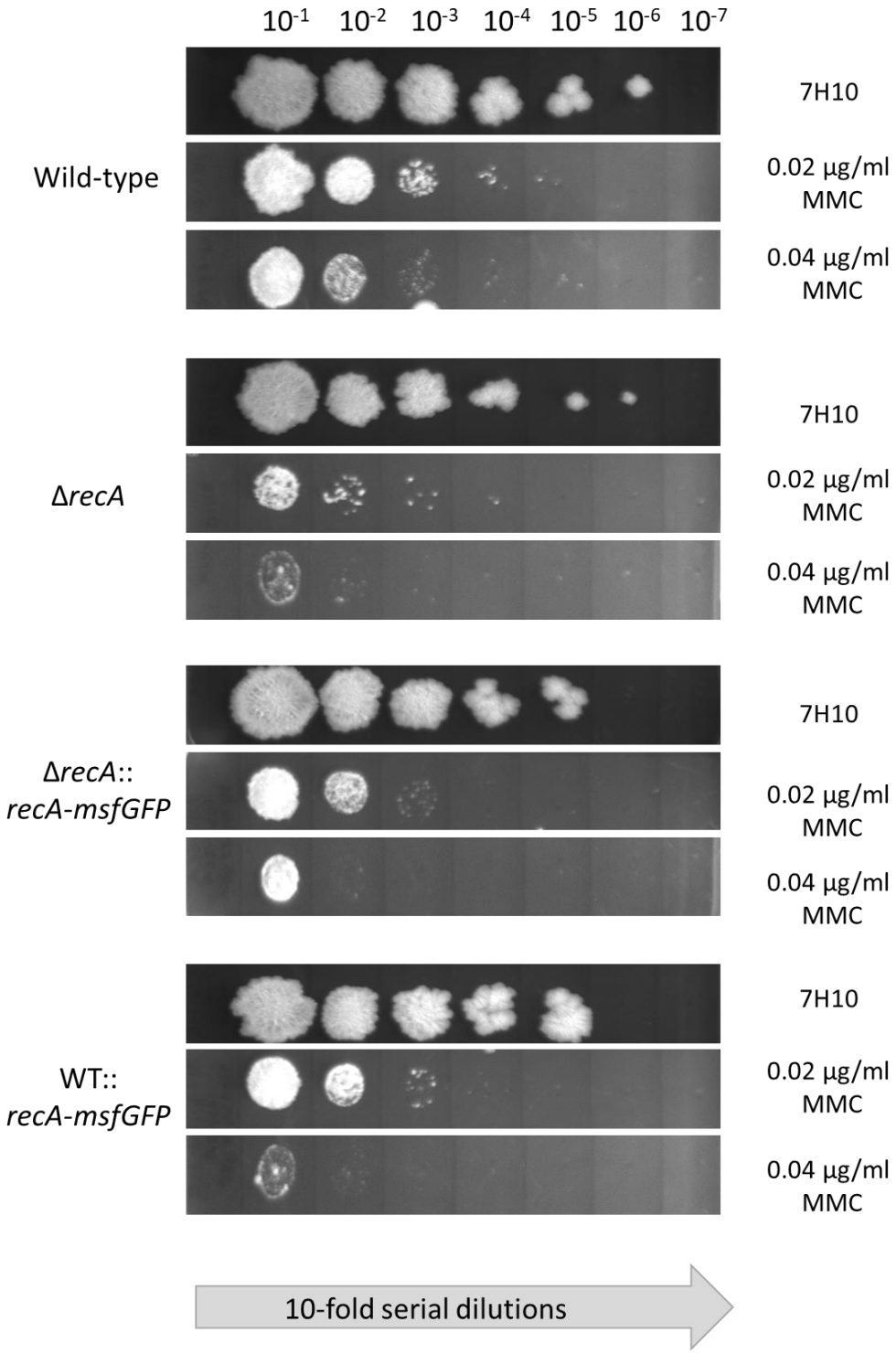

Figure 3.11: RecA-msfGFP DNA damage tolerance assay. DNA damage tolerance of WT, ΔrecA, WT::recA-msfGFP and ΔrecA::recA-msfGFP was determined following exposure to MMC. Cells were grown to mid-log phase and ten-fold serial dilutions spotted on solid 7H10 medium with or without 0.02 or 0.04 µg/ml MMC. The experiments were conducted as three independent biological replicates.

To investigate further the phenotypes observed with MMC, the RecA-msfGFP and mScarlet-ImuA' strains were tested for sensitivity against a range of DNA-damaging agents with different mechanisms of action; namely, Mox, Nfz, Nov, Ofx and UV irradiation. The applied concentrations were selected to allow for colony growth observation and damage tolerance sensitivity. When Δ*imuA′* and strains carrying the *mScarlet-imuA*' allele were exposed to Mox **(Fig 3.12A)**, Nfz **(Fig 3.12B)**, or Nov **(Fig 3.12D)**, all three showed sensitivity similar to WT at both concentrations. When exposed to UV, Δ*imuA′* displayed hypersensitivity at both 600 μJ/cm^2 and 750 μJ/cm^2. This was in contrast to both WT::*mScarlet-imuA′* and Δ*imuA′*:: *mScarlet-imuA′* which phenocopied WT at both 600 μJ/cm^2 and 750 μJ/cm^2 UV, displaying ~1 log sensitivity **(Fig 3.12C).** When exposed to Ofx, mScarlet-ImuA' strains partially phenocopied WT, displaying 3log sensitivity, whereas Δ*imuA′* grew at a level similar to WT showing 1 log sensitivity when exposed to 0.201 μg/ml Ofx. When exposed to a higher Ofx concentration, mScarlet-ImuA' strains were more sensitive, showing 1 log greater inhibition than WT and Δ*imuA′* **(Fig 3.12E)**.

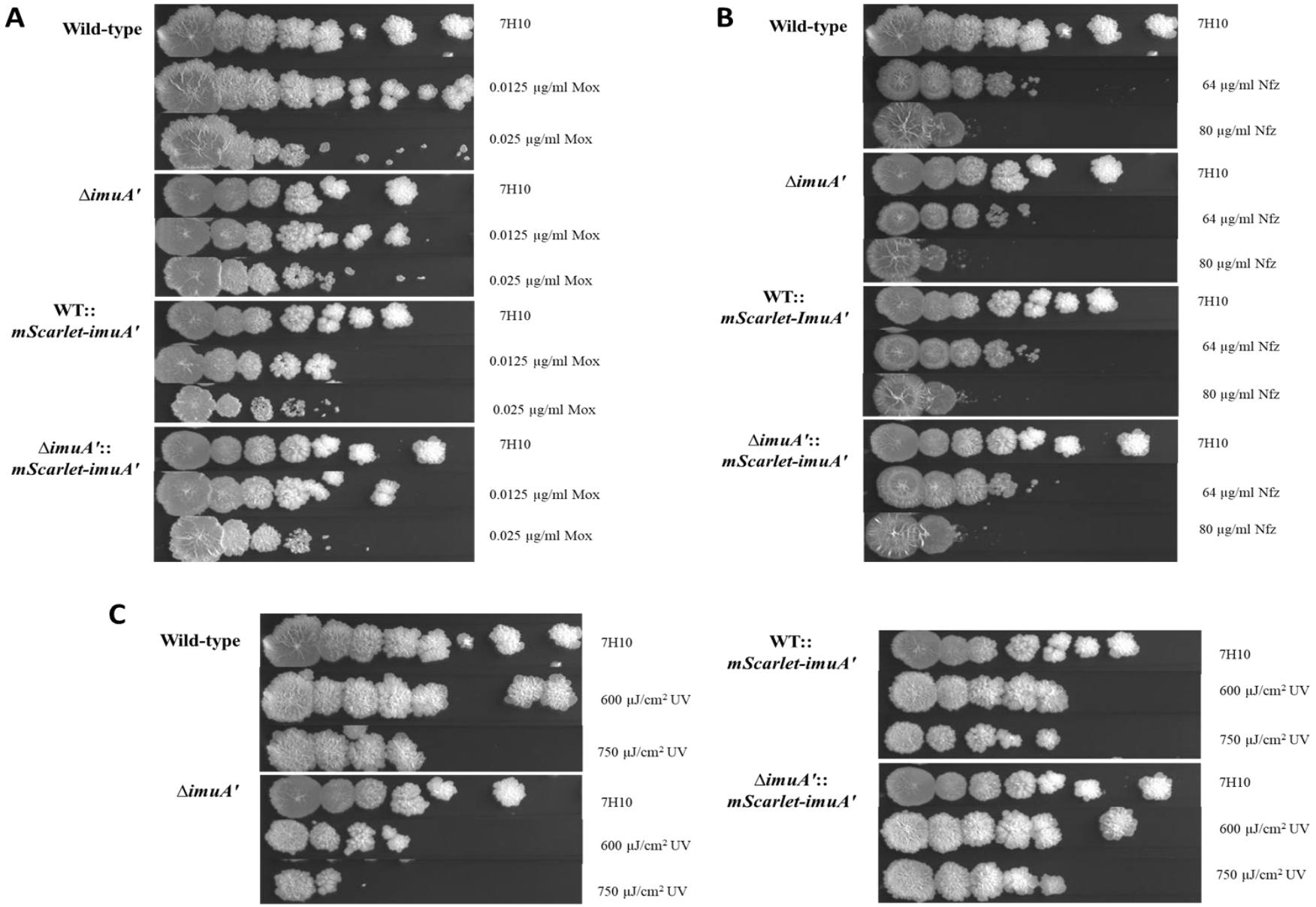
A
Wild-type
7H10
0.0125 µg/ml Mox
0.025 µg/ml Mox
ΔimuA'
7H10
0.0125 µg/ml Mox
0.025 µg/ml Mox
WT::
mScarlet-imuA'
7H10
0.0125 µg/ml Mox
0.025 µg/ml Mox
ΔimuA'::
mScarlet-imuA'
7H10
0.0125 µg/ml Mox
0.025 µg/ml Mox
B
Wild-type
7H10
64 µg/ml Nfz
80 µg/ml Nfz
ΔimuA'
7H10
64 µg/ml Nfz
80 µg/ml Nfz
WT::
mScarlet-ImuA'
7H10
64 µg/ml Nfz
80 µg/ml Nfz
ΔimuA'::
mScarlet-imuA'
7H10
64 µg/ml Nfz
80 µg/ml Nfz
C
Wild-type
7H10
600 µJ/cm² UV
750 µJ/cm² UV
ΔimuA'
7H10
600 µJ/cm² UV
750 µJ/cm² UV
WT::
mScarlet-imuA'
7H10
600 µJ/cm² UV
750 µJ/cm² UV
ΔimuA'::
mScarlet-imuA'
7H10
600 µJ/cm² UV
750 µJ/cm² UV

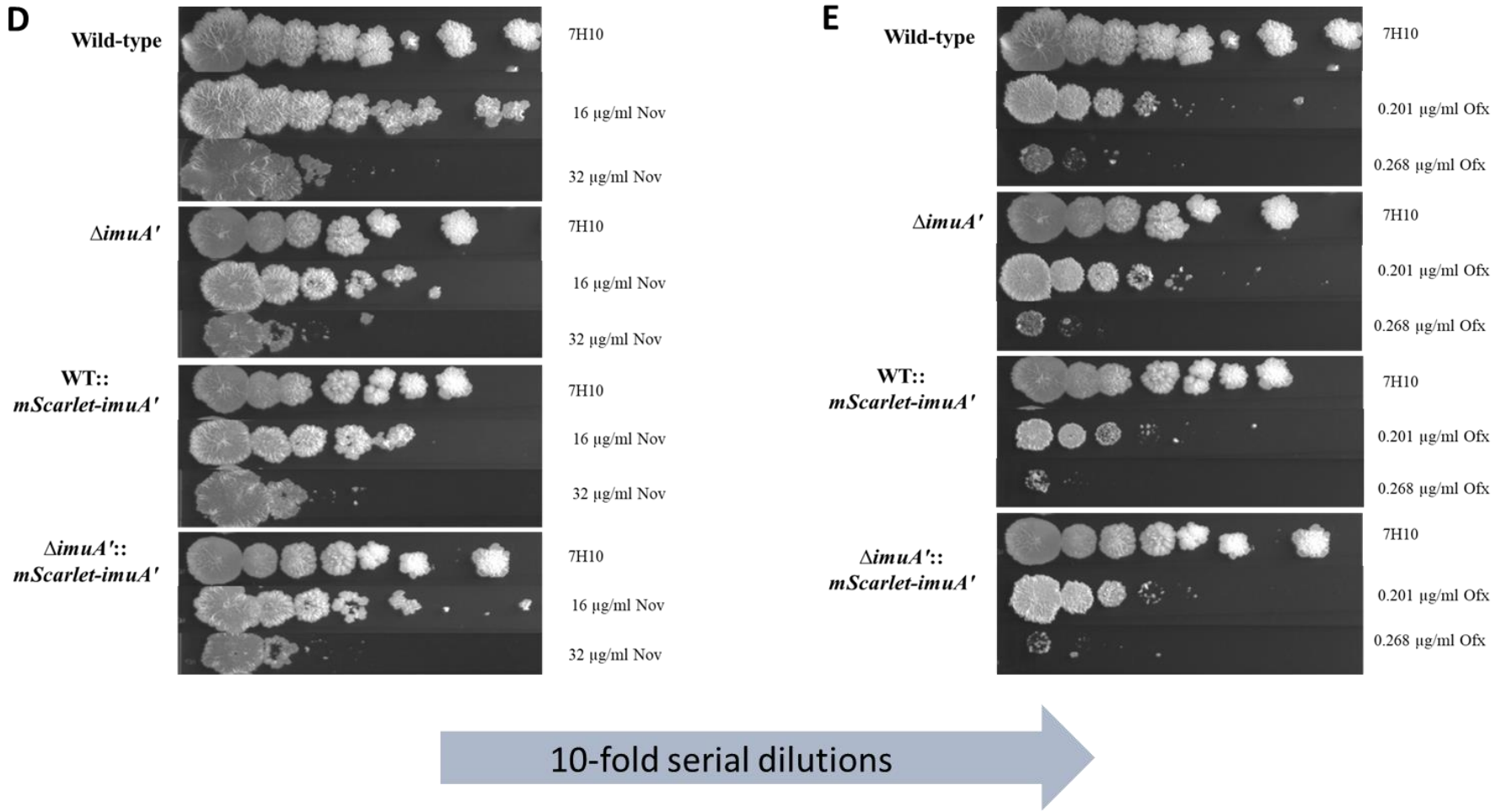

Figure 3.12. DNA damage sensitivity in mScarlet-ImuA' Msm strains. DNA damage sensitivity was determined for WT, ΔimuA', WT::mScarlet-ImuA' and ΔimuA'::mScarlet-ImuA' against a range of DNA-damaging agents. Cells were grown to mid-log phase and ten-fold dilutions were spotted on solid media plates (7H10) only and plates supplemented with varying concentrations of each antimicrobial compound. For UV, cells were plated on 7H10 only plates and exposed to UV irradiation at different range. The experiments were conducted as three independent biological replicates.

When exposed to Mox, Δ*recA*::*recA-msfGFP*, Δ*recA* and WT::*recA-msfGFP* showed growth that looks like that of WT **(Fig. 3.13A)**. For Nfz, Δ*recA* showed the highest level of sensitivity (3 log-fold at 64 μg/ml) whereas the RecA-msfGFP strains were less sensitive (2log-fold sensitivity) than Δ*recA*, although still more sensitive than WT (1 log-fold sensitivity). When exposed to a higher concentration of Nfz, Δ*recA*::*recA-msfGFP* and Δ*recA* strains were hypersensitive completely abolishing growth, whereas WT::*recA-msfGFP* was less sensitive showing 4 log sensitivity **(Fig. 3.13B)**. When exposed to UV **(Fig. 3.13C)** and Nov **(Fig. 3.13D)**, all strains showed growth that looked like WT. Finally, Ofx fully inhibited growth of Δ*recA* and Δ*recA*::*recA-msfGFP* whereas WT::*recA-msfGFP* showed slight growth exhibiting 4 log sensitivity compared to WT which exhibited 3 log sensitivity at 32 μg/ml Ofx. However, when exposed to a lower concentration of 16 μg/ml Ofx, WT::*recA-msfGFP* showed less sensitivity when compared Δ*recA* and Δ*recA*::*recA-msfGFP* which was more hypersensitive **(Fig. 3.13E).**

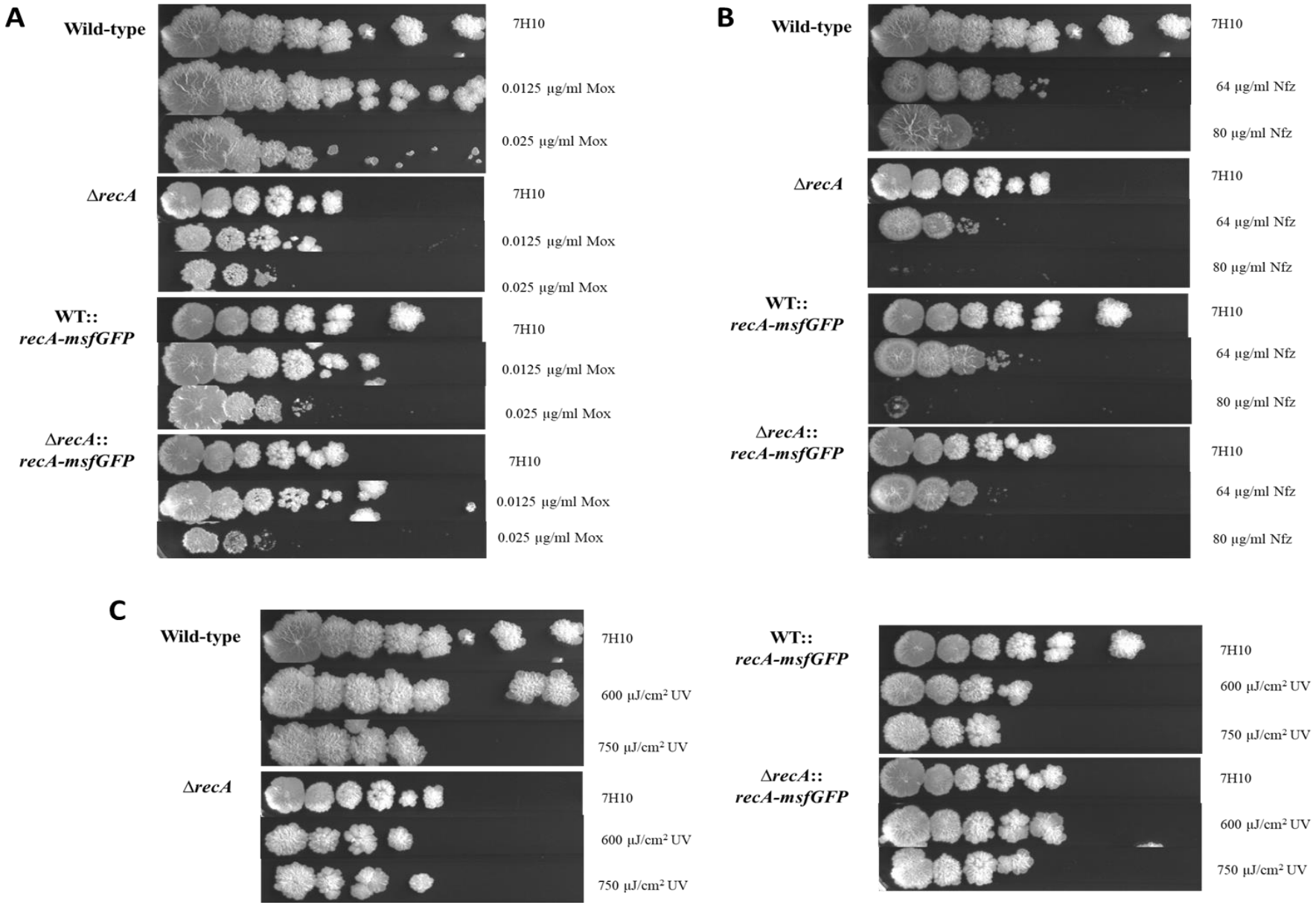
A
Wild-type
7H10
0.0125 µg/ml Mox
0.025 µg/ml Mox
ΔrecA
7H10
0.0125 µg/ml Mox
0.025 µg/ml Mox
WT::
recA-msfGFP
7H10
0.0125 µg/ml Mox
0.025 µg/ml Mox
ΔrecA::
recA-msfGFP
7H10
0.0125 µg/ml Mox
0.025 µg/ml Mox
B
Wild-type
7H10
64 µg/ml Nfz
80 µg/ml Nfz
ΔrecA
7H10
64 µg/ml Nfz
80 µg/ml Nfz
WT::
recA-msfGFP
7H10
64 µg/ml Nfz
80 µg/ml Nfz
ΔrecA::
recA-msfGFP
7H10
64 µg/ml Nfz
80 µg/ml Nfz
C
Wild-type
7H10
600 µJ/cm² UV
750 µJ/cm² UV
ΔrecA
7H10
600 µJ/cm² UV
750 µJ/cm² UV
WT::
recA-msfGFP
7H10
600 µJ/cm² UV
750 µJ/cm² UV
ΔrecA::
recA-msfGFP
7H10
600 µJ/cm² UV
750 µJ/cm² UV

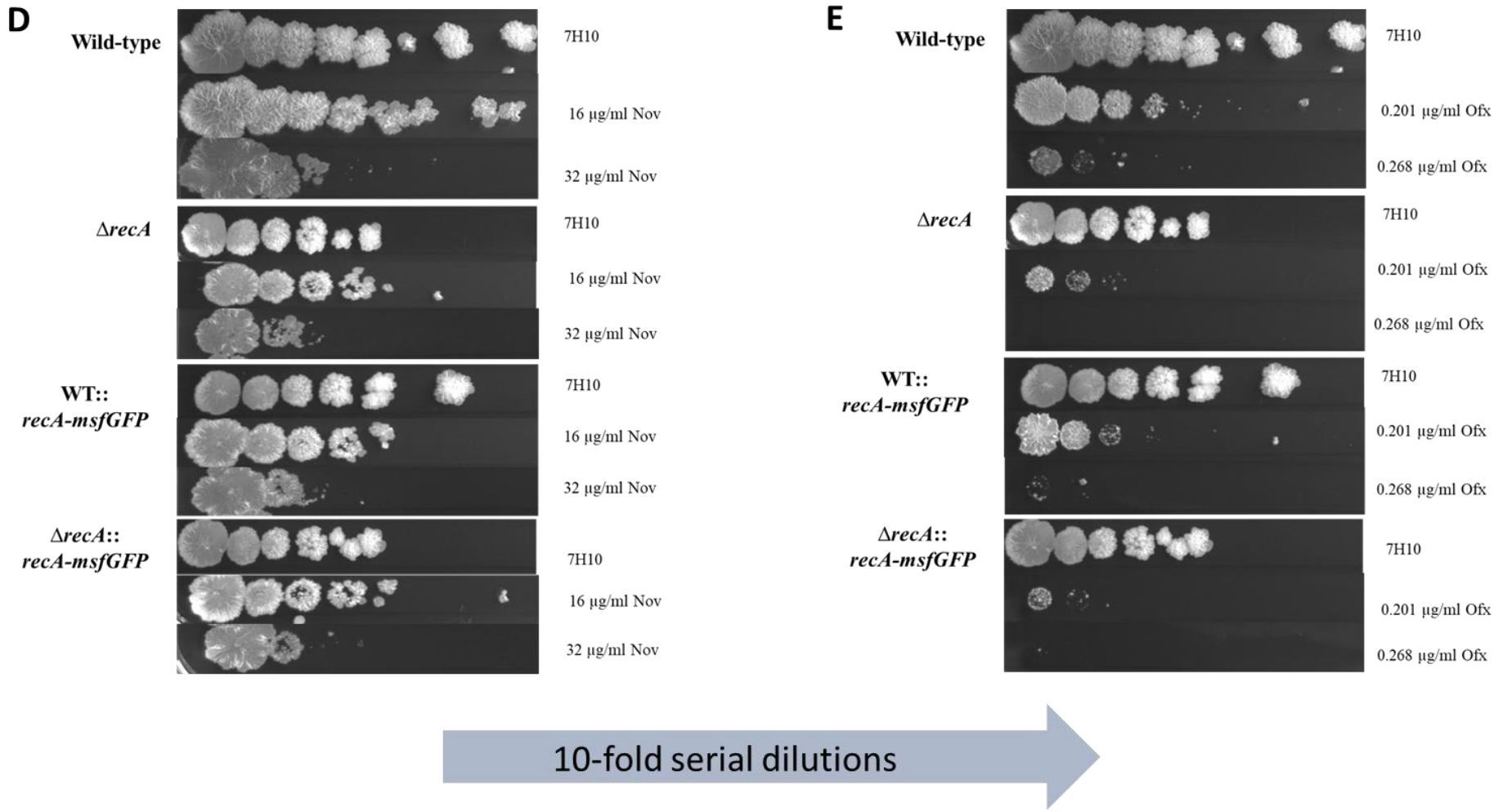

Figure 3.13. DNA damage sensitivity in RecA-msfGFP Msm strains. DNA damage sensitivity of WT, ΔrecA, WT::RecA-msfGFP and ΔrecA::RecA-msfGFP strains was assayed for a range of DNA-damaging agents. Cells were grown to mid-log phase and ten-fold dilutions were spotted on solid media plates (7H10) only and plates supplemented with varying concentrations of different antimicrobial drugs. For UV, cells were plated on 7H10 only plates and exposed to UV irradiation at different range. The experiments were conducted as three independent biological replicates.

4.3. Visualisation of the fluorescently tagged ImuA' and RecA bioreporters.

4.3.1. Localization of mScarlet-ImuA′ using fluorescence imaging.

Following the introduction of the mScarlet-ImuA′ and RecA-msfGFP constructs into WT and corresponding knockout backgrounds (Δ*imuA′* and Δ*recA*, respectively), the next objective was to observe the cells under different genotoxic stress conditions. To visualise strains using fluorescence microscopy, cells were grown to an OD_{600}~0.2 followed by a 4 hr treatment with 1x MIC MMC or exposure to UV (250 μJ/cm^2) to allow DNA damage induced expression of the SOS-regulated genes. To eliminate the possibility of non-specific fluorescence, WT mc^2155 was exposed to the same conditions and imaged using the same microscope settings. Although low level background fluorescence was detectable in all conditions, the fluorescence signal was much less than the mScarlet-ImuA′ and RecA-msfGFP containing strains. This background was subtracted from all images to ensure that only the signal from the fluorescently-tagged fusion proteins was recorded. **(Fig. 3.14, 3.17A)**. As expected, when Δ*imuA′*:: *mScarlet-imuA′* and WT:: *mScarlet-imuA′* were grown in untreated conditions, no fluorescence expression was observed **(Fig. 3.15, 3.16)**. In contrast, when the strains were exposed to UV and MMC-induced DNA damage, a diffuse red fluorescence signal was detected throughout the cells after 4 hrs of treatment (**Fig. 3.15, 3.16**).

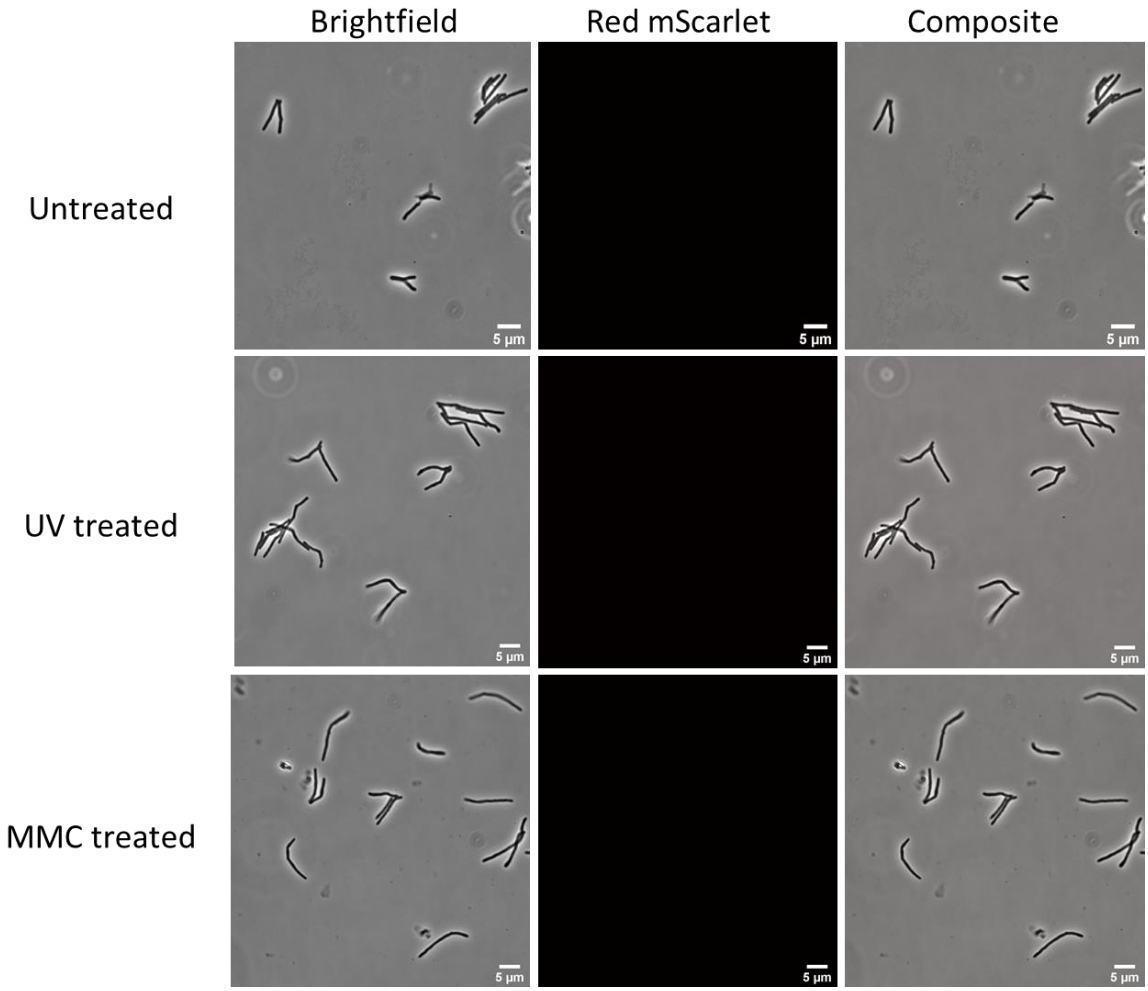

Figure 3.14: Microscopic imaging of WT *Msm* under normal growth and following genotoxic stress. The growth conditions are represented as untreated, UV-treated and MMC-treated, respectively. For each condition, the left panel illustrates brightfield micrographs of bacilli; middle panel illustrates the red mScarlet fluorescence signal; right panel is a composite of red fluorescence signal and brightfield micrographs. These images are representative of 3 repeats. Scale bars, 5 µm.

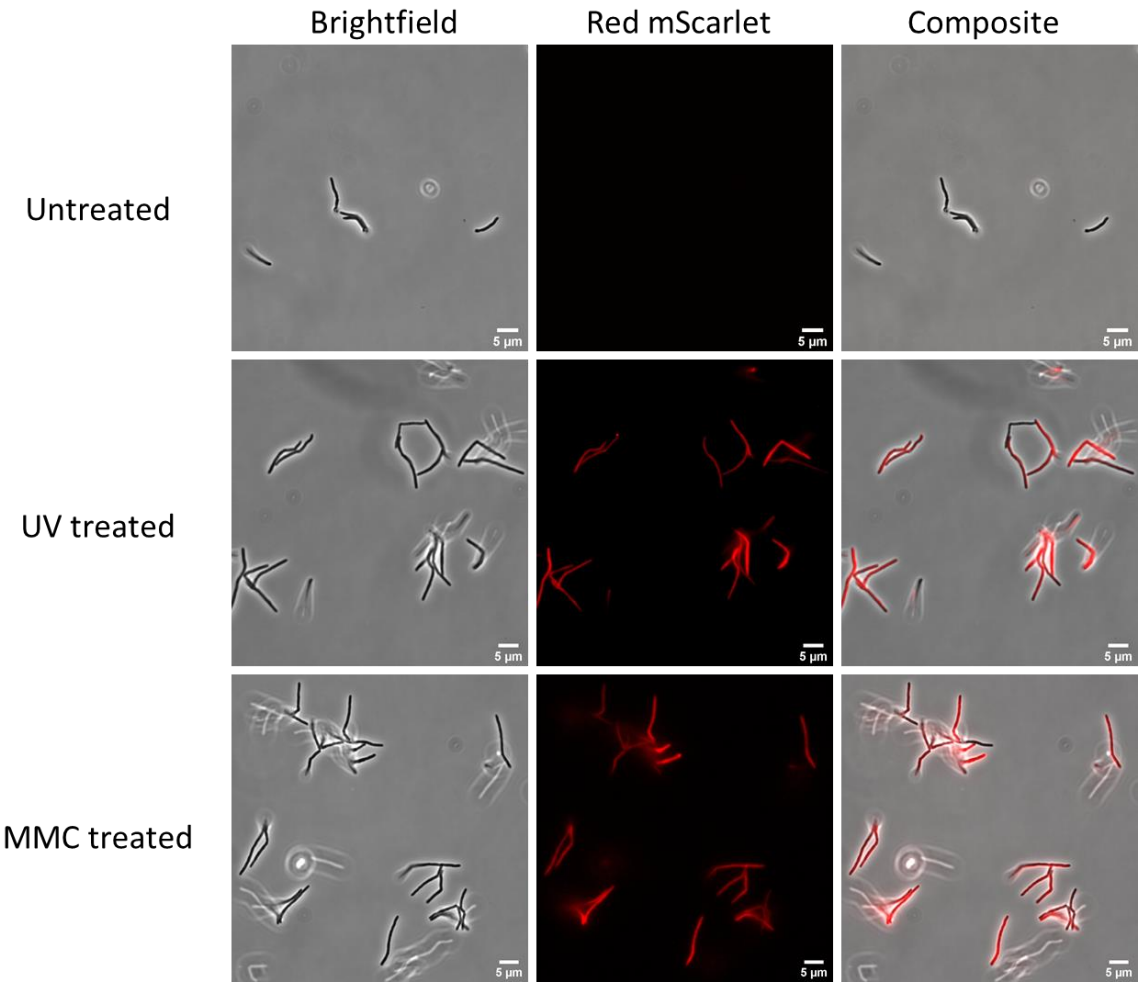

Figure 3.15: Visualization of mScarlet-ImuA′ in Δ*imuA′::mScarlet-ImuA′* during growth under normal conditions and following genotoxic stress. The growth conditions are represented as untreated, UV-treated, and MMC-treated by the top, middle, and bottom rows, respectively. Left panel illustrates brightfield micrographs of bacilli; middle panel illustrates the red mScarlet fluorescence signal; right panel is a composite of red fluorescence signal and brightfield micrographs. Images are representative of 3 repeats. Scale bars, 5 µm.

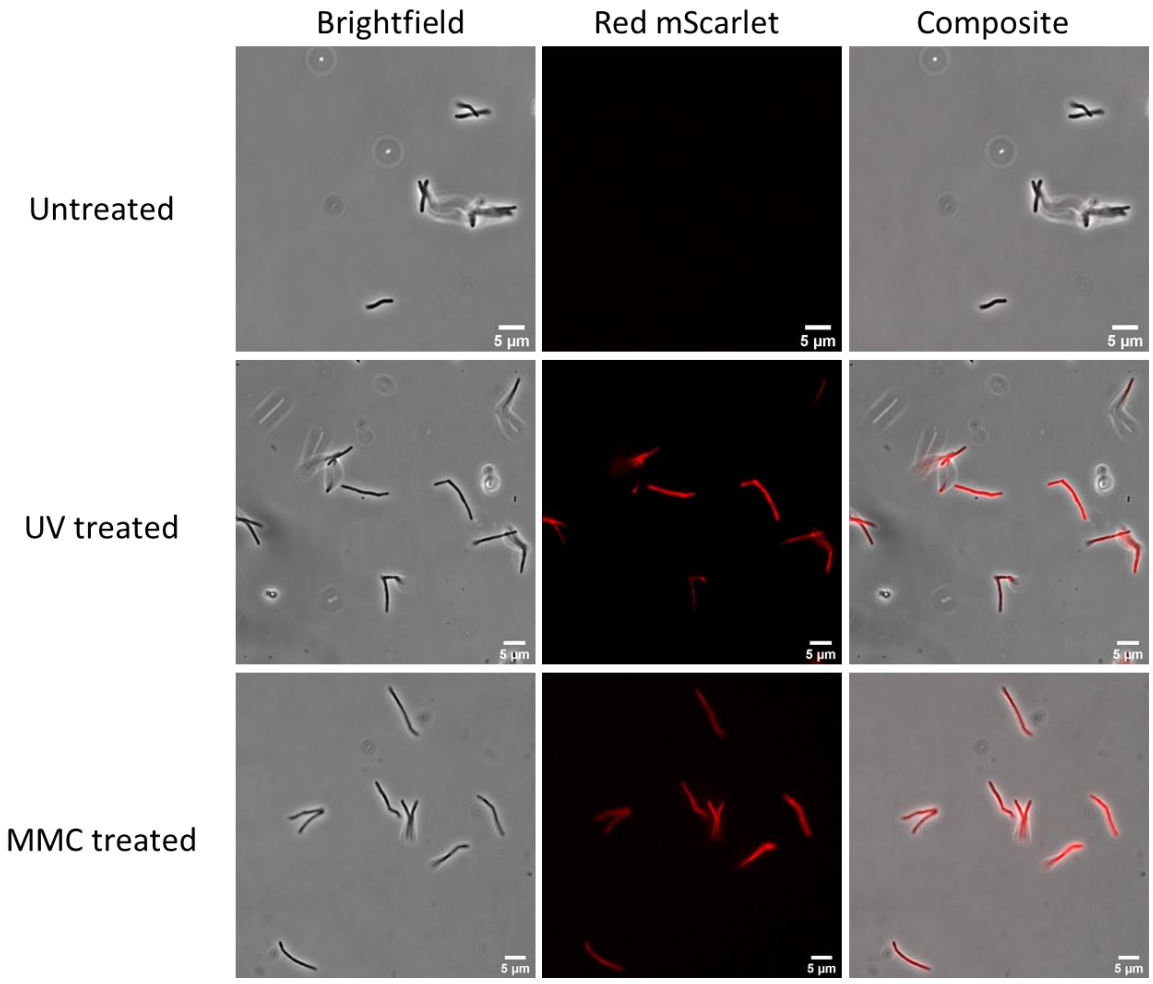

Figure 3.16: Expression of mScarlet-ImuA′ in WT::*mScarlet-imuA′* under normal conditions and following genotoxic stress. WT::mScarlet-imuA′ was imaged in untreated, UV-treated, and MMC-treated conditions as depicted in the top, middle, and bottom rows, respectively. Left panel illustrates brightfield micrographs of bacilli; middle panel illustrates the red mScarlet fluorescence signal; right panel is a composite of red fluorescence signal and brightfield micrographs. Images are representative of 3 repeats. Scale bars, 5 µm.

In support of the imaging data, fluorescence signal was quantified and averaged across multiple cells of a given strain under the different conditions. As mentioned previously, low level background fluorescence was detected in the WT mc^2155 parental strain, which lacks any fluorescent constructs, under all conditions, and this autofluorescence signal increased following DNA damage. To enable determination of the signal from the fusion protein only, this background (non-specific) fluorescence was subtracted from all images **(Fig. 3.14, 317A)**. An increase in fluorescence was observed when WT::*mScarlet-imuA′* and Δ*imuA′*::*mScarlet-imuA′* strains were treated with UV and MMC **(Fig. 3.17A)**. Moreover, there was no discernible difference in fluorescence intensity when comparing UV-treated and MMC-treated conditions

for both strains (p=0.7102 for Δ*imuA′*::*mScarlet-imuA′* and p=0.0799 for WT::*mScarlet-imuA′*). As expected given DNA damage induction of the SOS response, exposure to UV and MMC led to bacillary filamentation which was observed as an increase in average cell length. Although there was no visually discernible difference between UV and MMC treated cells **(Fig 3.14-3.16)**, quantification of cell lengths revealed a slight, but statistically significant, difference between UV-treated and MMC-treated cells **(Fig. 3.17B)**.

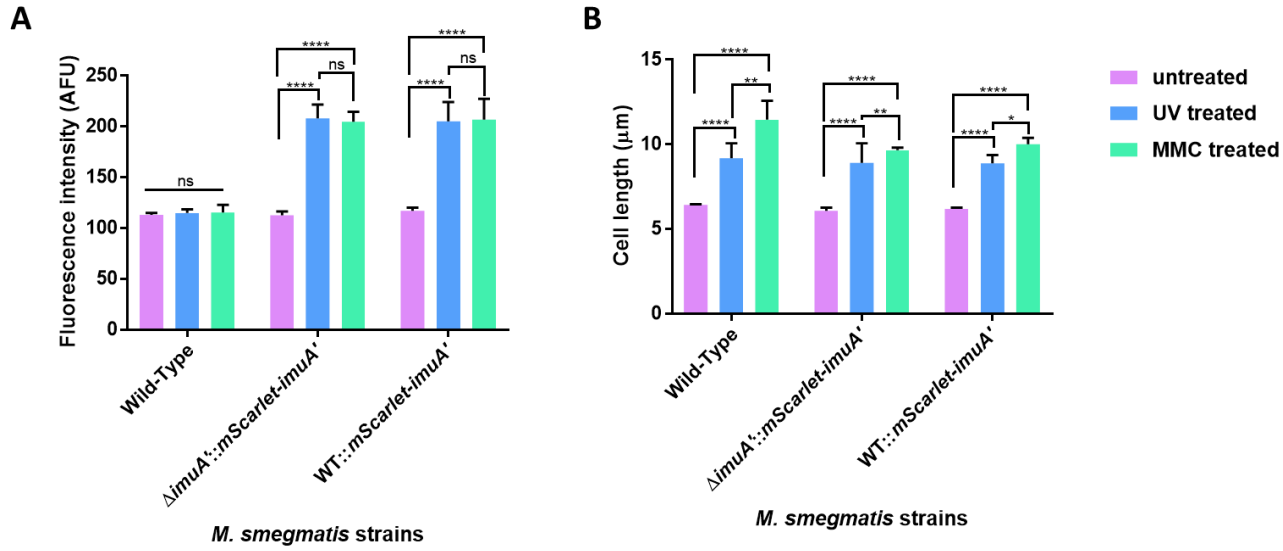

Figure 3.17: Quantification of fluorescence intensities and cell lengths in *Msm* mScarlet-ImuA′ reporter strains. A. Fluorescence intensities and **B.** cell lengths were determined for WT, WT::mScarlet-imuA′ and ΔimuA′::mScarlet-imuA′ before treatment (pink), after UV treatment (blue) and after MMC exposure (green). Data represent an average of three independent experiments in which 50 to 150 cells were counted per strain: ns=non-significant, *=P<0.05, **=P<0.01, ****=P<0.0001.

4.3.2. Expression and localization of RecA-msfGFP expression using fluorescence imaging.

Similar to mScarlet-ImuA′, the fluorescence intensities and cell lengths were quantified and averaged across multiple cells of a given strain under different conditions. Again, no strong fluorescence signal was detected for wild-type *Msm* lacking the fluorescent construct **(Fig. 3.18)**; however, low level background fluorescence was detected under all conditions, and this fluorescence signal increased following DNA damage. As before, this background (non-specific) fluorescence was subtracted from all images. When RecA-msfGFP strains were visualised with fluorescence microscopy, RecA-msfGFP expression was observed under both treated and untreated conditions **(Fig. 3.19, 3.20, 3.21A)**, consistent with the multiple roles of

RecA in mycobacterial DNA replication and repair. Decreased expression was observed in untreated RecA-msfGFP strains compared to UV and MMC treated cells which showed an increased msfGFP expression (Fig. 3.21A). Again, there was no discernible difference in fluorescence between UV and MMC treated cells (p=0.6825 for Δ*recA*::*recA-msfGFP* and p=0.0716 for WT::*recA-msfGFP*). However, when the strains were exposed to UV and MMC and visualised with fluorescence microscopy, filamentous cells were observed (Fig 3.18-3.20). When cell length was quantified for each strain and condition, there was a slight difference between UV treated and MMC treated cells (p=0.0130 for Δ*recA*::*recA-msfGFP* and p=0.0013 for WT::*recA-msfGFP*) (Fig. 3.21B).

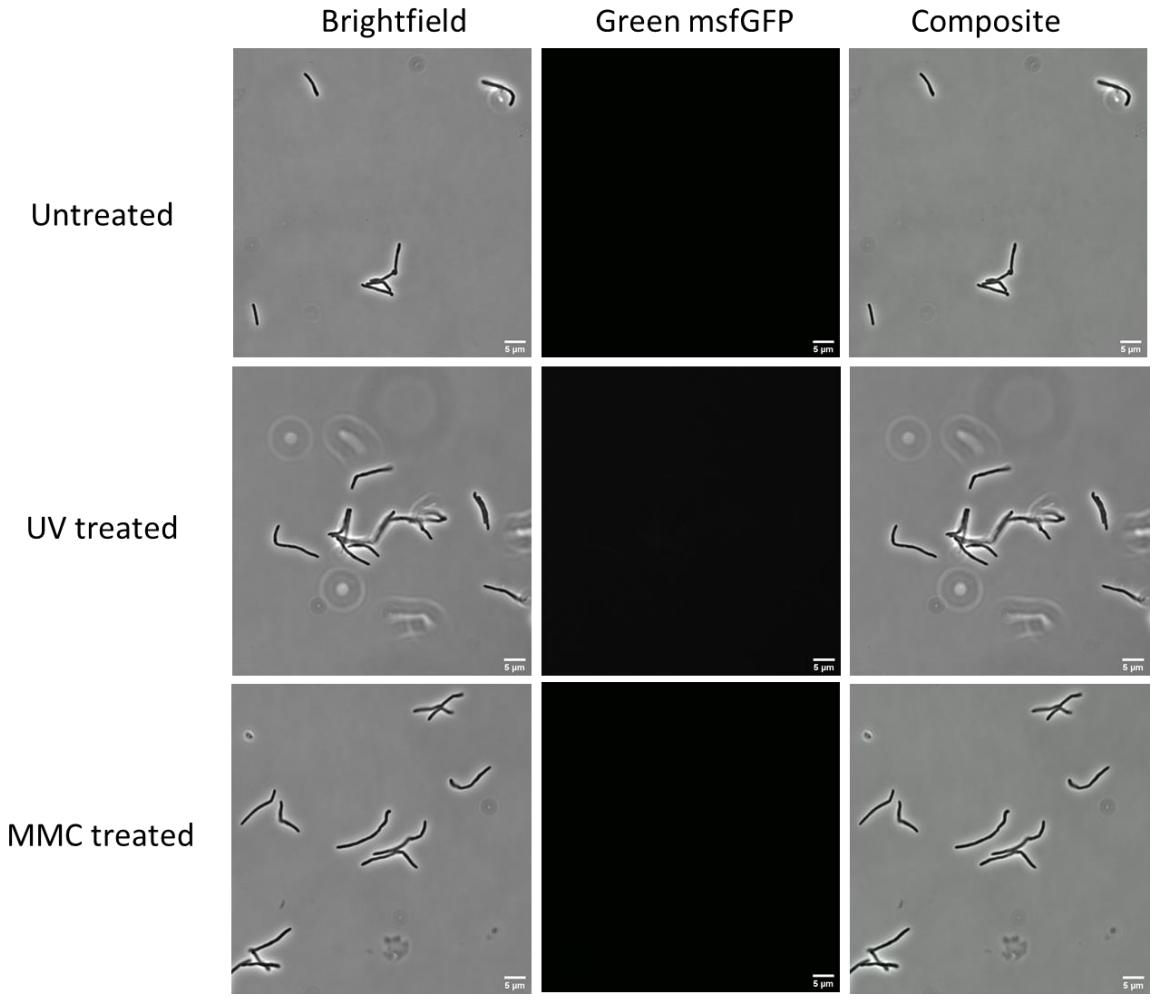

Figure 3.18: Visualisation of WT *Msm* under normal conditions and following genotoxic stress. Cells were untreated, UV-treated and MMC-treated as indicated in the top, middle, and bottom rows, respectively. Left panel illustrates brightfield micrographs of bacilli; middle panel illustrates the green msfGFP fluorescence signal; right panel is a composite of green fluorescence signal and brightfield micrographs. Images are representative of 3 repeats. Scale bars, 5 μm.

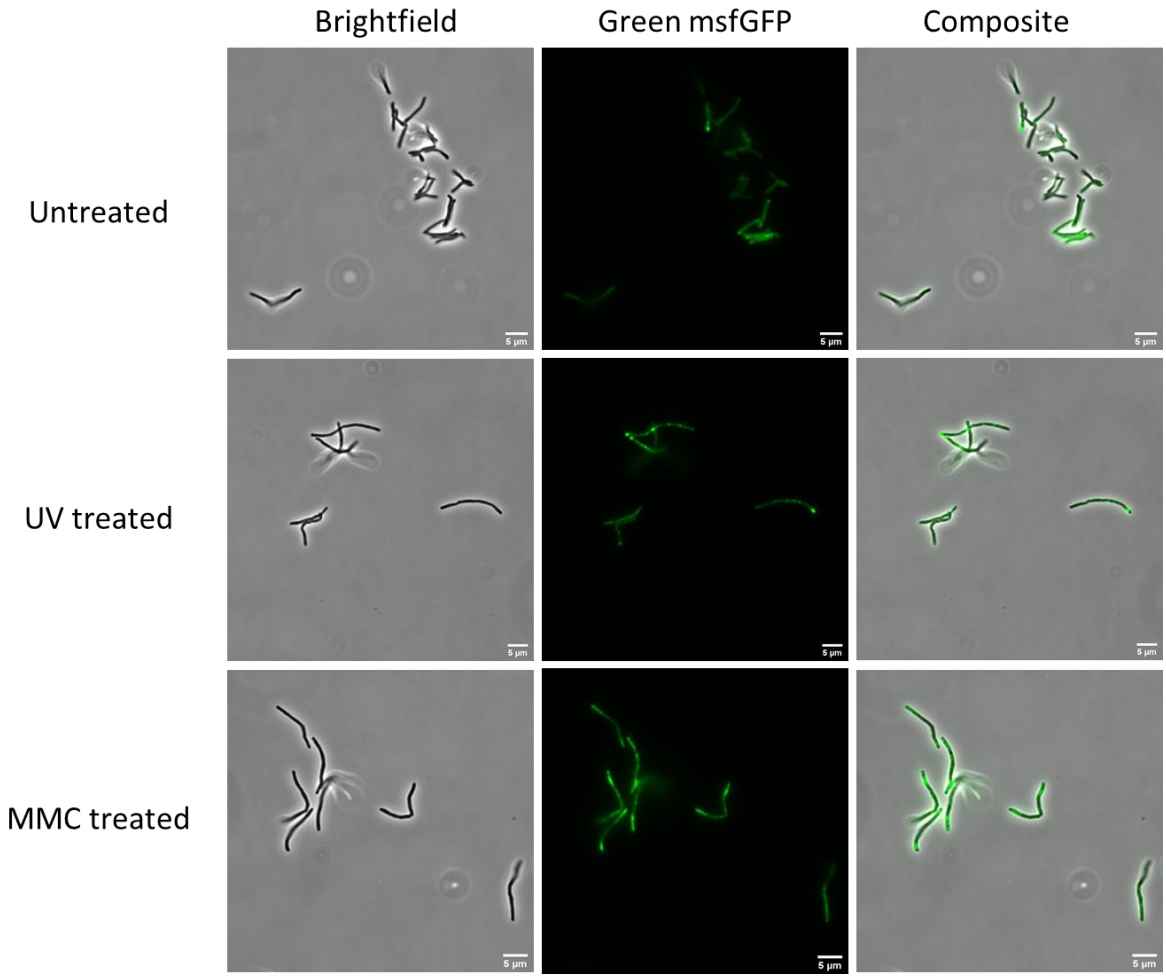

Figure 3.19: Localization of RecA-msfGFP in WT::*recA-msfGFP* under normal conditions and following genotoxic stress. The growth conditions are represented as untreated, UV-treated and MMC-treated by the top, middle, and bottom rows, respectively. Left panel illustrates brightfield micrographs of bacilli; middle panel illustrates the green msfGFP fluorescence signal; right panel is a composite of green fluorescence signal and brightfield micrographs. Images are representative of 3 repeats. Scale bars, 5 μm.

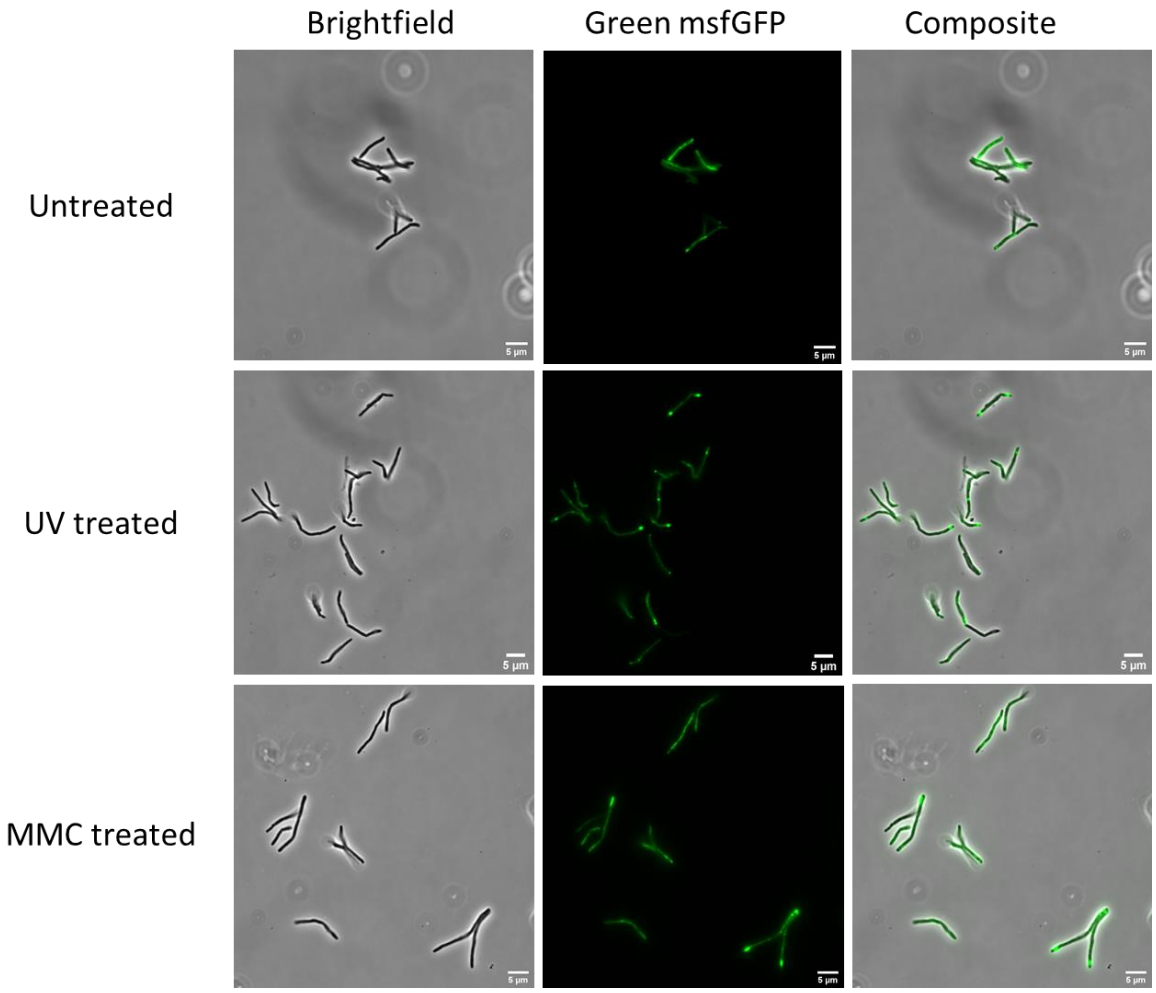

Figure 3.20: Localization of RecA-msfGFP in *Msm* Δ*recA*::*recA-msfGFP* under normal conditions and following genotoxic stress. The growth conditions are represented as untreated, UV treated and MMC treated by the top, middle, and bottom rows, respectively. Left panel illustrates brightfield micrographs of bacilli; middle panel illustrates the green msfGFP fluorescence signal; right panel is a composite of green fluorescence signal and brightfield micrographs. Images are representative of 3 repeats. Scale bars, 5 μm.

To determine whether exposure to UV or MMC influences RecA focus formation, the number of foci formed per cell was quantified in untreated WT::*recA-msfGFP* and Δ*recA*::*recA-msfGFP* **(Fig. 3.22A)**. As a control, the *Msm* WT strain was visualised under the same conditions and as expected, no foci were observed within WT cells. Small numbers (3.28, 3.33) of msfGFP-RecA foci were observed in the untreated reporter mutants, WT::*recA-msfGFP* and Δ*recA*::*recA-msfGFP*. In contrast, elevated numbers of RecA foci were observed following both MMC (6.67 and 6.60 foci per cell for WT::*recA-msfGFP* and Δ*recA*::*recA-msfGFP*, respectively) and UV (6.46 and 6.52 foci/cell, respectively) treatments **(Fig. 3.22A)**. It was also observed that, when the RecA-msfGFP was exposed to UV and MMC, the foci formed within the cells were larger in size (p=0.3479 and p=0.1547 for Δ*recA*::*recA-msfGFP* and WT::*recA-*

msfGFP, respectively) compared to those in untreated conditions **(Fig 3.22B)**. Similar to mScarlet-ImuA′ expressing strains, there was increased filamentation following UV and MMC treated conditions **(Fig. 3.21 B)**. To determine if there was a relationship between cell length and the number of foci, a Spearman correlation analysis was performed. Although the number of foci increased when cells were exposed to both UV and MMC, there was weak to very little correlation between cell length and number of foci in both RecA-msfGFP strains **(Fig. 3.23A, B)**.

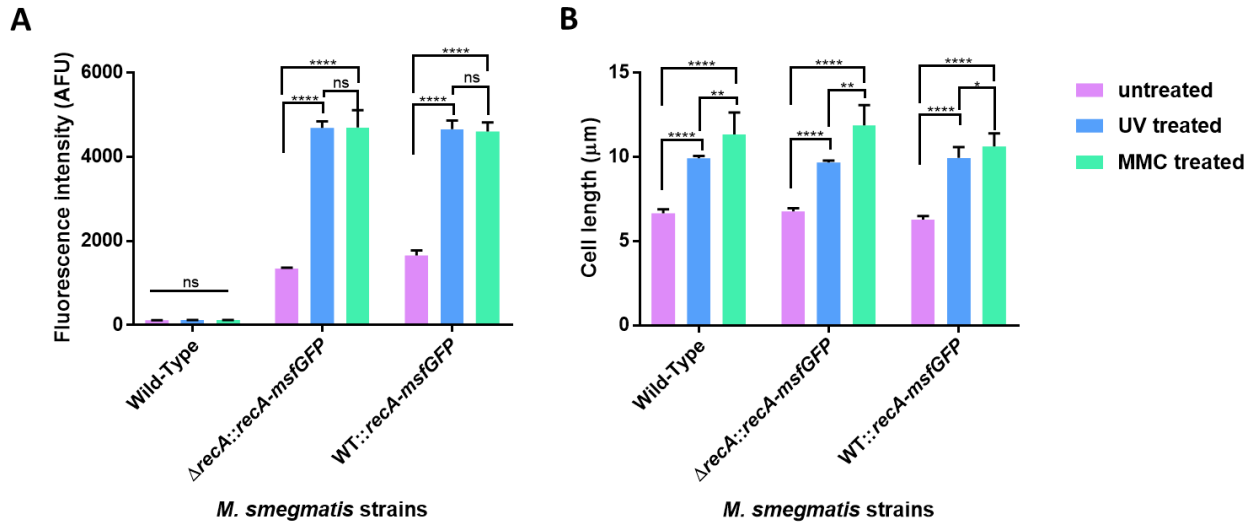

Figure 3.21: Quantification of fluorescence intensities and cell lengths in *Msm* RecA-msfGFP reporter strains. A. Fluorescence intensities and **B.** cell lengths were determined for WT, WT::recA-msfGFP and ΔimuA′::recA-msfGFP before treatment (pink), after UV treatment (blue) and after MMC exposure (green). Data represent an average of three independent experiments in which 50 to 150 cells were counted per strain: ns=non-significant, *=P<0.05, **=P<0.01, ****=P<0.0001.

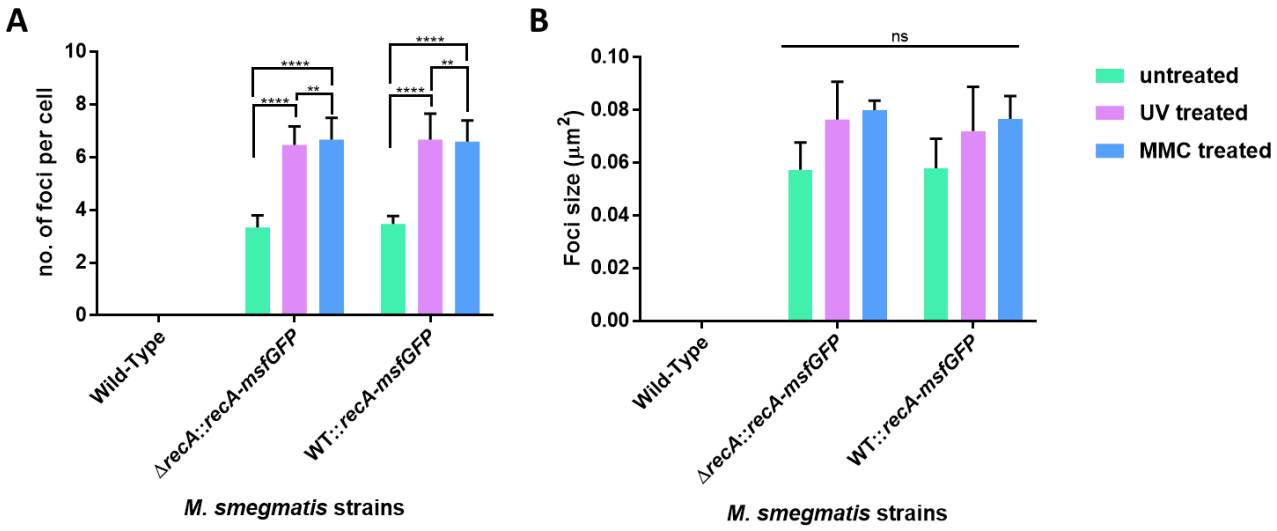

Figure 3.22: Quantification of RecA focus formation. A. The number of RecA foci and **B.** size of RecA foci was determined in WT, WT::recA-msfGFP and ΔrecA::recA-msfGFP strains before treatment (green), after exposure to UV (pink) and following MMC treatment (blue). Data represent an average of three independent experiments in which 50 to 150 cells were counted per strain: ns=non-significant, **=P<0.01, ****=P<0.0001.

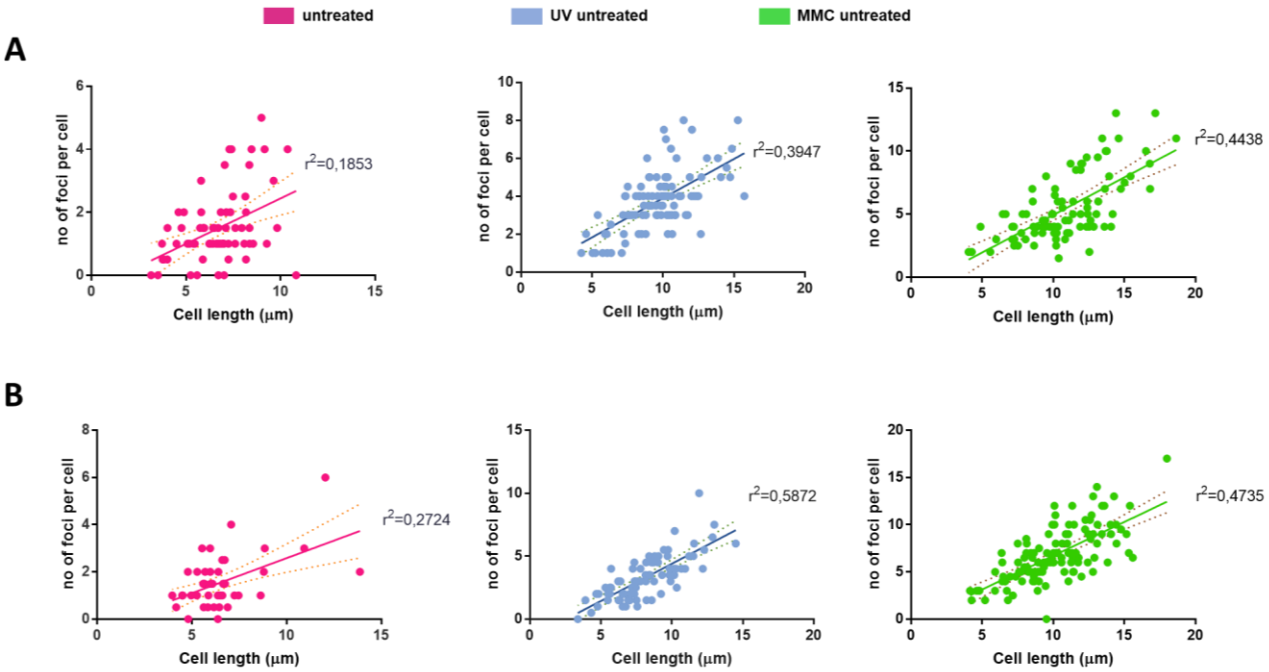

Figure 3.23: Quantification of RecA focus formation and cell length. Correlation plots for number of RecA foci and cell length were determined in **A.** ΔrecA::recA-msfGFP and **B.** WT::recA-msfGFP strains before treatment (pink), after exposure to UV (blue) and following MMC treatment (green). Data represent an average of three independent experiments in which 50 to 150 cells were counted per strain.

4.3.3. Dual mScarlet-ImuA′ and RecA-msfGFP expression using fluorescence imaging.

To determine the localization patterns of mScarlet-ImuA′ and RecA-msfGFP in the same cells, mScarlet-ImuA′ and RecA-msfGFP were electroporated into Δ*recA*::*recA-msfGFP* and Δ*imuA′*::*mScarlet-imuA′*, respectively. Consistent with the RecA-msfGFP strains, both Δ*imuA′*-T*mScarlet-imuA′*::P*recA-msfGFP* **(Fig. 3.24)** and Δ*recA*-P*recA-msfGFP*::T*mScarlet-imuA′* **(Fig. 3.25)** strains showed green, fluorescent signal with distinct foci under normal untreated conditions. As expected, an increase in expression of both RecA-msfGFP and mScarlet-ImuA′ was observed when the cells were exposed to either UV or MMC, and this was visible as a combination of red diffuse fluorescent signal and green, fluorescent signal with multiple clearly defined foci **(Fig. 3.24, 3.25, 3.26A and B)**. Again, for both constructs in both strains (Δ*imuA′*-T*mScarlet-imuA′*::P*recA-msfGFP* and Δ*recA*-P*recA-msfGFP*::T*mScarlet-imuA′*), there was a slight difference in fluorescence signal between UV-treated (p= 0.0134 and p= 0.0037, respectively) and MMC-treated cells (p=.0.0009 and p=0.0003, respectively).

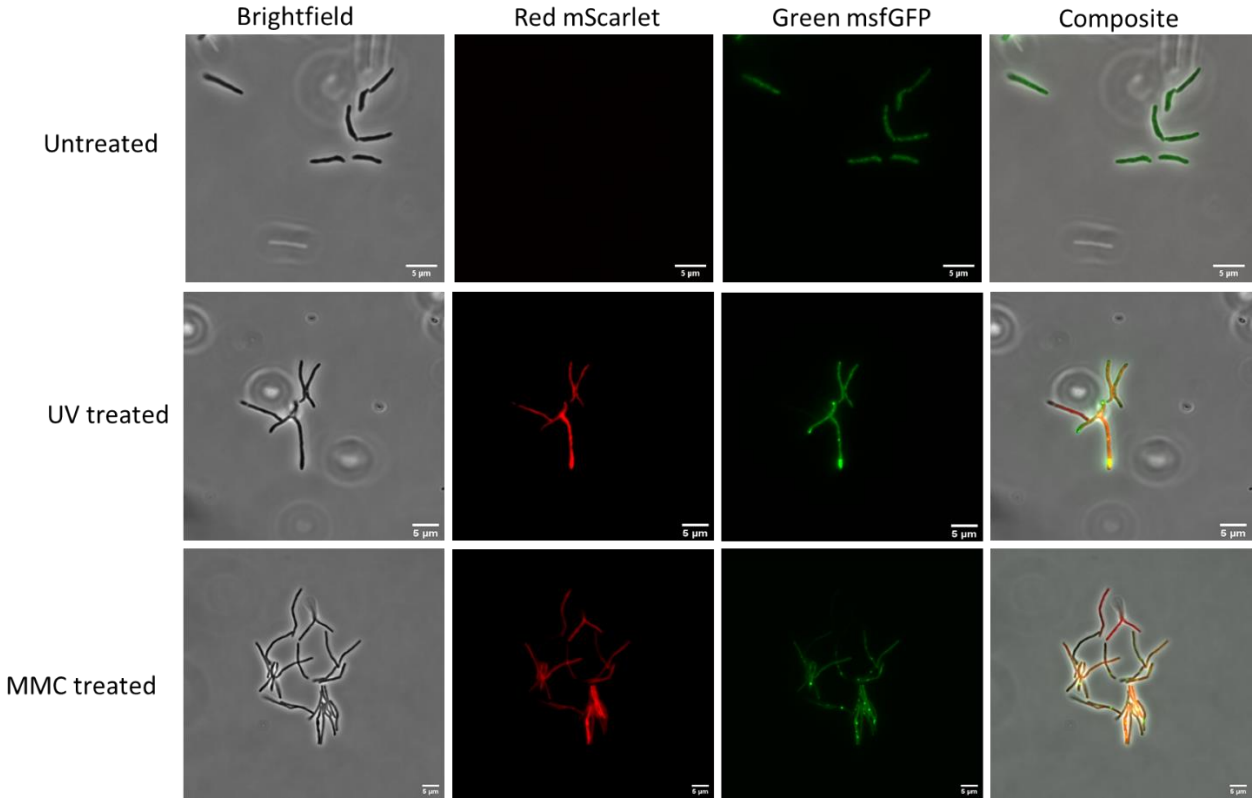

Figure 3.24: Localization of RecA-msfGFP and mScarlet-ImuA′ in *Msm* Δ*imuA′*-T*mScarlet-ImuA′*::P*recA-msfGFP* under normal conditions and following genotoxic stress. The growth conditions are represented as untreated, UV treated and MMC treated by the top, middle, and bottom rows, respectively. First panel illustrates brightfield micrographs of bacilli; second panel illustrates the green mScarlet fluorescence signal; third panel illustrates

the green msfGFP fluorescence signal and last panel is a composite of green fluorescence signal, red fluorescence and brightfield micrographs. Images are representative of 3 biological repeats. Scale bars, 5 μm.

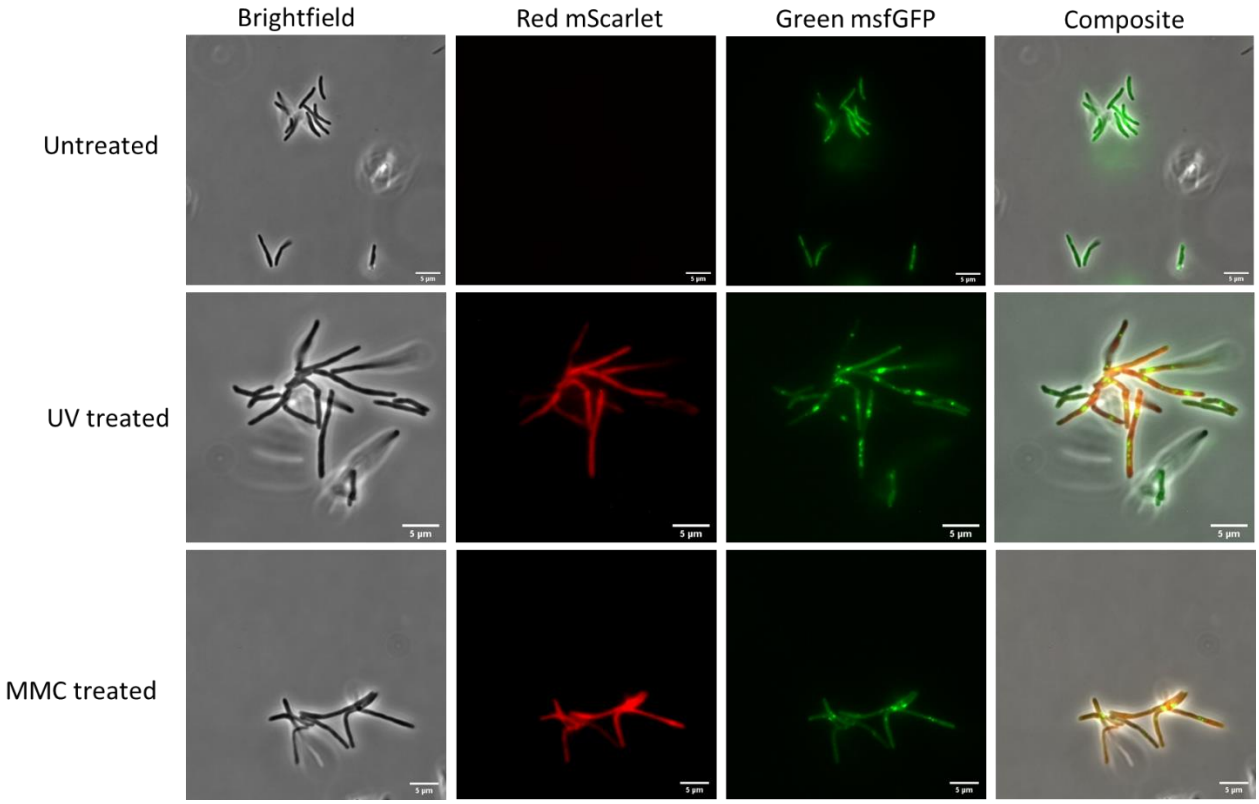

Figure 3.25: Localization of RecA-msfGFP and mScarlet-ImuA′ in *Msm* Δ*recA*-P*recA*-*msfGFP*::T*mScarlet-imuA′* under normal conditions and following genotoxic stress. The growth conditions are represented as untreated, UV treated and MMC treated by the top, middle, and bottom rows, respectively. First panel illustrates brightfield micrographs of bacilli; second panel illustrates the green mScarlet fluorescence signal; third panel illustrates the green msfGFP fluorescence signal and last panel is a composite of green fluorescence signal, red fluorescence and brightfield micrographs. Images are representative of 3 biological repeats. Scale bars, 5 μm.

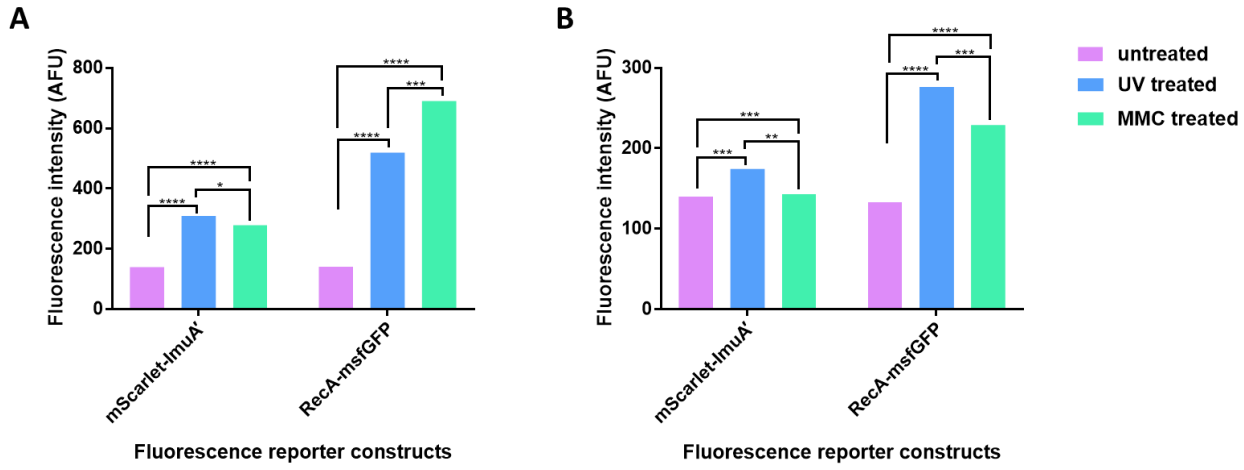

Figure 3.26: Quantification of fluorescence intensities in *Msm* reporter strains. Fluorescence intensities were determined for **A.** ΔimuA′::mScarlet-imuA′(recA-msfGFP), and **B.** ΔrecA::recA-msfGFP(mScarlet-imuA′) before treatment (pink), after UV treatment (blue) and after MMC exposure (green). Data for represent an average of a single, in which 50 to 150 cells were counted per strain. *=P<0.05, **=P<0.01, ***=P<0.001, ****=P<0.0001.

Similar to the single RecA-msfGFP strains, an increase in number of foci within cells was observed when bacilli were exposed to UV and MMC compared to untreated cells **(Fig. 3.27A)**. As expected, when the strains were exposed to UV and MMC, filamentous cells were observed which were not evident in untreated cells **(Fig. 3.27B)**. To determine if there was a correlation between the intensity of the two constructs, Spearman correlation plots were generated. No correlation was observed between RecA-msfGFP and mScarlet-ImuA′ fluorescent signal when Δ*imuA′*-T*mScarlet-ImuA′*::P*recA-msfGFP* was exposed to different conditions **(Fig. 3.28A)**. However, when Δ*recA*-P*recA-msfGFP*::T*mScarlet-imuA′* was exposed to UV and MMC, a stronger correlation was observed **(Fig. 3.28B)**.

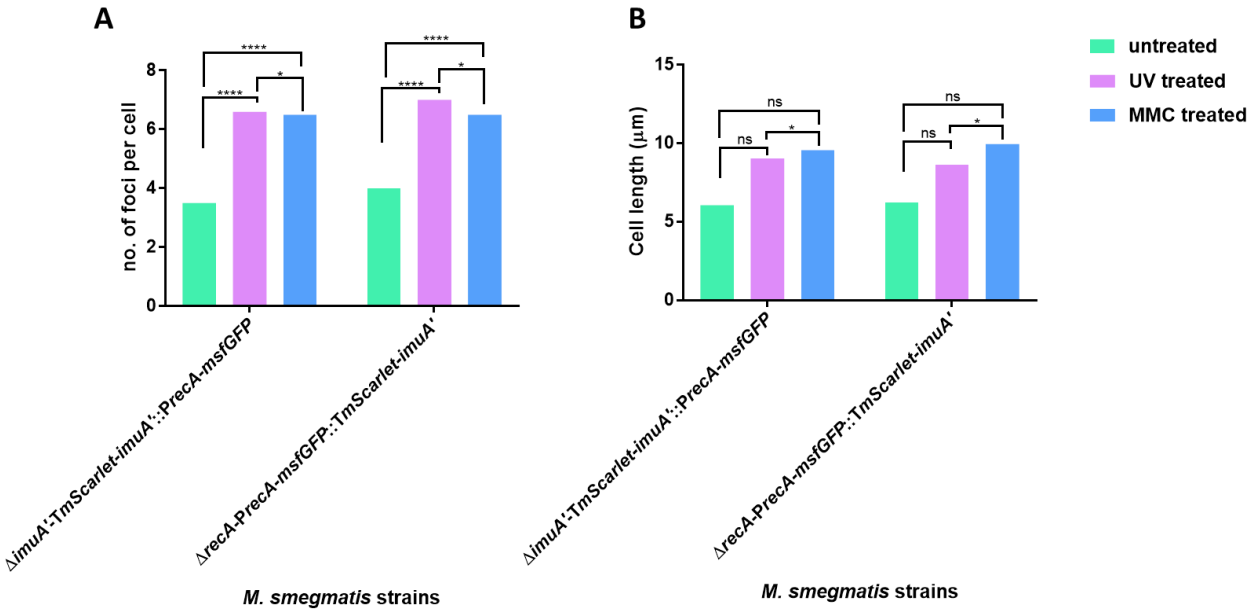

Figure 3.27: Quantification of RecA focus formation and cell length. **A.** The number of RecA foci and **B.** cell length was determined in WT, WT::recA-msfGFP and ΔrecA::recA-msfGFP strains before treatment (green), after exposure to UV (pink) and following MMC treatment (blue). Data represent a single experiment in which 50 to 150 cells were counted per strain: ns=non-significant, *=P<0.05, ****=P<0.0001.

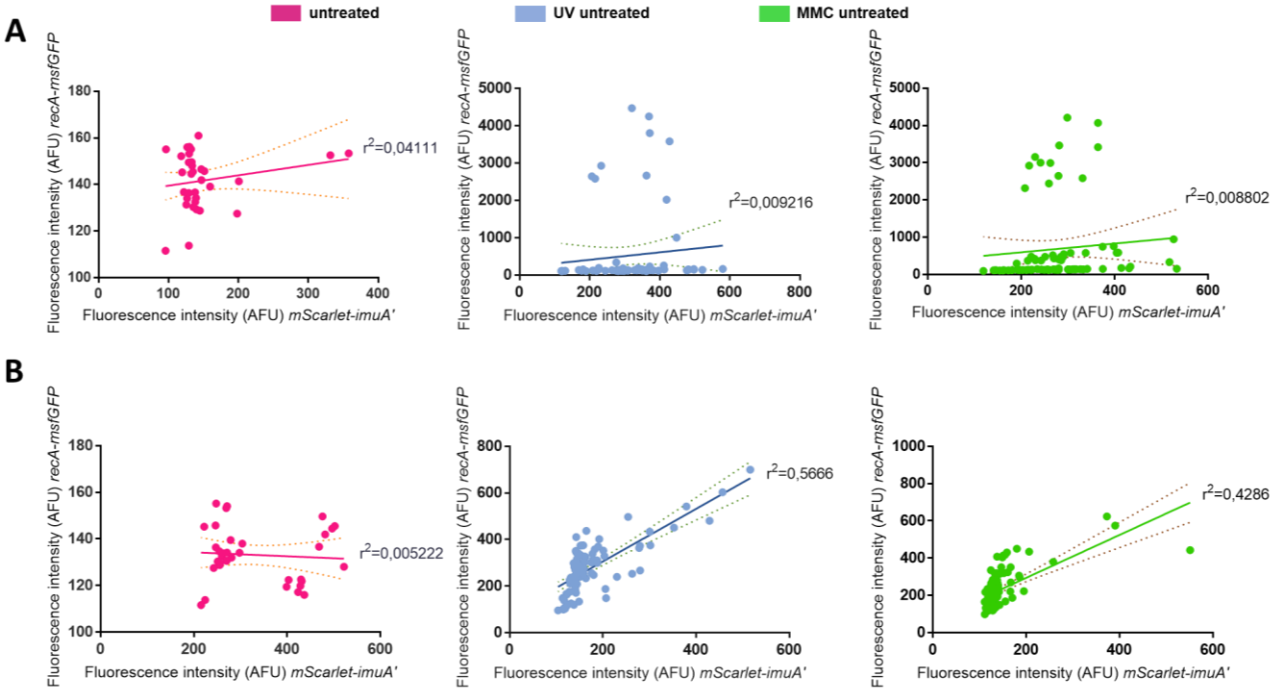

Figure 3.28: Quantification of fluorescence intensities in dual complementation strains. Correlation plots for RecA-msfGFP and mScarlet-ImuA′ fluorescence intensities were determined in **A.** ΔimuA′::mScarlet-imuA′(recA-msfGFP) and **B.** ΔrecA::recA-msfGFP(mScarlet-imuA′) strains before treatment (pink), after exposure to UV (blue) and following MMC treatment (green). Data represent a single experiment in which 50 to 150 cells were counted per strain.

5. Discussion.

Mycobacteria employ different mechanisms in response to DNA damaging conditions and the timing and potential hierarchies of pathway usage and DNA damage selectivity (*i.e.*, which repair pathways are preferentially invoked for different lesion types) remain to be determined. In the classical SOS response pathway regulated by RecA and LexA (Brooks et al., 2001, Smollett et al., 2012), RecA functions to orchestrate the response to DNA damage by releasing expression of the genes repressed by LexA. In addition to its role in regulating LexA, RecA has also been implicated in other major pathways such as homologous recombination repair at sites of single-strand gaps and DSBs (Little and Mount, 1982, Lusetti and Cox, 2002, Robinson et al., 2015, Sassanfar and Roberts, 1990). Included in the SOS regulon is ImuA′, a protein of unknown function which forms part of the ImuA′/ImuB-DnaE2 mutasome (Warner et al., 2010). Mycobacterial ImuA′ is distantly homologous to *E. coli* RecA at a structural level but lacks the C-terminal RecA-like ATP binding motif, suggesting that it is unable to bind DNA (Datta et al., 2003b). The distinct C-terminal region of ImuA′ serves to interact with ImuB in induced mutagenesis (Warner et al., 2010), suggesting a regulatory role analogous to the C-terminal RecA domain which, when deleted, enhances RecA function (Cox, 2007). To gain a better understanding of the localization of ImuA′ and RecA in the mycobacterial DNA damage response, we designed reporter constructs comprising translational fusions of spectrally compatible fluorescent tags to our proteins of interest: RecA and ImuA′. Expression and localization of the reporters were determined following exposure to DNA damaging treatments, UV irradiation and MMC.

A similar approach was previously pursued in our laboratory in which VFP-ImuA′ was visualised (Reiche, 2018)(Gessner, Martin, Reiche *et al*., in preparation). Using VFP-ImuA′, diffuse localization was observed, however this diffuse signal was confounded by a low signal to noise ratio. Therefore, in this study, ImuA′ was fused to mScarlet owing to its bright red fluorescent expression (Bindels et al., 2017). The *mScarlet-imuA′* construct was designed in a similar way to the previously reported VFP-ImuA′ (Reiche, 2018). Here, the *imuA′* promoter and first two codons of *imuA′* were placed at the beginning of the mScarlet encoding gene. The mScarlet stop codon was removed at the end of the tag to allow uninterrupted translation of *imuA′* and *mScarlet* as a fusion protein. In addition to ImuA′, RecA was tagged using a modified GFP known as the monomeric super folder GFP (msfGFP) based on previous studies (Ghodke

et al., 2019, Renzette et al., 2005). According to prior observations in other bacteria (Ghodke et al., 2019, Renzette et al., 2005), a C-terminal fusion was designed to avoid interfering with the folding of RecA. To design the C-terminal fusion, the RecA stop codon was removed at the end of *recA* and placed at the end of the msfGFP encoding gene. The tagged fluorescent protein encoding constructs were cloned into two different integrating plasmids that target different *attB* integration sites, thus allowing them to be integrated into a single *Msm* genome at the same time.

The use of fluorescent proteins is associated with many challenges; for example, the bulky fluorophore could disrupt (or eliminate) the function of the tagged protein, in turn interfering with the normal biological processes of the cell (Carter et al., 2014). We were able to investigate whether the fluorescent proteins disrupt the functions of the proteins since cells lacking *recA* (Ghodke et al., 2019, Keyamura et al., 2013, Renzette et al., 2005) and *imuA′* (Warner et al., 2010) are hypersensitive to DNA damage. Therefore, we introduced the fusion proteins into strains lacking *imuA′* (Δ*imuA′*) and *recA* (Δ*recA*), respectively. To test whether the fusion constructs retained native protein function, UV-induced mutagenesis and MMC damage sensitivity of Δ*recA* and Δ*imuA′* and complemented strains were evaluated. *Msm* cells that were lacking the RecA and ImuA' proteins were highly sensitive to DNA damage and showed reduced induced mutagenesis, consistent with previous observations (Boshoff et al., 2003, Gupta et al., 2011, Warner et al., 2010). In Δ*imuA′*::*mScarlet-imuA′* and Δ*recA*::*recA-msfGFP*, the tagged proteins were able to restore induced mutagenesis to wild-type levels, suggesting that the tags do not interfere with normal protein function in induced mutagenesis. However, when the mScarlet-ImuA' complemented strain (Δ*imuA′*::*mScarlet-imuA′*) was exposed to MMC, which induces DNA damage by causing DNA inter-strand and intra-strand crosslinks (Tomasz et al., 1988), the bioreporter exhibited growth which phenocopied the *imuA′* knockout, suggesting a failure to complement loss of ImuA′ function. Similar results were obtained in a previous study, where VFP-ImuA′ failed to complement Δ*imuA′* in MMC damage sensitivity assays but appeared to fully complement loss of ImuA′ function in UV-induced mutagenesis assays (Reiche, 2018). The results presented here are therefore important in establishing the reproducibility of this observation – in which complementation is achieved for induced mutagenesis but not MMC tolerance – and for confirming that these (discrepant) complementation phenotypes are not attributable to a particular fluorophore. Instead, the results

imply the possible disruption a key protein-protein interaction(s) required for MMC damage tolerance.

Analogous to the imuA' results, when the RecA-msfGFP complemented strains were exposed to MMC, Δ*recA*::RecA-msfGFP largely phenocopied the Δ*recA* knockout, exhibiting hypersensitivity to MMC. This finding could be explained by previous reports that fluorescent protein fusions to RecA have resulted in reduced RecA functionality (Ghodke et al., 2019, Renzette et al., 2005). The reason the fusion protein can complement loss of function in one assay but not the other is unclear. However, one possible explanation could be that, in the induced mutagenesis assay, cells are exposed to UV irradiation transiently and allowed to recover before plating on Rif-containing media whereas, in damage tolerance, the cells are exposed to MMC throughout the duration of the experiment; that is, exposure to the DNA damaging agent is prolonged for MMC. Additionally, it is important to remember that the nature of lesion caused by UV *versus* MMC differs, with UV producing pyrimidine dimers (Janion, 2008) and MMC resulting in inter- and intra-strand DNA crosslinks (Tomasz et al., 1988). In this context, it is interesting to note that the *mScarlet-imuA'* allele restored wild-type UV sensitivity to the imuA' mutant, suggesting that repair/tolerance of this type of lesion was unaffected by the fluorescently tagged protein.

Alternatively, it's possible that the fluorescent tag blocks protein-protein interactions that are essential for damage tolerance but not mutagenesis. Although tantalising, this latter notion is speculative, and more work is required to test this possibility. It was notable that the presence of a WT copy of *imuA'* seemed to have an impact on the protein function. When the fusion construct was introduced into a WT strain (as opposed to Δ*imuA'*), it appeared to be much more sensitive to MMC compared to all the other strains including the Δ*imuA'* strain. Similar to the inhibitory/toxic effect in WT::*mScarlet-imuA'*, the WT::*recA-msfGFP* showed growth like WT at 0.1× MIC MMC but was highly sensitive to MMC at a higher concentration, presenting a phenotype which more closely resembled the Δ*recA* strain. This finding was unexpected since wild-type copy of the protein is present and expected to function at WT level. It is possible that there is some interaction between the WT protein and the tagged version which eliminates the function of both. However, the reason these strains have impaired growth remains unclear.

The strains were then exposed additional DNA-damaging agents to extend the results obtained in the MMC tolerance assay. The DNA-damaging agents that were selected had different

mechanisms of action which could explain the different phenotypes observed. Ofx and Mox are, respectively, second- and third-generation fluoroquinolones which block DNA replication by binding to DNA gyrase, inhibiting its DNA unwinding activity (Drlica and Zhao, 1997, Reece and Maxwell, 1991); Nfz induces lethal N2-deoxyguanosine adducts and lethal DNA lesions (Jarosz et al., 2006); Nov is a coumarin which, like. Fluoroquinolones inhibit DNA gyrase but by a different mechanism that targets gyrase B (GyrB) action (Chopra et al., 2012); and UV irradiation causes DNA lesions which result in cyclobutene pyrimidine and pyrimidine 6-4 photoproducts (Janion, 2008). Exposure to most of these additional agents showed that all the tested strains phenocopied WT, including the deletion strains. This finding indicates that, although putatively sampling different lesion types, the different genotoxic agents were not useful in revealing additional insights into differential functional complementation of the fusion proteins. Future work could, however, explore the use of 2-fold spotting dilutions to increase the potential to identify differences in sensitivity, albeit subtle.

With the objective of visualising the location of mScarlet-ImuA′ and RecA-msfGFP in *Msm* live cells, the fluorescent protein expressing strains were imaged using fluorescence microscopy. To gain insight into the level of background fluorescence, WT cells that were not expressing the fluorescent proteins were also treated and analysed. The fluorescent signal detected in WT cells was regarded as noise and was used to normalise fluorescence signals derived from the fluorescent protein expressing strains. As expected, the expression levels of ImuA′ during normal growth were too low to detect any fluorescence signal in both Δ*imuA′* and WT *Msm* strains. However, after exposure to MMC and UV irradiation, when *imuA′* expression is induced, diffuse red fluorescent signal was detected at a level above that observed for the WT control. These findings are consisted with those reported previously in our laboratory using the VFP-tagged ImuA′ reporter (Reiche, 2018), suggesting that the observation is not the artefact of the fluorescent tag. Again, there were no distinct foci or regions of dense mScarlet-ImuA′ localisation. Moreover, there was no difference in fluorescence intensity or visible localization when the cells were exposed to either UV irradiation or MMC. When the *Msm* strains were exposed to UV and MMC treatment, increased cell lengths were observed compared to cells that were grown in normal untreated conditions. The formation of the filamentous cells is likely due to SOS induction, so that exposure to UV and MMC inhibits cell division, resulting in growth without division.

Previous work in *E. coli* has demonstrated ten-fold upregulation of *recA* expression within minutes in cells exposed to DNA damage (Renzette et al., 2005). When RecA was C-terminally fused to GFP and placed under the *recA* native promoter, distinct localization was observed in the form of GFP foci (Lesterlin et al., 2014, Renzette et al., 2005). Visualization of RecA in response to SOS induction in live *E. coli* cells revealed that, under normal conditions that are not damaging to DNA, RecA is largely concealed in DNA-free aggregates known as storage structures (Ghodke et al., 2019). Following exposure of the bacteria to UV irradiation, the storage structures dissolve and cytosolic RecA nucleates on DNA to form early SOS signalling complexes that later form long thread-like structures termed RecA bundles. Upon completion of repair, RecA storage structures re-form (Ghodke et al., 2019). Given this observation in *E. coli*, it would be really useful to see if mycobacterial RecA is similarly confined in storage structures which dissolve to allow formation of nucleoprotein filaments during DNA damage. However, this will require further investigations using time-lapse microscopy as well as possible single-molecule tracking. Like *E. coli*, RecA-msfGFP foci were visible during normal growth in all the RecA-msfGFP expressing strains. These findings suggest that, even in the absence of externally induced DNA damage, RecA is sequestered. An increase in fluorescence intensity, number of RecA-msfGFP foci, and RecA-msfGFP foci size were observed following DNA damage induced by both UV and MMC, consistent with the fact that RecA forms part of the SOS response. The observed increase in RecA-GFP foci for the treated strains is hypothesised to be due to an increased level of RecA that is recruited within the cell when the bacterium is exposed to DNA damage compared to when the bacterium is growing under normal conditions. A previous study indicated that RecA expression was distributed throughout the cells, becoming more intense when cells were exposed to DNA damaging agents (Manina et al., 2019). However, there was no visible difference in fluorescence intensity or the number of foci following treatment with UV and MMC, which would suggest that RecA gets recruited in a similar manner following different types of DNA damage. Seeing as filamentation is a result of the SOS response, it raised a question as to whether there is a relationship between cell length and number of foci formed within cells. From this analysis we were able to determine that, although number of foci increased following treatment, there was weak correlation between cell length and number of foci. This suggests that longer filamentous cells don’t necessarily have more foci than shorter cells.

A recent study in *M. xanthus* determined that ImuA interacts with RecA1, suggesting that both proteins are involved in TLS (Sheng et al., 2020). Since ImuA lacks DNA-binding loops as well as N-terminal of RecA, ImuA appeared to interact with DNA through RecA1 (Sheng et al., 2020). Moreover, an increasing concentration of ImuA decreased formation of RecA nucleoprotein filaments, implying ImuA-mediated inhibition of RecA filament formation (Sheng et al., 2020). This finding suggests that ImuA binds to RecA1 preventing filament extension, inhibiting RecA-mediated recombination and template switching while improving DnaE2-induced mutagenesis; that is, there appears to be competition between the two proteins (Sheng et al., 2020). In our study, we introduced RecA-msfGFP and mScarlet-ImuA′ to Δ*imuA′*::*mScarlet-ImuA′* and Δ*recA*::*recA-msfGFP*, respectively, to determine the localization patterns of ImuA′ and RecA at the same time in a single cell. Fluorescence signal was observed when both strains were exposed to UV and MMC. mScarlet-ImuA′ was associated with bright red diffuse signal, whereas RecA-msfGFP was associated with green signal which, although diffuse, showed definite localization hotspots in the form of focus formation. The observation that both proteins were expressed following exposure to MMC, and UV was expected. However, the diffuse nature of mScarlet-ImuA′ expression made it difficult to ascertain whether there was any true colocalization of the two proteins. Consistent with a high level of heterogeneity often associated with mycobacterial cells (de Wet et al., 2020), fluorescence signal was observed for only one construct (either mScarlet-ImuA′ or RecA-msfGFP) in some. cells. However, in both backgrounds, mScarlet-ImuA′ fluorescent signal was reduced compared to RecA-msfGFP signal and a slight difference was observed between UV and MMC treated cells with both constructs.

An interesting observation was that the fluorescent intensities of the fusion proteins in these strains was much lower compared to those with single fusion proteins. It was also notable that the fusion proteins gave different significantly different results in different backgrounds. One could speculate that both fusion proteins in one cell causes the SOS response to be reduced. Similar to previous observations (Sheng et al., 2020), it's possible that the presence of the extra *imuA′* could inhibit the activity of RecA in the dual construct strains, resulting in much lower fluorescence signal of RecA-msfGFP compared to single construct strains (RecA-msfGFP strains). As expected, RecA signal was expressed under normal conditions, whereas ImuA′ signal was not detected. Interestingly, when the strains were evaluated to determine if there was any correlation between the fluorescence intensity of the constructs in each strain, it was observed that there was a weak correlation in fluorescence intensity following treatment in one

strain and not the other. A key limitation of the work presented in this dissertation is that the results were determined solely from end-point microscopy. Future work should include time-lapse experiments in which expression dynamics can be monitored in real-time to see how foci or structures are altered in response to treatment.

6. Conclusions.

RecA and ImuA′ are SOS-inducible proteins that have been shown to be involved damage tolerance in *Mtb*. RecA plays a central role in regulating the SOS response and ImuA′ forms part of the mycobacterial mutasome which has been shown to elevate mutation rates in stressed cells. Mycobacterial ImuA′ is distantly related to RecA which suggest that it may play a role in DnaE2-mediated mutasome, similar to that described for *E. coli* in activating PolV ($UmuD'_2C$) mutasome. However, it lacks the C-terminus region responsible for binding ssDNA, the conserved ATPase core domain and the ability to self-associate. Despite these differences, ImuA may play an analogous role to RecA (activating PolV in *E. coli*) in activating the TLS polymerase DnaE2 in mycobacteria. However, since ImuA was not seen to directly interact with DnaE2, its role in DnaE2 catalysed TLS may not entirely resemble that of RecA in PolV system. This suggests that ImuA may have evolved from RecA, losing sites required for homologous recombination and not those needed in TLS. Mycobacterial mutasome components ImuA′, ImuB and DnaE2 have been of great interest in our research group. It is interesting that ImuA′ shows weak homology to RecA which together with PolV forms the mutasome in *E. coli*. However, *E. coli* lacks ImuA and, since mycobacteria have both ImuA′ and RecA, how these two proteins functions together in the same cell is unknown.

In this study, we constructed fluorescently tagged versions of the DNA damage response proteins ImuA′ and RecA. mScarlet-ImuA' and RecA-msfGFP were shown to mostly retain WT protein function. However, the presence of the fluorescently labelled protein seemed to have an inhibitory/toxic effect in the presence of a WT copy. Future studies should investigate why the fluorescently tagged proteins appear to interfere with the function, rendering even wild-type cells sensitive to damage. Additionally, future work should also be aimed at investigating why the two protein functionality assays (DNA damage-induced mutagenesis and DNA damage tolerance) exhibit different results. We observed that mScarlet-ImuA′ was induced in response to DNA damaging conditions, whereas RecA-msfGFP was expressed without DNA damage but highly induced when exposed to DNA damage, consistent with previously reported expression data. The diffuse nature of mScarlet-ImuA′ makes it difficult to make any conclusions about recruitment and localizations patterns; more sensitive approaches like single molecule tracking will have to be explored. Unlike mScarlet-ImuA′, RecA-msfGFP visibly gets recruited into foci, even in the absence of DNA damage. These foci clearly increase

in number and fluorescent intensity following DNA damage. Future work will be aimed at tracking RecA-msfGFP in the presence of DNA damage markers and/or other genotoxic agents and visualising the cells using time-lapse microscopy.

Appendices

Appendix 1: Culture media

1. 2TY broth media
    - 4 g NaCl
    - 10 g yeast extract
    - 16 g tryptone
    - 1000 ml dH_2O
    - Autoclave and store at RT

2. 7H10 agar
    - 19 g Difco™ Middlebrook 7H10 Agar (BD Biosciences, USA)
    - 5 ml Glycerol (Sigma, USA)
    - 100 ml BBL™ *Middlebrook OADC Enrichment* (BD Biosciences, USA)
    - 900 ml distilled water
    - Autoclave and pour into petri dishes

3. 7H9 broth
    - 4.7g Difco™ Middlebrook 7H10 Agar (BD Biosciences, USA)
    - 2 ml Glycerol (Sigma, USA)
    - 2 ml 25% Tween 80 (Sigma, USA)
    - 100 ml BBL™ *Middlebrook* OADC Enrichment (BD Biosciences, USA)
    - 900 ml distilled water
    - Autoclave and store at 37 °C

4. Luria Bertani Agar media
    - 10 g Bacto™ Tryptone (BD Biosciences, USA)
    - 10 g sodium chloride (Sigma, USA)
    - 15 g Difco™ Yeast Extract (BD Biosciences, USA)
    - 15 g 15 g Bacto™ Agar (BD Biosciences, USA)
    - 1000 ml dH_2O
    - Autoclave and pour into petri dishes

5. Luria Bertani Broth Media
    - 10 g Bacto™ Tryptone (BD Biosciences, USA)
    - 10 g sodium chloride (Sigma, USA)
    - 5 g Difco™ Yeast Extract (BD Biosciences, USA)
    - 1000 ml dH_2O
    - Autoclave and store at RT

Appendix 2: Communal antibiotics

1. Ampicillin (100 mg/ml)
    - 1 g Ampicillin powder
    - 10 ml dH2O
    - Filter sterilize with 0.22 µm filters (Merck Millipore, USA) and store at 4°C

2. Gentamycin (10 mg/ml)
    - 100 mg Gentamycin powder (Sigma, USA)
    - 10 ml dH_2O
    - Filter sterilize with 0.22 µm filters (Merck Millipore, USA) and store at 4°C

3. Kanamycin sulphate (50 mg/ml)
    - 500 mg kanamycin powder (Sigma, USA)
    - 10 ml dH2O
    - Filter sterilize with 0.22 µm filters (Merck Millipore, USA) and store at 4°C

4. Mitomycin C (0.5 mg/ml)
    - mitomycin C from *Streptomyces caespitosus* (Sigma, USA)
    - 4 ml dH2O
    - Filter sterilize with 0.22 µm filters (Merck Millipore, USA) and store at 4°C

5. Rifampicin (200 mg/ml)
    - 1 g Rifampicin powder
    - 5 ml DMSO
    - Store at -20°C

Appendix 3: Communal solutions

1. 5-Bromo-4-chloro-3-indolyl-β-D-galactopyranoside (2% X-gal)
    - 1g X-gal powder
    - 50 ml deionised DMSO
    - Filter sterilize with 0.22 µm filters (Merck Millipore, USA) and store at 4°C

2. Agarose 1%
    - 1 g agarose powder (Sigma, USA)
    - 1x TAE buffer (to make 100 ml)
    - Microwave to dissolve

3. Chloroform-Isoamyl alcohol (24:1)
    - 96 ml Chloroform
    - 4 ml Isoamyl alcohol (to make 100 ml)
    - Store at RT

4. Cetyltrimethylammonium bromide (CTAB)
    - 4.1 g NaCl
    - 10 g CTAB (Sigma)
    - 80 ml dH2O
    - Dissolve at 65 °C and add volume to 100 ml
    - Autoclave and store at RT

5. DNA molecular weight marker
    - 10 µl marker (New England Biolabs, USA)
    - 10 µl loading dye
    - 40 µl distilled water
    - Store at 4 °C

6. dNTPs
    - Deoxyribonucleotide triphosphates - dATPs, dCTPs, dGTPs, dTTPs (200 µM) (New England Biolabs, USA)
    - Store at -20°C

7. Ethanol 70%
    - 7 parts (70 ml) ethanol
    - 3 parts (30 ml) distilled water (to make 100 ml)

8. EDTA (0.5 M)
    - Ethylenediaminetetraacetic acid disodium salt dihydrate.
    - 37.32 g EDTA
    - 100 ml dH_2O and pH to 8.0
    - Add dH_2O to final volume of 200 ml
    - Autoclave and store at RT

9. Ethidium Bromide
    - 200 µl of 10 mg/ml ethidium Bromide concentrated solution (Sigma, USA)
    - 14 ml dH_2O
    - Add a drop to 30-50 ml agarose gel

10. Glucose (1 M)
    - 18.02 g powder (Sigma, USA)
    - 100 ml dH_2O
    - Autoclave and store at RT

11. Glycerol (10%)
    - 10 ml glycerol (Sigma, USA)
    - 90 ml dH_2O (to make 100 ml)

- Autoclave and store at 4 °C

12. Glycerol (66%)
    - 66 ml glycerol (Sigma, USA)
    - 33 ml dH_2O (to make 100 ml)
    - Autoclave and store at RT

13. Isopropanol
    - Obtained from Sigma, USA
    - Store at RT

14. DNA loading dye
    - 0.04 g bromophenol-blue (Sigma, USA)
    - 4.5 ml glycerol (Sigma, USA)
    - 10.5 ml dH_2O
    - Filter sterilize with 0.22 µm filters (Merck Millipore, USA) and store at 4 °C

15. Lysozyme (10 mg/ml)
    - 100 mg lysozyme powder (Sigma, USA)
    - 10 ml dH_2O
    - Store at -20 °C

16. Phenol: Chloroform (1:1)
    - 1-part Phenol (Sigma, USA)
    - 1-part Chloroform (Sigma, USA)
    - Mix and store at 4 °C

17. Potassium Acetate (5 M)
    - 49.08 g potassium acetate powder (Sigma, USA)
    - 100 ml dH_2O
    - Autoclave and store at RT

18. Proteinase K (10 mg/ml)
    - 100 mg proteinase K powder (Sigma, USA)
    - 10 ml dH2O
    - Store at -20°C

19. RNAse (10 mg/ml)
    - 100 mg of RNAse powder
    - 10 ml dH_2O
    - Boil for 10 min at 100 °C
    - Store at -20 °C

20. Sodium Acetate (3 M)
    - 40.82 g sodium acetate titradydrate (Sigma, USA)
    - 80 ml dH_2O
    - Adjust pH to with acetate 5.2
    - Dissolve and add volume to 100 ml
    - Store at RT

21. Sodium Chloride (5 M)
    - 29.22 g NaCl powder (Sigma, USA)
    - 80 ml dH_2O and stir
    - Dissolve at 65 °C and add volume to 100 ml
    - Autoclave and store at RT

22. Sodium Dodecyl Sulphate (10%)
    - 10 g SDS
    - 100 ml dH_2O
    - Heat to dissolve
    - Store at RT

23. Sodium Hydroxide (10 M)
    - 40 g NaOH powder (Sigma, USA)
    - 100 ml dH_2O
    - Autoclave and store at RT

24. Solution I (Lysis buffer)
    - 5 ml 1 M Glucose
    - 2.5 ml 1 M Tris-HCL
    - 2 ml 0.5 M EDTA
    - 90.5 dH_2O
    - Autoclave and store at 4 °C

25. Solution II (Neutralisation buffer)
    - 2 ml 10 M NaOH
    - 10 ml 10% SDS
    - 88 ml dH_2O
    - Filter sterilize with 0.22 µm filters (Merck Millipore, USA) and store at RT

26. Solution III (Precipitation buffer)
    - 60 ml 5 M potassium acetate
    - 11,5 ml glacial acetic acid (Sigma, USA)
    - 28.5 ml dH_2O
    - Store at 4 °C

27. Sucrose (60%)

- 60 g Sucrose powder (Sigma,USA)
- 100 ml dH2O
- Use at a final concentration of 5%
- Autoclave and store at RT

28. Transformation buffer I (TFBI)
    - 0.588 g (30 mM) potassium acetate
    - 2.42 g (100 mM) Rubidium chloride
    - 0.294 g (10 mM) Calcium chloride
    - 2.0 g (50 mM) Manganese chloride
    - 30 ml (15% v/v) Glycerol
    - 200 ml dH_2O
    - pH to 5.8 with dilute acetic acid and filter sterilize

29. Transformation buffer II (TFBII)
    - 0.21 g (10 mM) MOPS
    - 1.1 g (75 mM) Calcium Chloride
    - 0.121 g (10 mM) Rubidium Chloride
    - 15 (15% v/v)
    - 100 ml dH_2O
    - pH to 6.5 with dilute NaOH and filter sterilize

30. Tris-Acetic EDTA (TAE) buffer (50x)
    - 242 g Tris(hydroxymethyl)aminomethane (Sigma, USA)
    - 500 ml dH_2O
    - 100 ml 0.5 M EDTA (pH 8.0)
    - 57.1 glacial acetic acid (Sigma, USA)
    - Adjust volume to 1000 ml with dH2O
    - Store at RT

31. Tris-EDTA (TE) buffer (1x)
    - Make up 1x working solution by mixing 1-part TAE with 49 parts dH2O
    - 1 ml 1 M Tris-HCL
    - 20 µl 0.5 EDTA
    - Adjust volume to 100 ml with dH_2O
    - Store at RT

32. Tris-HCl (1M)
    - 30.6 g Tris
    - 150 ml dH_2O
    - Adjust pH to 8.0 with HCl and add dH_2O volume to 250 ml
    - Autoclave and store @ RT

33. Tween 80 (25%)
    - 25 ml Tween 80

- 75 ml dH_2O
- Heat at 55 °C to dissolve
- Store at RT

References

1. ABELLA, M., CAMPOY, S., ERILL, I., ROJO, F. & BARBÉ, J. 2007. Cohabitation of two different lexA regulons in Pseudomonas putida. *Journal of bacteriology,* 189**,** 8855-8862.
2. ABELLA, M., ERILL, I., JARA, M., MAZÓN, G., CAMPOY, S. & BARBÉ, J. 2004. Widespread distribution of a lexA-regulated DNA damage-inducible multiple gene cassette in the Proteobacteria phylum. *Molecular microbiology,* 54**,** 212-222.
3. ADAMS, L., DINAUER, M., MORGENSTERN, D. & KRAHENBUHL, J. 1997. Comparison of the roles of reactive oxygen and nitrogen intermediates in the host response to Mycobacterium tuberculosis using transgenic mice. *Tubercle and Lung Disease,* 78**,** 237-246.
4. AGASHE, D. 2017. The road not taken: Could stress-specific mutations lead to different evolutionary paths? *PLoS biology,* 15**,** e2002862.
5. ALAM, M. K., ALHHAZMI, A., DECOTEAU, J. F., LUO, Y. & GEYER, C. R. 2016. RecA inhibitors potentiate antibiotic activity and block evolution of antibiotic resistance. *Cell chemical biology,* 23**,** 381-391.
6. ALEKSEEV, A., SERDAKOV, M., POBEGALOV, G., YAKIMOV, A., BAKHLANOVA, I., BAITIN, D. & KHODORKOVSKII, M. 2020. Single-molecule analysis reveals two distinct states of the compressed RecA filament on single-stranded DNA. *FEBS letters,* 594**,** 3464-3476.
7. AMARH, V., WHITE, M. A. & LEACH, D. R. 2018. Dynamics of RecA-mediated repair of replication-dependent DNA breaks. *Journal of Cell Biology,* 217**,** 2299-2307.
8. ANDERSSON, D. I., KOSKINIEMI, S. & HUGHES, D. 2010. Biological roles of translesion synthesis DNA polymerases in eubacteria. *Molecular microbiology,* 77**,** 540-548.
9. ANKLEY, L., THOMAS, S. & OLIVE, A. J. 2020. Fighting persistence: how chronic infections with Mycobacterium tuberculosis Evade T cell-mediated clearance and new strategies to defeat them. *Infection and immunity,* 88**,** e00916-19.
10. BAÑOS-MATEOS, S., VAN ROON, A.-M. M., LANG, U. F., MASLEN, S. L., SKEHEL, J. M. & LAMERS, M. H. 2017. High-fidelity DNA replication in Mycobacterium tuberculosis relies on a trinuclear zinc center. *Nature communications,* 8**,** 1-10.

11. BARRY, C. E., BOSHOFF, H. I., DARTOIS, V., DICK, T., EHRT, S., FLYNN, J., SCHNAPPINGER, D., WILKINSON, R. J. & YOUNG, D. 2009. The spectrum of latent tuberculosis: rethinking the biology and intervention strategies. *Nature Reviews Microbiology,* 7**,** 845-855.
12. BEARD, W. A. & WILSON, S. H. 2003. Structural insights into the origins of DNA polymerase fidelity. *Structure,* 11**,** 489-496.
13. BIANCO, P. R. & KOWALCZYKOWSKI, S. C. 2005. RecA protein. *Encyclopedia of Life Sciences (eLS),* 1-8.
14. BINDELS, D. S., HAARBOSCH, L., VAN WEEREN, L., POSTMA, M., WIESE, K. E., MASTOP, M., AUMONIER, S., GOTTHARD, G., ROYANT, A. & HINK, M. A. 2017. mScarlet: a bright monomeric red fluorescent protein for cellular imaging. *Nature methods,* 14**,** 53-56.
15. BOSHOFF, H. I., MYERS, T. G., COPP, B. R., MCNEIL, M. R., WILSON, M. A. & BARRY, C. E. 2004. The transcriptional responses of Mycobacterium tuberculosis to inhibitors of metabolism: novel insights into drug mechanisms of action. *Journal of Biological Chemistry,* 279**,** 40174-40184.
16. BOSHOFF, H. I., REED, M. B., BARRY III, C. E. & MIZRAHI, V. 2003. DnaE2 polymerase contributes to in vivo survival and the emergence of drug resistance in Mycobacterium tuberculosis. *Cell,* 113**,** 183-193.
17. BOZZANO, F., MARRAS, F. & DE MARIA, A. 2014. Immunology of tuberculosis. *Mediterranean journal of hematology and infectious diseases,* 6.
18. BRIDGES, B. A. 2005a. Error-prone DNA repair and translesion DNA synthesis: II: The inducible SOS hypothesis. *DNA repair,* 4**,** 725-739.
19. BRIDGES, B. A. 2005b. Error-prone DNA repair and translesion synthesis: focus on the replication fork. *DNA repair,* 4**,** 618-634.
20. BROOKS, P. C., MOVAHEDZADEH, F. & DAVIS, E. O. 2001. Identification of some DNA damage-inducible genes of Mycobacterium tuberculosis: apparent lack of correlation with LexA binding. *Journal of bacteriology,* 183**,** 4459-4467.
21. BRUCK, I., WOODGATE, R., MCENTEE, K. & GOODMAN, M. F. 1996. Purification of a Soluble UmuD′ C Complex from Escherichia coli: COOPERATIVE BINDING OF UmuD′ C TO SINGLE-STRANDED DNA (∗). *Journal of Biological Chemistry,* 271**,** 10767-10774.

22. BURNEY, S., CAULFIELD, J. L., NILES, J. C., WISHNOK, J. S. & TANNENBAUM, S. R. 1999. The chemistry of DNA damage from nitric oxide and peroxynitrite. *Mutation Research/Fundamental and Molecular Mechanisms of Mutagenesis,* 424**,** 37-49.
23. BUSSI, C. & GUTIERREZ, M. G. 2019. Mycobacterium tuberculosis infection of host cells in space and time. *FEMS microbiology reviews,* 43**,** 341-361.
24. CAMBIER, C., FALKOW, S. & RAMAKRISHNAN, L. 2014. Host evasion and exploitation schemes of Mycobacterium tuberculosis. *Cell,* 159**,** 1497-1509.
25. CARTER, K. P., YOUNG, A. M. & PALMER, A. E. 2014. Fluorescent sensors for measuring metal ions in living systems. *Chemical reviews,* 114**,** 4564-4601.
26. CARVALHO, R., DE SONNEVILLE, J., STOCKHAMMER, O. W., SAVAGE, N. D., VENEMAN, W. J., OTTENHOFF, T. H., DIRKS, R. P., MEIJER, A. H. & SPAINK, H. P. 2011. A high-throughput screen for tuberculosis progression. *PloS one,* 6**,** e16779.
27. CASTAÑEDA-GARCÍA, A., MARTÍN-BLECUA, I., CEBRIÁN-SASTRE, E., CHINER-OMS, A., TORRES-PUENTE, M., COMAS, I. & BLÁZQUEZ, J. 2020. Specificity and mutagenesis bias of the mycobacterial alternative mismatch repair analyzed by mutation accumulation studies. *Science advances,* 6**,** eaay4453.
28. CASTANEDA-GARCIA, A., PRIETO, A., RODRIGUEZ-BELTRAN, J., ALONSO, N., CANTILLON, D., COSTAS, C., PÉREZ-LAGO, L., ZEGEYE, E., HERRANZ, M. & PLOCIŃSKI, P. 2017. A non-canonical mismatch repair pathway in prokaryotes. *Nature communications,* 8**,** 1-10.
29. CHANDANI, S., JACOBS, C. & LOECHLER, E. L. 2010. Architecture of y-family DNA polymerases relevant to translesion DNA synthesis as revealed in structural and molecular modeling studies. *Journal of nucleic acids,* 2010.
30. CHANDRAN, A. V., JAYANTHI, S. & VIJAYAN, M. 2018. Structure and interactions of RecA: plasticity revealed by molecular dynamics simulations. *Journal of Biomolecular Structure and Dynamics,* 36**,** 98-111.
31. CHAO, M. C. & RUBIN, E. J. 2010. Letting sleeping dos lie: does dormancy play a role in tuberculosis? *Annual review of microbiology,* 64**,** 293-311.
32. CHEN, J. M., POJER, F., BLASCO, B. & COLE, S. T. 2010. Towards anti-virulence drugs targeting ESX-1 mediated pathogenesis of Mycobacterium tuberculosis. *Drug Discovery Today: Disease Mechanisms,* 7**,** e25-e31.
33. CHOPRA, S., MATSUYAMA, K., TRAN, T., MALERICH, J. P., WAN, B., FRANZBLAU, S. G., LUN, S., GUO, H., MAIGA, M. C. & BISHAI, W. R. 2012.

Evaluation of gyrase B as a drug target in Mycobacterium tuberculosis. *Journal of antimicrobial chemotherapy,* 67**,** 415-421.

34. CIRZ, R. T., CHIN, J. K., ANDES, D. R., DE CRÉCY-LAGARD, V., CRAIG, W. A. & ROMESBERG, F. E. 2005. Inhibition of mutation and combating the evolution of antibiotic resistance. *PLoS biology,* 3**,** e176.
35. CLARK, A. J. & MARGULIES, A. D. 1965. Isolation and characterization of recombination-deficient mutants of Escherichia coli K12. *Proceedings of the National Academy of Sciences of the United States of America,* 53**,** 451.
36. COX, M. M. 2007. Regulation of bacterial RecA protein function. *Critical reviews in biochemistry and molecular biology,* 42**,** 41-63.
37. CULYBA, M. J., MO, C. Y. & KOHLI, R. M. 2015. Targets for combating the evolution of acquired antibiotic resistance. *Biochemistry,* 54**,** 3573-3582.
38. DA ROCHA, R. P., DE MIRANDA PAQUOLA, A. C., DO VALLE MARQUES, M., MENCK, C. F. M. & GALHARDO, R. S. 2008. Characterization of the SOS regulon of Caulobacter crescentus. *Journal of bacteriology,* 190**,** 1209-1218.
39. DARWIN, K. H. & NATHAN, C. F. 2005. Role for nucleotide excision repair in virulence of Mycobacterium tuberculosis. *Infection and immunity,* 73**,** 4581-4587.
40. DATTA, S., GANESH, N., CHANDRA, N. R., MUNIYAPPA, K. & VIJAYAN, M. 2003a. Structural studies on MtRecA-nucleotide complexes: Insights into DNA and nucleotide binding and the structural signature of NTP recognition. *Proteins: Structure, Function, and Bioinformatics,* 50**,** 474-485.
41. DATTA, S., KRISHNA, R., GANESH, N., CHANDRA, N. R., MUNIYAPPA, K. & VIJAYAN, M. 2003b. Crystal structures of Mycobacterium smegmatis RecA and its nucleotide complexes. *Journal of bacteriology,* 185**,** 4280-4284.
42. DATTA, S., PRABU, M., VAZE, M., GANESH, N., CHANDRA, N. R., MUNIYAPPA, K. & VIJAYAN, M. 2000. Crystal structures of Mycobacterium tuberculosis RecA and its complex with ADP–AlF4: implications for decreased ATPase activity and molecular aggregation. *Nucleic acids research,* 28**,** 4964-4973.
43. DAVIS, E. O., DULLAGHAN, E. M. & RAND, L. 2002. Definition of the mycobacterial SOS box and use to identify LexA-regulated genes in Mycobacterium tuberculosis. *Journal of bacteriology,* 184**,** 3287-3295.

44. DAVIS, E. O., JENNER, P. J., BROOKS, P. C., COLSTON, M. J. & SEDGWICK, S. G. 1992. Protein splicing in the maturation of M. tuberculosis recA protein: a mechanism for tolerating a novel class of intervening sequence. *Cell,* 71**,** 201-210.
45. DAVIS, E. O., THANGARAJ, H. S., BROOKS, P. C. & COLSTON, M. J. 1994. Evidence of selection for protein introns in the recAs of pathogenic mycobacteria. *The EMBO Journal,* 13**,** 699-703.
46. DE WET, T. J., WINKLER, K. R., MHLANGA, M., MIZRAHI, V. & WARNER, D. F. 2020. Arrayed CRISPRi and quantitative imaging describe the morphotypic landscape of essential mycobacterial genes. *Elife,* 9**,** e60083.
47. DEL VAL, E., NASSER, W., ABAIBOU, H. & REVERCHON, S. 2019. RecA and DNA recombination: a review of molecular mechanisms. *Biochemical Society Transactions,* 47**,** 1511-1531.
48. DHEDA, K., GUMBO, T., GANDHI, N. R., MURRAY, M., THERON, G., UDWADIA, Z., MIGLIORI, G. & WARREN, R. 2014. Global control of tuberculosis: from extensively drug-resistant to untreatable tuberculosis. *The lancet Respiratory medicine,* 2**,** 321-338.
49. DHEDA, K., GUMBO, T., MAARTENS, G., DOOLEY, K. E., MCNERNEY, R., MURRAY, M., FURIN, J., NARDELL, E. A., LONDON, L. & LESSEM, E. 2017. The epidemiology, pathogenesis, transmission, diagnosis, and management of multidrug-resistant, extensively drug-resistant, and incurable tuberculosis. *The lancet Respiratory medicine,* 5**,** 291-360.
50. DILLINGHAM, M. S. & KOWALCZYKOWSKI, S. C. 2008. RecBCD enzyme and the repair of double-stranded DNA breaks. *Microbiology and Molecular Biology Reviews,* 72**,** 642-671.
51. DITSE, Z., LAMERS, M. H. & WARNER, D. F. 2017. DNA Replication in Mycobacterium tuberculosis. *Microbiology spectrum,* 5**,** 5.2. 20.
52. DOS VULTOS, T., MESTRE, O., TONJUM, T. & GICQUEL, B. 2009. DNA repair in Mycobacterium tuberculosis revisited. *FEMS microbiology reviews,* 33**,** 471-487.
53. DOVER, L. G. & COXON, G. D. 2011. Current status and research strategies in tuberculosis drug development: miniperspective. *Journal of medicinal chemistry,* 54**,** 6157-6165.
54. DRLICA, K. & ZHAO, X. 1997. DNA gyrase, topoisomerase IV, and the 4-quinolones. *Microbiology and molecular biology reviews,* 61**,** 377-392.

55. ECHEVERRIA-VALENCIA, G., FLORES-VILLALVA, S. & ESPITIA, C. I. 2018. Virulence factors and pathogenicity of Mycobacterium. *Mycobacterium—Research and Development; Tech: Rijeka, Croatia,* 231-255.
56. EHRT, S. & SCHNAPPINGER, D. 2009. Mycobacterial survival strategies in the phagosome: defence against host stresses. *Cellular microbiology,* 11**,** 1170-1178.
57. ERILL, I., CAMPOY, S., MAZON, G. & BARBÉ, J. 2006. Dispersal and regulation of an adaptive mutagenesis cassette in the bacteria domain. *Nucleic acids research,* 34**,** 66-77.
58. FIJALKOWSKA, I. J., SCHAAPER, R. M. & JONCZYK, P. 2012. DNA replication fidelity in Escherichia coli: a multi-DNA polymerase affair. *FEMS microbiology reviews,* 36**,** 1105-1121.
59. FRIEDBERG, E. 1995. In Friedberg, EC, Walker, GC and Siede, W. *DNA Repair and Mutagenesis,* 1-7.
60. FRIEDBERG, E. C., FISCHHABER, P. L. & KISKER, C. 2001. Error-prone DNA polymerases: novel structures and the benefits of infidelity. *Cell,* 107**,** 9-12.
61. FRIEDBERG, E. C., WALKER, G. C., SIEDE, W. & WOOD, R. D. 2005. *DNA repair and mutagenesis,* American Society for Microbiology Press.
62. FRISCHKORN, K., SANDER, P., SCHOLZ, M., TESCHNER, K., PRAMMANANAN, T. & BÖTTGER, E. C. 1998. Investigation of mycobacterial recA function: protein introns in the RecA of pathogenic mycobacteria do not affect competency for homologous recombination. *Molecular microbiology,* 29**,** 1203-1214.
63. FUCHS, R. P. & FUJII, S. 2013. Translesion DNA synthesis and mutagenesis in prokaryotes. *Cold Spring Harbor Perspectives in Biology,* 5**,** a012682.
64. GALHARDO, R. S., DO, R., YAMADA, M., FRIEDBERG, E. C., HASTINGS, P., NOHMI, T. & ROSENBERG, S. M. 2009. DinB upregulation is the sole role of the SOS response in stress-induced mutagenesis in Escherichia coli. *Genetics,* 182**,** 55-68.
65. GALHARDO, R. S., ROCHA, R. P., MARQUES, M. V. & MENCK, C. F. 2005. An SOS-regulated operon involved in damage-inducible mutagenesis in Caulobacter crescentus. *Nucleic Acids Research,* 33**,** 2603-2614.
66. GAMULIN, V., CETKOVIC, H. & AHEL, I. 2004. Identification of a promoter motif regulating the major DNA damage response mechanism of Mycobacterium tuberculosis. *FEMS microbiology letters,* 238**,** 57-63.
67. GESSNER, S. J. 2017. Molecular mechanisms of DNA repair in Mycobacterium tuberculosis.

68. GHODKE, H., PAUDEL, B. P., LEWIS, J. S., JERGIC, S., GOPAL, K., ROMERO, Z. J., WOOD, E. A., WOODGATE, R., COX, M. M. & VAN OIJEN, A. M. 2019. Spatial and temporal organization of RecA in the Escherichia coli DNA-damage response. *Elife,* 8**,** e42761.
69. GOODMAN, M. F. 2002. Error-prone repair DNA polymerases in prokaryotes and eukaryotes. *Annual review of biochemistry,* 71**,** 17-50.
70. GOODMAN, M. F., MCDONALD, J. P., JASZCZUR, M. M. & WOODGATE, R. 2016. Insights into the complex levels of regulation imposed on Escherichia coli DNA polymerase V. *DNA repair,* 44**,** 42-50.
71. GOODMAN, M. F. & WOODGATE, R. 2013. Translesion DNA polymerases. *Cold Spring Harbor perspectives in biology,* 5**,** a010363.
72. GOPAUL, K. K., BROOKS, P. C., PROST, J.-F. & DAVIS, E. O. 2003. Characterization of the two Mycobacterium tuberculosis recA promoters. *Journal of bacteriology,* 185**,** 6005-6015.
73. GORNA, A. E., BOWATER, R. P. & DZIADEK, J. 2010. DNA repair systems and the pathogenesis of Mycobacterium tuberculosis: varying activities at different stages of infection. *Clinical science,* 119**,** 187-202.
74. GU, S., LI, W., ZHANG, H., FLEMING, J., YANG, W., WANG, S., WEI, W., ZHOU, J., ZHU, G. & DENG, J. 2016. The β 2 clamp in the Mycobacterium tuberculosis DNA polymerase III αβ 2 ε replicase promotes polymerization and reduces exonuclease activity. *Scientific reports,* 6**,** 1-13.
75. GUPTA, R., BARKAN, D., REDELMAN-SIDI, G., SHUMAN, S. & GLICKMAN, M. S. 2011. Mycobacteria exploit three genetically distinct DNA double-strand break repair pathways. *Molecular microbiology,* 79**,** 316-330.
76. GYGLI, S. M., BORRELL, S., TRAUNER, A. & GAGNEUX, S. 2017. Antimicrobial resistance in Mycobacterium tuberculosis: mechanistic and evolutionary perspectives. *FEMS microbiology reviews,* 41**,** 354-373.
77. HOAGLAND, D. T., LIU, J., LEE, R. B. & LEE, R. E. 2016. New agents for the treatment of drug-resistant Mycobacterium tuberculosis. *Advanced drug delivery reviews,* 102**,** 55-72.
78. HUANG, L., NAZAROVA, E. V. & RUSSELL, D. G. 2019. Mycobacterium tuberculosis: bacterial fitness within the host macrophage. *Microbiology spectrum,* 7**,** 7.2. 04.

79. HUANG, X., LU, Y., WANG, S., SUI, M., LI, J., MA, J., MA, D., JIA, Q., HU, S. & XU, C. 2020. Mismatch sensing by nucleofilament deciphers mechanism of RecA-mediated homologous recombination. *Proceedings of the National Academy of Sciences,* 117**,** 20549-20554.
80. INDIANI, C., LANGSTON, L. D., YURIEVA, O., GOODMAN, M. F. & O'DONNELL, M. 2009. Translesion DNA polymerases remodel the replisome and alter the speed of the replicative helicase. *Proceedings of the National Academy of Sciences,* 106**,** 6031-6038.
81. INDIANI, C., MCINERNEY, P., GEORGESCU, R., GOODMAN, M. F. & O'DONNELL, M. 2005. A sliding-clamp toolbelt binds high-and low-fidelity DNA polymerases simultaneously. *Molecular cell,* 19**,** 805-815.
82. IPPOLITI, P. J., DELATEUR, N. A., JONES, K. M. & BEUNING, P. J. 2012. Multiple strategies for translesion synthesis in bacteria. *Cells,* 1**,** 799-831.
83. JANION, C. 2008. Inducible SOS response system of DNA repair and mutagenesis in Escherichia coli. *International journal of biological sciences,* 4**,** 338.
84. JASIN, M. & ROTHSTEIN, R. 2013. Repair of strand breaks by homologous recombination. *Cold Spring Harbor perspectives in biology,* 5**,** a012740.
85. JASZCZUR, M., BERTRAM, J. G., ROBINSON, A., VAN OIJEN, A. M., WOODGATE, R., COX, M. M. & GOODMAN, M. F. 2016. Mutations for worse or better: low-fidelity DNA synthesis by SOS DNA polymerase V is a tightly regulated double-edged sword. *Biochemistry,* 55**,** 2309-2318.
86. JASZCZUR, M. M., VO, D. D., STANCIAUSKAS, R., BERTRAM, J. G., SIKAND, A., COX, M. M., WOODGATE, R., MAK, C. H., PINAUD, F. & GOODMAN, M. F. 2019. Conformational regulation of Escherichia coli DNA polymerase V by RecA and ATP. *PLoS genetics,* 15**,** e1007956.
87. JATSENKO, T., SIDORENKO, J., SAUMAA, S. & KIVISAAR, M. 2017. DNA polymerases ImuC and DinB are involved in DNA alkylation damage tolerance in Pseudomonas aeruginosa and Pseudomonas putida. *PloS one,* 12**,** e0170719.
88. JOHNSON, A. & O'DONNELL, M. 2005. Cellular DNA replicases: components and dynamics at the replication fork. *Annu. Rev. Biochem.,* 74**,** 283-315.
89. KANA, B. D., ABRAHAMS, G. L., SUNG, N., WARNER, D. F., GORDHAN, B. G., MACHOWSKI, E. E., TSENOVA, L., SACCHETTINI, J. C., STOKER, N. G. & KAPLAN, G. 2010. Role of the DinB homologs Rv1537 and Rv3056 in Mycobacterium tuberculosis. *Journal of bacteriology,* 192**,** 2220-2227.

90. KEYAMURA, K., SAKAGUCHI, C., KUBOTA, Y., NIKI, H. & HISHIDA, T. 2013. RecA protein recruits structural maintenance of chromosomes (SMC)-like RecN protein to DNA double-strand breaks. *Journal of Biological Chemistry,* 288**,** 29229-29237.
91. KOORITS, L., TEGOVA, R., TARK, M., TARASSOVA, K., TOVER, A. & KIVISAAR, M. 2007. Study of involvement of ImuB and DnaE2 in stationary-phase mutagenesis in Pseudomonas putida. *DNA repair,* 6**,** 863-868.
92. KUMAR, A., FARHANA, A., GUIDRY, L., SAINI, V., HONDALUS, M. & STEYN, A. J. 2011. Redox homeostasis in mycobacteria: the key to tuberculosis control? *Expert reviews in molecular medicine,* 13.
93. KURTHKOTI, K. & VARSHNEY, U. 2012. Distinct mechanisms of DNA repair in mycobacteria and their implications in attenuation of the pathogen growth. *Mechanisms of ageing and development,* 133**,** 138-146.
94. LANGE, S. S., TAKATA, K.-I. & WOOD, R. D. 2011. DNA polymerases and cancer. *Nature reviews cancer,* 11**,** 96-110.
95. LESTERLIN, C., BALL, G., SCHERMELLEH, L. & SHERRATT, D. J. 2014. RecA bundles mediate homology pairing between distant sisters during DNA break repair. *Nature,* 506**,** 249.
96. LIN, P. L., FORD, C. B., COLEMAN, M. T., MYERS, A. J., GAWANDE, R., IOERGER, T., SACCHETTINI, J., FORTUNE, S. M. & FLYNN, J. L. 2014. Sterilization of granulomas is common in active and latent tuberculosis despite within-host variability in bacterial killing. *Nature medicine,* 20**,** 75-79.
97. LINDAHL, T. 1996. The Croonian Lecture, 1996: endogenous damage to DNA. *Philosophical Transactions of the Royal Society of London. Series B: Biological Sciences,* 351**,** 1529-1538.
98. LING, H., BOUDSOCQ, F., WOODGATE, R. & YANG, W. 2001. Crystal structure of a Y-family DNA polymerase in action: a mechanism for error-prone and lesion-bypass replication. *Cell,* 107**,** 91-102.
99. LITTLE, J. 1991. Mechanism of specific LexA cleavage: autodigestion and the role of RecA coprotease. *Biochimie,* 73**,** 411-421.
100. LITTLE, J. W. 1982. Control of the SOS regulatory system by the level of RecA protease. *Biochimie,* 64**,** 585-589.
101. LITTLE, J. W. & MOUNT, D. W. 1982. The SOS regulatory system of Escherichia coli. *Cell,* 29**,** 11-22.

102. LITTLE, J. W., MOUNT, D. W. & YANISCH-PERRON, C. R. 1981. Purified lexA protein is a repressor of the recA and lexA genes. *Proceedings of the National Academy of Sciences,* 78**,** 4199-4203.

103. LIU, B., XUE, Q., TANG, Y., CAO, J., GUENGERICH, F. P. & ZHANG, H. 2016. Mechanisms of mutagenesis: DNA replication in the presence of DNA damage. *Mutation Research/Reviews in Mutation Research,* 768**,** 53-67.

104. LODISH, H. 1995. Cell organization, subcellular structure, and cell division In: Lodish H, Baltimore D, Berk A, Zipursky SL, Matsudaira P, Darnell J,(eds) Molecular cell biology 3rd ed. Scientific American Books, New York.

105. LUSETTI, S. L. & COX, M. M. 2002. The bacterial RecA protein and the recombinational DNA repair of stalled replication forks. *Annual review of biochemistry,* 71**,** 71-100.

106. MAHAJAN, R. 2013. Bedaquiline: first FDA-approved tuberculosis drug in 40 years. *International Journal of Applied and Basic Medical Research,* 3**,** 1.

107. MANGANELLI, R., PROVEDDI, R., RODRIGUE, S., BEAUCHER, J., GAUDREAU, L. & SMITH, I. 2004. σ factors and global gene regulation in Mycobacterium tuberculosis. *Journal of bacteriology,* 186**,** 895-902.

108. MANINA, G., GRIEGO, A., SINGH, L. K., MCKINNEY, J. D. & DHAR, N. 2019. Preexisting variation in DNA damage response predicts the fate of single mycobacteria under stress. *The EMBO journal,* 38**,** e101876.

109. MANJELIEVSKAIA, J., ERCK, D., PIRACHA, S. & SCHRAGER, L. 2016. Drug-resistant TB: deadly, costly and in need of a vaccine. *Transactions of the Royal Society of Tropical Medicine and Hygiene,* 110**,** 186-191.

110. MASLOWSKA, K. H., MAKIELA-DZBENSKA, K. & FIJALKOWSKA, I. J. 2019. The SOS system: a complex and tightly regulated response to DNA damage. *Environmental and molecular mutagenesis,* 60**,** 368-384.

111. MAYITO, J., ANDIA, I., BELAY, M., JOLLIFFE, D. A., KATEETE, D. P., REECE, S. T. & MARTINEAU, A. R. 2019. Anatomic and cellular niches for Mycobacterium tuberculosis in latent tuberculosis infection. *The Journal of infectious diseases,* 219**,** 685-694.

112. MCGREW, D. A. & KNIGHT, K. L. 2003. Molecular design and functional organization of the RecA protein. *Critical Reviews in Biochemistry and Molecular Biology,* 38**,** 385-432.

113. MCHENRY, C. S. 2011a. Bacterial replicases and related polymerases. *Current opinion in chemical biology,* 15**,** 587-594.

114. MCHENRY, C. S. 2011b. Breaking the rules: bacteria that use several DNA polymerase IIIs. *EMBO reports,* 12**,** 408-414.

115. MCKENNA, L. & FURIN, J. 2019. Are pretomanid-containing regimens for tuberculosis a victory or a victory narrative? *The Lancet Respiratory Medicine,* 7**,** 999-1000.

116. MIGGIANO, R., MORRONE, C., ROSSI, F. & RIZZI, M. 2020. Targeting genome integrity in Mycobacterium tuberculosis: From nucleotide synthesis to DNA replication and repair. *Molecules,* 25**,** 1205.

117. MINIAS, A., BRZOSTEK, A. & DZIADEK, J. 2019. Targeting DNA repair systems in antitubercular drug development. *Current medicinal chemistry,* 26**,** 1494-1505.

118. MITTAL, P., SINHA, R., KUMAR, A., SINGH, P., NGASAINAO, M. R., SINGH, A. & SINGH, I. K. 2020. Focusing on DNA repair and damage tolerance mechanisms in mycobacterium tuberculosis: an emerging therapeutic theme. *Current topics in medicinal chemistry,* 20**,** 390-408.

119. MIZRAHI, V. & ANDERSEN, S. J. 1998. DNA repair in Mycobacterium tuberculosis. What have we learnt from the genome sequence? *Molecular microbiology,* 29**,** 1331-1339.

120. MORIMATSU, K. & KOWALCZYKOWSKI, S. C. 2003. RecFOR proteins load RecA protein onto gapped DNA to accelerate DNA strand exchange: a universal step of recombinational repair. *Molecular cell,* 11**,** 1337-1347.

121. MÜLLER, A. U., IMKAMP, F. & WEBER-BAN, E. 2018. The mycobacterial LexA/RecA-independent DNA damage response is controlled by PafBC and the Pup-proteasome system. *Cell reports,* 23**,** 3551-3564.

122. MÜLLER, A. U., LEIBUNDGUT, M., BAN, N. & WEBER-BAN, E. 2019. Structure and functional implications of WYL-domain-containing transcription factor PafBC involved in the mycobacterial DNA damage response. *bioRxiv***,** 612655.

123. MUTTUCUMARU, D. & PARISH, T. 2004. The molecular biology of recombination in Mycobacteria: what do we know and how can we use it? *Current issues in molecular biology,* 6**,** 145-158.

124. NAMOUCHI, A., GÓMEZ-MUÑOZ, M., FRYE, S. A., MOEN, L. V., ROGNES, T., TØNJUM, T. & BALASINGHAM, S. V. 2016. The Mycobacterium tuberculosis transcriptional landscape under genotoxic stress. *BMC genomics,* 17**,** 1-13.

125. NAPOLITANO, R., JANEL-BINTZ, R., WAGNER, J. & FUCHS, R. 2000. All three SOS-inducible DNA polymerases (Pol II, Pol IV and Pol V) are involved in induced mutagenesis. *The EMBO journal,* 19**,** 6259-6265.

126. NAUTIYAL, A., PATIL, K. N. & MUNIYAPPA, K. 2014. Suramin is a potent and selective inhibitor of Mycobacterium tuberculosis RecA protein and the SOS response: RecA as a potential target for antibacterial drug discovery. *Journal of Antimicrobial Chemotherapy,* 69**,** 1834-1843.

127. NOHMI, T. 2006. Environmental stress and lesion-bypass DNA polymerases. *Annu. Rev. Microbiol.,* 60**,** 231-253.

128. NOHMI, T., BATTISTA, J. R., DODSON, L. A. & WALKER, G. C. 1988. RecA-mediated cleavage activates UmuD for mutagenesis: mechanistic relationship between transcriptional derepression and posttranslational activation. *Proceedings of the National Academy of Sciences,* 85**,** 1816-1820.

129. OHMORI, H., FRIEDBERG, E. C., FUCHS, R. P., GOODMAN, M. F., HANAOKA, F., HINKLE, D., KUNKEL, T. A., LAWRENCE, C. W., LIVNEH, Z. & NOHMI, T. 2001. The Y-family of DNA polymerases. *Molecular cell,* 8**,** 7-8.

130. OJHA, D. & PATIL, K. N. 2019. p-Coumaric acid inhibits the Listeria monocytogenes RecA protein functions and SOS response: An antimicrobial target. *Biochemical and biophysical research communications,* 517**,** 655-661.

131. OLIVENCIA, B. F., MÜLLER, A. U., ROSCHITZKI, B., BURGER, S., WEBER-BAN, E. & IMKAMP, F. 2017. Mycobacterium smegmatis PafBC is involved in regulation of DNA damage response. *Scientific reports,* 7**,** 1-13.

132. ORGANIZATION, W. H. 2020. Global tuberculosis report 2020: executive summary.

133. PAGÈS, V. 2016. Single-strand gap repair involves both RecF and RecBCD pathways. *Current Genetics,* 62**,** 519-521.

134. PAPAVINASASUNDARAM, K., ANDERSON, C., BROOKS, P. C., THOMAS, N. A., MOVAHEDZADEH, F., JENNER, P. J., COLSTON, M. J. & DAVIS, E. O. 2001. Slow induction of RecA by DNA damage in Mycobacterium tuberculosis. *Microbiology,* 147**,** 3271-3279.

135. PARISH, T. & STOKER, N. G. 1998. *Mycobacteria protocols*, Springer.

136. PATEL, M., JIANG, Q., WOODGATE, R., COX, M. M. & GOODMAN, M. F. 2010. A new model for SOS-induced mutagenesis: how RecA protein activates DNA polymerase V. *Critical reviews in biochemistry and molecular biology,* 45**,** 171-184.

137. PATTERSON, B. & WOOD, R. 2019. Is cough really necessary for TB transmission? *Tuberculosis,* 117**,** 31-35.

138. PAVLOPOULOU, A. 2018. RecA: a universal drug target in pathogenic bacteria. *Front. Biosci.(Landmark Ed.),* 23**,** 36-42.

139. PHAM, P., BERTRAM, J. G., O'DONNELL, M., WOODGATE, R. & GOODMAN, M. F. 2001. A model for SOS-lesion-targeted mutations in Escherichia coli. *Nature,* 409**,** 366-370.

140. PHILIPS, J. A. & ERNST, J. D. 2011. Directly observing therapy: a new view of drug tolerance in tuberculosis. *Cell,* 145**,** 13-14.

141. PONTALI, E., SOTGIU, G., D'AMBROSIO, L., CENTIS, R. & MIGLIORI, G. B. 2016. Bedaquiline and multidrug-resistant tuberculosis: a systematic and critical analysis of the evidence. Eur Respiratory Soc.

142. PRABU, J. R., MANJUNATH, G., CHANDRA, N. R., MUNIYAPPA, K. & VIJAYAN, M. 2008. Functionally important movements in RecA molecules and filaments: studies involving mutation and environmental changes. *Acta Crystallographica Section D: Biological Crystallography,* 64**,** 1146-1157.

143. PRASAD, D., ARORA, D., NANDICOORI, V. K. & MUNIYAPPA, K. 2019. Elucidating the functional role of Mycobacterium smegmatis recX in stress response. *Scientific reports,* 9**,** 1-16.

144. PRASAD, R., SINGH, A., BALASUBRAMANIAN, V. & GUPTA, N. 2017. Extensively drug-resistant tuberculosis in India: Current evidence on diagnosis & management. *The Indian journal of medical research,* 145**,** 271.

145. QUEVAL, C. J., BROSCH, R. & SIMEONE, R. 2017. The macrophage: a disputed fortress in the battle against Mycobacterium tuberculosis. *Frontiers in microbiology,* 8**,** 2284.

146. RADMAN, M. 1975. SOS repair hypothesis: phenomenology of an inducible DNA repair which is accompanied by mutagenesis. *Molecular mechanisms for repair of DNA***,** 355-367.

147. RAND, L., HINDS, J., SPRINGER, B., SANDER, P., BUXTON, R. S. & DAVIS, E. O. 2003. The majority of inducible DNA repair genes in Mycobacterium tuberculosis are induced independently of RecA. *Molecular microbiology,* 50**,** 1031-1042.

148. RANGARAJAN, S., WOODGATE, R. & GOODMAN, M. F. 2002. Replication restart in UV-irradiated Escherichia coli involving pols II, III, V, PriA, RecA and RecFOR proteins. *Molecular microbiology,* 43**,** 617-628.

149. RAVIMOHAN, S., KORNFELD, H., WEISSMAN, D. & BISSON, G. P. 2018. Tuberculosis and lung damage: from epidemiology to pathophysiology. *European Respiratory Review,* 27.

150. REECE, R. J. & MAXWELL, A. 1991. DNA gyrase: structure and function. *Critical reviews in biochemistry and molecular biology,* 26**,** 335-375.

151. REICHE, M. A. 2018. *Visualising the mycobacterial mutasome.* University of Cape Town.

152. REICHE, M. A., WARNER, D. F. & MIZRAHI, V. 2017. Targeting DNA replication and repair for the development of novel therapeutics against tuberculosis. *Frontiers in molecular biosciences,* 4**,** 75.

153. RENZETTE, N., GUMLAW, N., NORDMAN, J. T., KRIEGER, M., YEH, S. P., LONG, E., CENTORE, R., BOONSOMBAT, R. & SANDLER, S. J. 2005. Localization of RecA in Escherichia coli K-12 using RecA–GFP. *Molecular microbiology,* 57**,** 1074-1085.

154. REUVEN, N. B., ARAD, G., MAOR-SHOSHANI, A. & LIVNEH, Z. 1999. The mutagenesis protein UmuC is a DNA polymerase activated by UmuD′, RecA, and SSB and is specialized for translesion replication. *Journal of Biological Chemistry*, 274**,** 31763-31766.

155. ROBINSON, A., MCDONALD, J. P., CALDAS, V. E., PATEL, M., WOOD, E. A., PUNTER, C. M., GHODKE, H., COX, M. M., WOODGATE, R. & GOODMAN, M. F. 2015. Regulation of mutagenic DNA polymerase V activation in space and time. *PLoS genetics,* 11**,** e1005482.

156. ROCK, J. M., LANG, U. F., CHASE, M. R., FORD, C. B., GERRICK, E. R., GAWANDE, R., COSCOLLA, M., GAGNEUX, S., FORTUNE, S. M. & LAMERS, M. H. 2015. DNA replication fidelity in Mycobacterium tuberculosis is mediated by an ancestral prokaryotic proofreader. *Nature genetics,* 47**,** 677-681.

157. RUSSELL, D. G. 2007. Who puts the tubercle in tuberculosis? *Nature Reviews Microbiology,* 5**,** 39-47.

158. SAMBROOK, J., FRITSCH, E. F. & MANIATIS, T. 1989. *Molecular cloning: a laboratory manual*, Cold spring harbor laboratory press.

159. SAMBROOK, J. & RUSSELL, D. 2001. Molecular cloning: A laboratory manual. Mol. *Cloning A Lab. Man*.

160. SANDERS, L. H., ROCKEL, A., LU, H., WOZNIAK, D. J. & SUTTON, M. D. 2006. Role of Pseudomonas aeruginosa dinB-encoded DNA polymerase IV in mutagenesis. *Journal of bacteriology,* 188**,** 8573-8585.

161. SASSANFAR, M. & ROBERTS, J. W. 1990. Nature of the SOS-inducing signal in Escherichia coli: the involvement of DNA replication. *Journal of molecular biology,* 212**,** 79-96.

162. SCHLACHER, K., LESLIE, K., WYMAN, C., WOODGATE, R., COX, M. M. & GOODMAN, M. F. 2005. DNA polymerase V and RecA protein, a minimal mutasome. *Molecular cell,* 17**,** 561-572.

163. SCHLACHER, K., PHAM, P., COX, M. M. & GOODMAN, M. F. 2006. Roles of DNA polymerase V and RecA protein in SOS damage-induced mutation. *Chemical reviews,* 106**,** 406-419.

164. SHASHKOVA, S. & LEAKE, M. C. Single-molecule fluorescence microscopy: shedding new light on old problems.

165. SHENG, D., WANG, Y., JIANG, Z., LIU, D. & LI, Y. 2020. ImuA participates in SOS mutagenesis by interacting with RecA1 and ImuB in Myxococcus xanthus. *bioRxiv*.

166. SHIN, H.-J. & KWON, Y.-S. 2015. Treatment of drug susceptible pulmonary tuberculosis. *Tuberculosis and respiratory diseases,* 78**,** 161-167.

167. SHINAGAWA, H. 1996. SOS response as an adaptive response to DNA damage in prokaryotes. *Stress-inducible cellular responses***,** 221-235.

168. SIA, J. K. & RENGARAJAN, J. 2019. Immunology of Mycobacterium tuberculosis infections. *Microbiology spectrum,* 7**,** 7.4. 6.

169. SIMMONS, L. A., GROSSMAN, A. D. & WALKER, G. C. 2007. Replication is required for the RecA localization response to DNA damage in Bacillus subtilis. *Proceedings of the National Academy of Sciences,* 104**,** 1360-1365.

170. SINGH, A. 2017. Guardians of the mycobacterial genome: A review on DNA repair systems in Mycobacterium tuberculosis. *Microbiology,* 163**,** 1740-1758.

171. SINGH, A., BHAGAVAT, R., VIJAYAN, M. & CHANDRA, N. 2016. A comparative analysis of the DNA recombination repair pathway in mycobacterial genomes. *Tuberculosis,* 99**,** 109-119.

172. SINGH, V. & MIZRAHI, V. 2017. Identification and validation of novel drug targets in Mycobacterium tuberculosis. *Drug Discovery Today,* 22**,** 503-509.

173. SMITH, K. C. 2004. Recombinational DNA repair: the ignored repair systems. *Bioessays,* 26**,** 1322-1326.

174. SMOLLETT, K. L., SMITH, K. M., KAHRAMANOGLOU, C., ARNVIG, K. B., BUXTON, R. S. & DAVIS, E. O. 2012. Global analysis of the regulon of the transcriptional repressor LexA, a key component of SOS response in Mycobacterium tuberculosis. *Journal of Biological Chemistry,* 287**,** 22004-22014.

175. SPRING, K. & DAVIDSON, M. Introduction to Fluorescence Microscopy. Nikon Microscopy U; 2008.

176. STAGG, H., HARRIS, R. J., HATHERELL, H., OBACH, D., ZHAO, H., TSUCHIYA, N., KRANZER, K., NIKOLAYEVSKYY, V., KIM, J. & LIPMAN, M. 2016. What are the most efficacious treatment regimens for isoniazid-resistant tuberculosis? A systematic review and network meta-analysis. *Thorax,* 71**,** 940-949.

177. STALLINGS, C. L. & GLICKMAN, M. S. 2010. Is Mycobacterium tuberculosis stressed out? A critical assessment of the genetic evidence. *Microbes and infection,* 12**,** 1091-1101.

178. STEPHANOU, N. C., GAO, F., BONGIORNO, P., EHRT, S., SCHNAPPINGER, D., SHUMAN, S. & GLICKMAN, M. S. 2007. Mycobacterial nonhomologous end joining mediates mutagenic repair of chromosomal double-strand DNA breaks. *Journal of bacteriology,* 189**,** 5237-5246.

179. STORY, R. M., WEBER, I. T. & STEITZ, T. A. 1992. The structure of the E. coli recA protein monomer and polymer. *Nature,* 355**,** 318-325.

180. SUTTON, M. D., SMITH, B. T., GODOY, V. G. & WALKER, G. C. 2000. The SOS response: recent insights into umuDC-dependent mutagenesis and DNA damage tolerance. *Annual review of genetics,* 34.

181. TANG, M., PHAM, P., SHEN, X., TAYLOR, J.-S., O'DONNELL, M., WOODGATE, R. & GOODMAN, M. F. 2000. Roles of E. coli DNA polymerases IV and V in lesion-targeted and untargeted SOS mutagenesis. *Nature,* 404**,** 1014-1018.

182. TANG, M., SHEN, X., FRANK, E. G., O'DONNELL, M., WOODGATE, R. & GOODMAN, M. F. 1999. UmuD′ 2C is an error-prone DNA polymerase, Escherichia coli pol V. *Proceedings of the National Academy of Sciences,* 96**,** 8919-8924.

183. TAYLOR, A. F. & SMITH, G. R. 2003. RecBCD enzyme is a DNA helicase with fast and slow motors of opposite polarity. *Nature,* 423**,** 889-893.

184. TIMINSKAS, K., BALVOČIŪTĖ, M., TIMINSKAS, A. & VENCLOVAS, Č. 2014. Comprehensive analysis of DNA polymerase III α subunits and their homologs in bacterial genomes. *Nucleic acids research,* 42**,** 1393-1413.

185. TIMINSKAS, K. & VENCLOVAS, Č. 2019. New insights into the structures and interactions of bacterial Y-family DNA polymerases. *Nucleic acids research,* 47**,** 4393-4405.

186. TIPPIN, B., PHAM, P. & GOODMAN, M. F. 2004. Error-prone replication for better or worse. *Trends in microbiology,* 12**,** 288-295.

187. TOMASZ, M., CHAWLA, A. K. & LIPMAN, R. 1988. Mechanism of monofunctional and bifunctional alkylation of DNA by mitomycin C. *Biochemistry,* 27**,** 3182-3187.

188. TSAI, H.-H., SHU, H.-W., YANG, C.-C. & CHEN, C. W. 2012. Translesion-synthesis DNA polymerases participate in replication of the telomeres in Streptomyces. *Nucleic acids research,* 40**,** 1118-1130.

189. TURNER, R. D., CHIU, C., CHURCHYARD, G. J., ESMAIL, H., LEWINSOHN, D. M., GANDHI, N. R. & FENNELLY, K. P. 2017. Tuberculosis infectiousness and host susceptibility. *The Journal of infectious diseases,* 216**,** S636-S643.

190. UPADHYAY, S., MITTAL, E. & PHILIPS, J. 2018. Tuberculosis and the art of macrophage manipulation. *Pathogens and disease,* 76**,** fty037.

191. WALKER, G. C. 1996. The SOS response of Escherichia coli. Escherichia coli and Salmonella: cellular and molecular biology.

192. WALSH, J. M., HAWVER, L. A. & BEUNING, P. J. 2011. Escherichia coli Y family DNA polymerases. *Front Biosci (Landmark Ed),* 16**,** 3164-3182.

193. WANG, Y., HUANG, Y., XUE, C., HE, Y. & HE, Z.-G. 2011. ClpR protein-like regulator specifically recognizes RecA protein-independent promoter motif and broadly regulates expression of DNA damage-inducible genes in mycobacteria. *Journal of Biological Chemistry,* 286**,** 31159-31167.

194. WARNER, D. F. 2010. The role of DNA repair in M. tuberculosis pathogenesis. *Drug Discovery Today: Disease Mechanisms,* 7**,** e5-e11.

195. WARNER, D. F., EVANS, J. C. & MIZRAHI, V. 2014. Nucleotide metabolism and DNA replication. *Microbiology Spectrum,* 2**,** 2.5. 01.

196. WARNER, D. F. & MIZRAHI, V. 2006. Tuberculosis chemotherapy: the influence of bacillary stress and damage response pathways on drug efficacy. *Clinical microbiology reviews,* 19**,** 558-570.

197. WARNER, D. F. & MIZRAHI, V. 2007. The survival kit of Mycobacterium tuberculosis. *Nature medicine,* 13**,** 282-284.

198. WARNER, D. F., NDWANDWE, D. E., ABRAHAMS, G. L., KANA, B. D., MACHOWSKI, E. E., VENCLOVAS, Č. & MIZRAHI, V. 2010. Essential roles for imuA′- and imuB-encoded accessory factors in DnaE2-dependent mutagenesis in Mycobacterium tuberculosis. *Proceedings of the National Academy of Sciences,* 107**,** 13093-13098.

199. WARNER, D. F., TØNJUM, T. & MIZRAHI, V. 2013. DNA metabolism in mycobacterial pathogenesis. *Pathogenesis of Mycobacterium tuberculosis and its Interaction with the Host Organism***,** 27-51.

200. WATSON, J. D., BAKER, T. A., BELL, S. P., GANN, A. & LEVINE, M. 2008. *Molecular biology of the gene*, 東京電機大学出版局.

201. WELLER, G. R., KYSELA, B., ROY, R., TONKIN, L. M., SCANLAN, E., DELLA, M., DEVINE, S. K., DAY, J. P., WILKINSON, A. & DI FAGAGNA, F. D. A. 2002. Identification of a DNA nonhomologous end-joining complex in bacteria. *Science,* 297**,** 1686-1689.

202. WIGLEY, D. B. 2013. Bacterial DNA repair: recent insights into the mechanism of RecBCD, AddAB and AdnAB. *Nature Reviews Microbiology,* 11**,** 9-13.

203. WIPPERMAN, M. F., HEATON, B. E., NAUTIYAL, A., ADEFISAYO, O., EVANS, H., GUPTA, R., VAN DITMARSCH, D., SONI, R., HENDRICKSON, R. & JOHNSON, J. 2018. Mycobacterial mutagenesis and drug resistance are controlled by phosphorylation- and cardiolipin-mediated inhibition of the RecA coprotease. *Molecular cell,* 72**,** 152-161. e7.

204. YANG, W. & GAO, Y. 2018. Translesion and repair DNA polymerases: diverse structure and mechanism. *Annual review of biochemistry,* 87**,** 239-261.

205. YANG, W. & WOODGATE, R. 2007. What a difference a decade makes: insights into translesion DNA synthesis. *Proceedings of the National Academy of Sciences,* 104**,** 15591-15598.

206. YI, C. & HE, C. 2013. DNA repair by reversal of DNA damage. *Cold Spring Harbor perspectives in biology,* 5**,** a012575.

207. ZHAI, W., WU, F., ZHANG, Y., FU, Y. & LIU, Z. 2019. The immune escape mechanisms of Mycobacterium tuberculosis. *International journal of molecular sciences,* 20**,** 340.

208. ZHAO, G., GLEAVE, E. S. & LAMERS, M. H. 2017. Single-molecule studies contrast ordered DNA replication with stochastic translesion synthesis. *Elife,* 6**,** e32177.

209. ZHAO, X.-Q., HU, J.-F. & YU, J. 2006. Comparative analysis of eubacterial DNA polymerase III alpha subunits. *Genomics, proteomics & bioinformatics,* 4**,** 203-211.